SAND2021-13981C

Thermal decoupling of deuterons and tritons during the shock-convergence phase in Inertial Confinement Fusion implosions

$$\left.\frac{T_T}{T_D}\right|_{t=0} = 1.5 = \frac{m_T}{m_D}$$

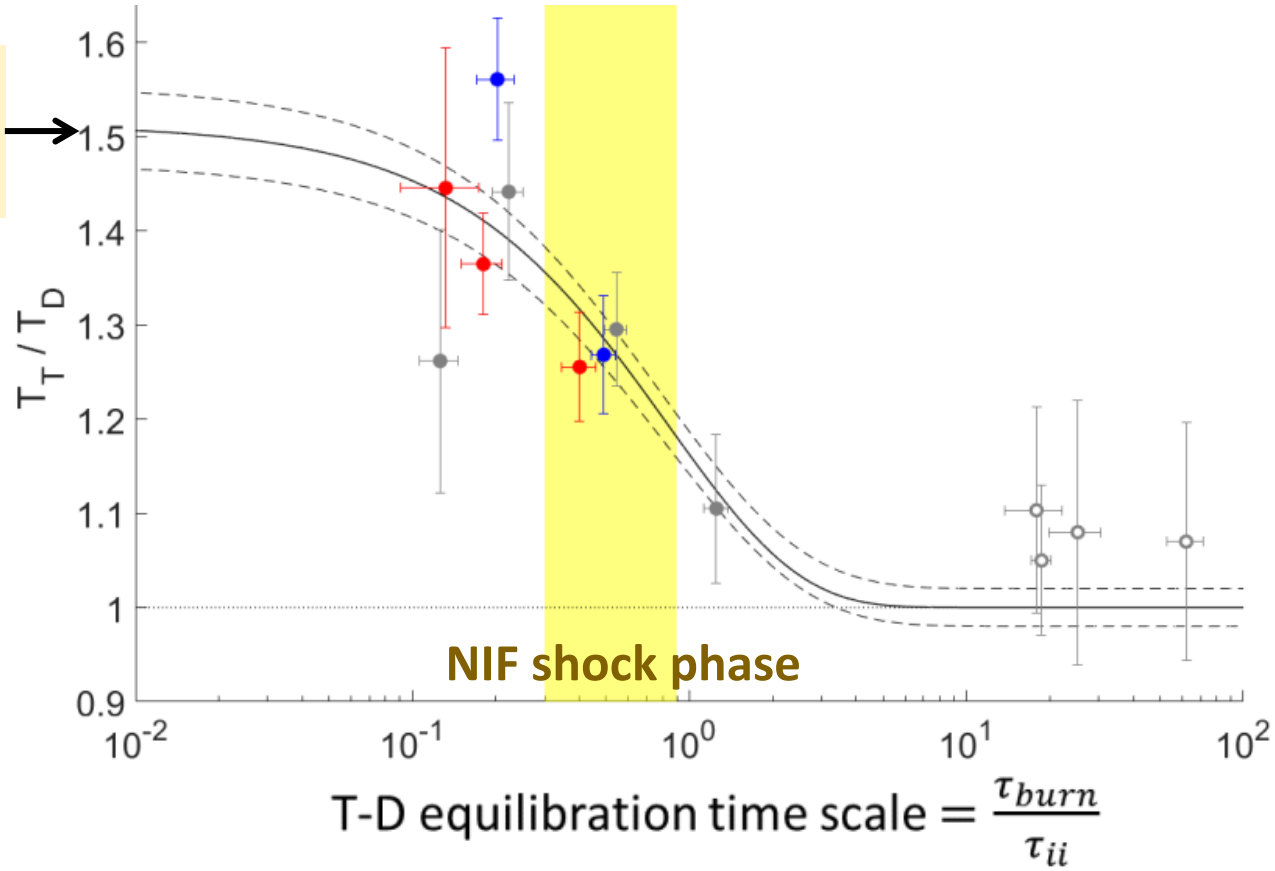

Neel Kabadi

10/2021

63rd Annual Meeting of the APS Division of Plasma Physics

Kabadi et al., Phys. Rev. E **104**, L013201 (2021)

LA-UR-21-30829

Collaborators and Sponsors

P. Adrian, R. Simpson, A. Bose, G. Sutcliffe, B. Lahmann, C. Parker, J. Pearcy, B. Reichelt, J. Frenje, M. Gatu Johnson, C. Li, and R. Petrasso
Plasma Science and Fusion Center, Massachusetts Institute of Technology

C. Forrest, V. Glebov, R. Janezic, O. Mannion*, C. Stoeckl, R. Betti
Laboratory for Laser Energetics, University of Rochester

L. Welch, B. Srinivasan
Virginia Tech

H. Sio, J. Sanchez
Lawrence Livermore National Laboratory

S. Atzeni
University of Rome Sapienza

J. Eriksson
Uppsala University

W. Taitano, B. Keenan, S. Anderson, A. Simakov, L. Chacón
Los Alamos National Laboratory

Brian Appelbe
Imperial College London

Supported by DOE/NNSA Contracts DE-NA0003868 and DE-NA0003938

*currently at Sandia National Laboratories

The observed difference between T_{DTn} and T_{DDn} is explained by shock coupling proportional to mass, and equilibration consistent with hydro theory.

- This is the first direct lab-based experimental measurement of shocks coupling directly proportional to mass in multi-ion plasmas, verifying a long standing prediction.

- For NIF ignition implosions, during the shock convergence phase the D and T ions are out of thermal equilibrium which greatly impacts the ion viscosity.

- iFP simulations indicate that this result is robust, even in the highly kinetic regime.

Outline

- Experimental Platform
- Measured T_{DDn} and T_{DTn}
- The mass dependence of ion shock coupling
- Impacts on ion viscosity
- Test of the impact of non-Maxwellian distributions
- Comparison to iFP Fokker-Planck

Outline

- Experimental Platform
- Measured T_{DDn} and T_{DTn}
- The mass dependence of ion shock coupling
- Impacts on ion viscosity
- Test of the impact of non-Maxwellian distributions
- Comparison to iFP Fokker-Planck

Thin shell shock driven implosions generate a shock convergence phase with similar conditions to ignition implosions

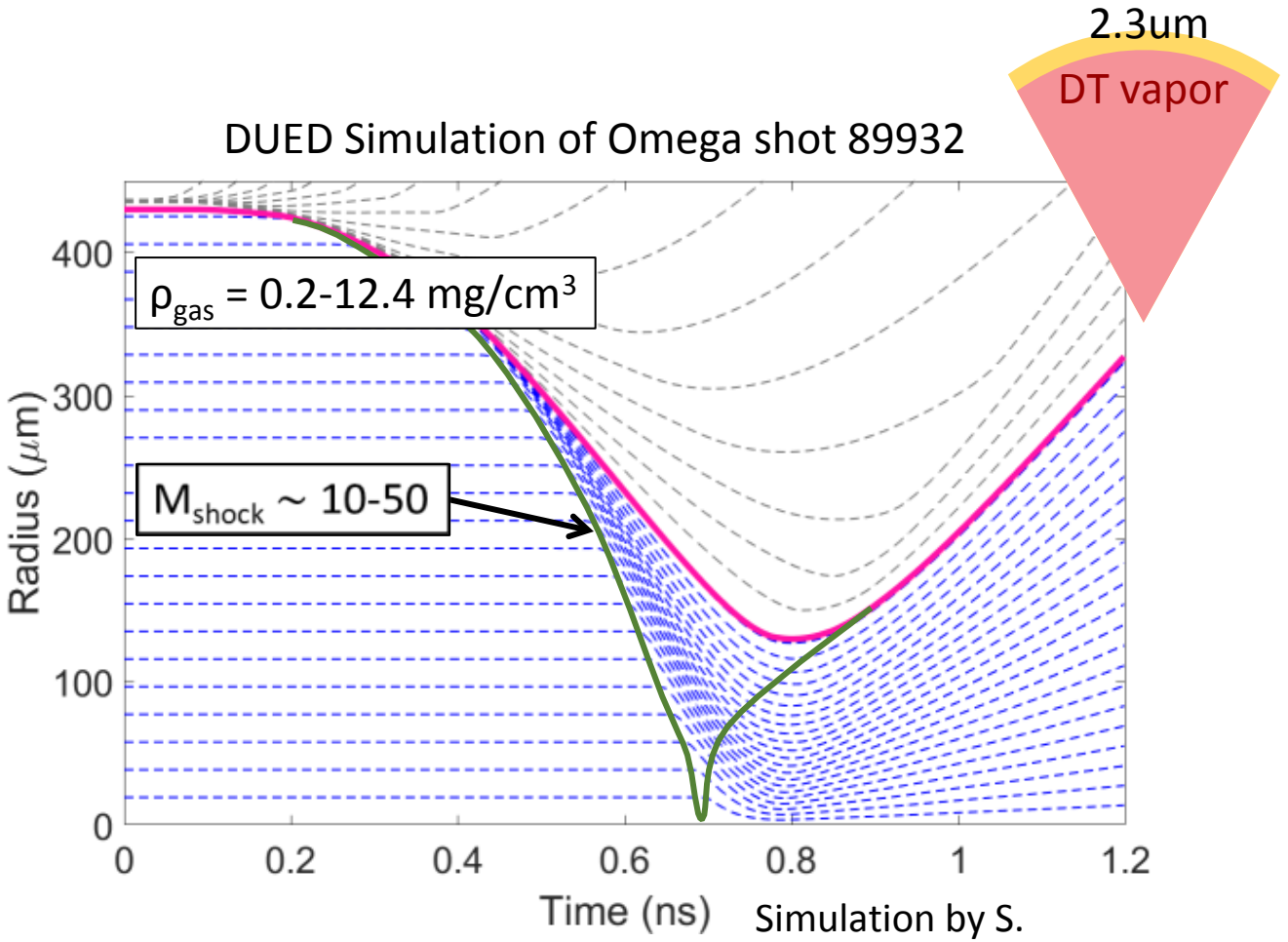

Simulation by S. Atzeni

Thin shell shock driven implosions generate a shock convergence phase with similar conditions to ignition implosions

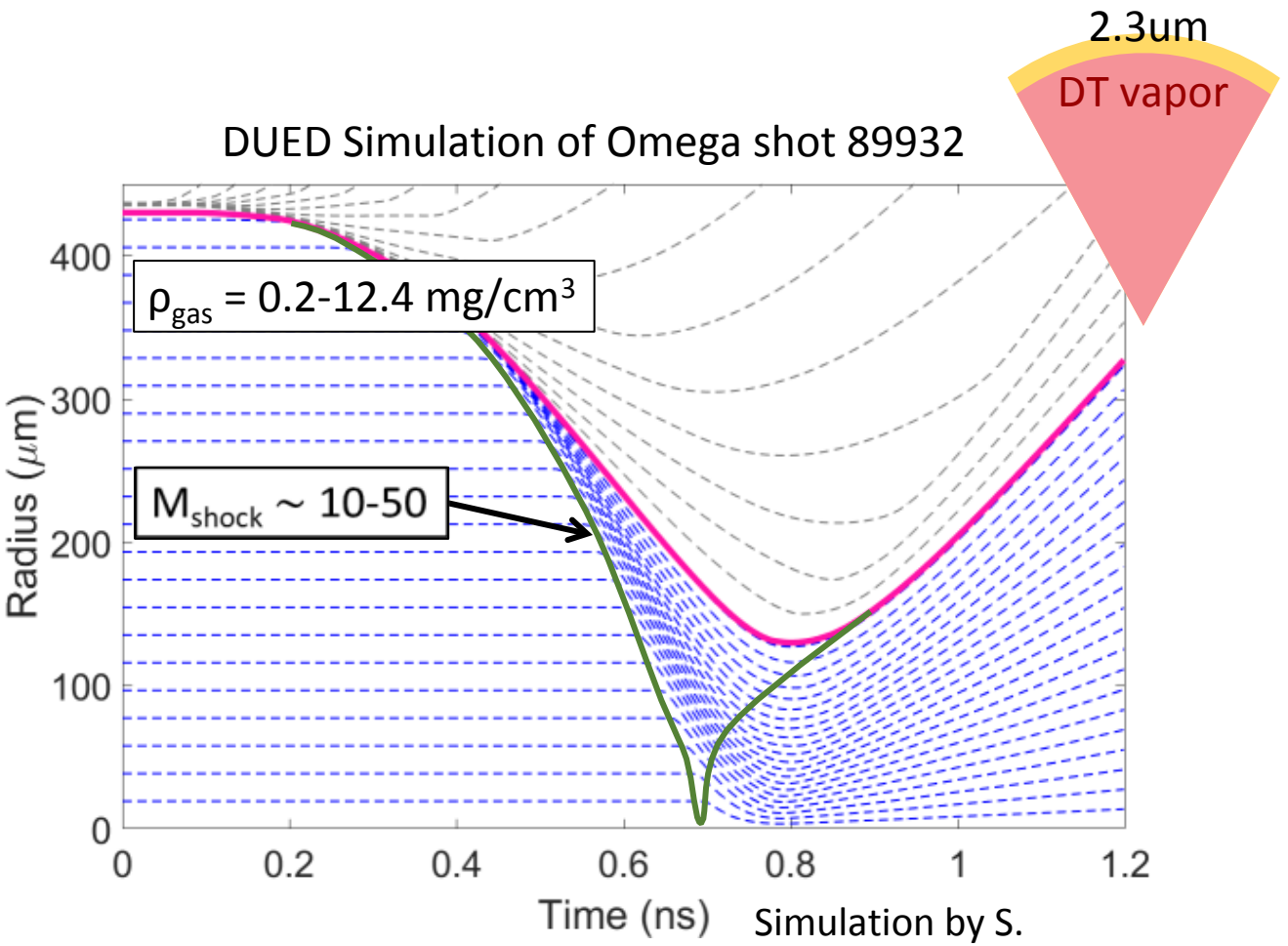

Simulation by S. Atzeni

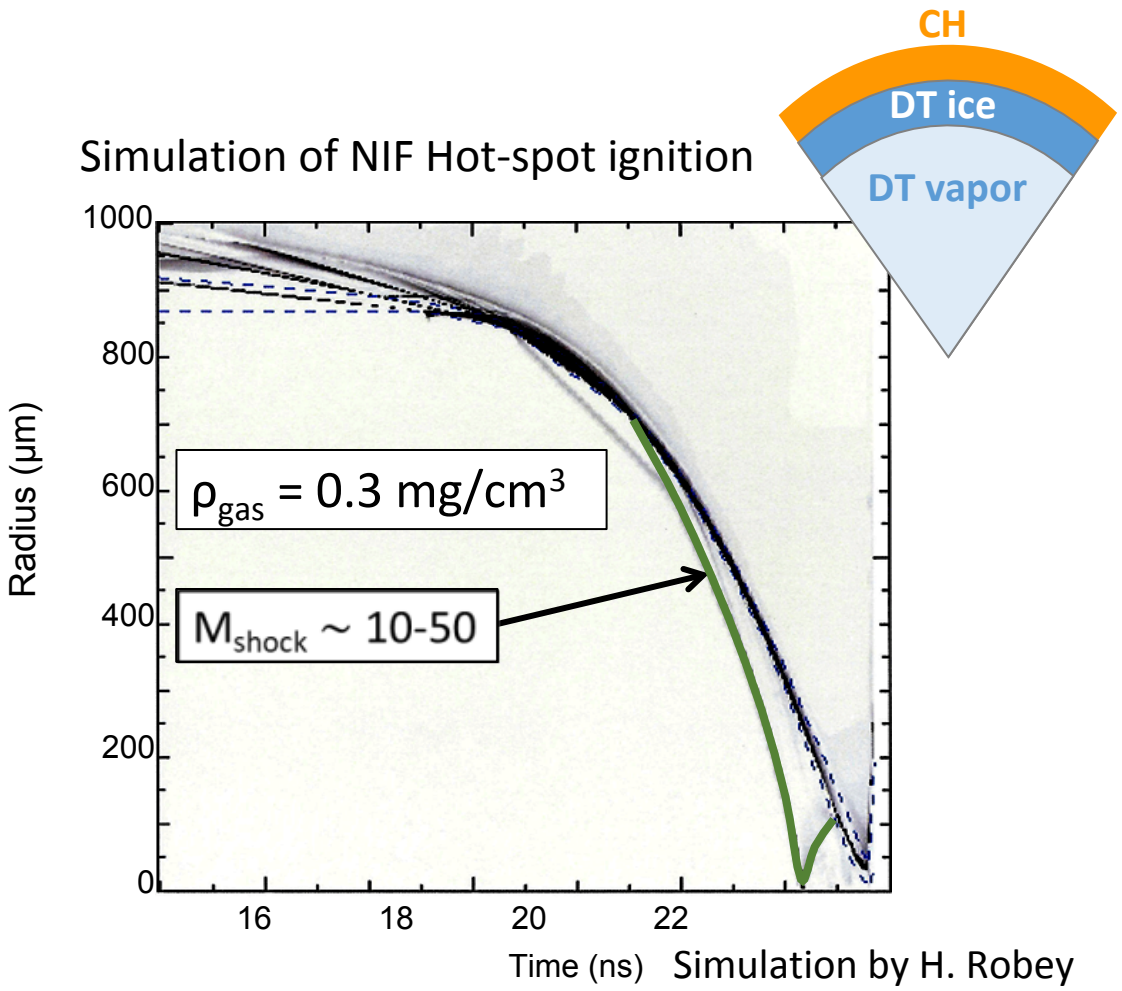

Simulation by H. Robey

Thin shell shock driven implosions generate a shock convergence phase with similar conditions to ignition implosions

DUED Simulation of Omega shot 89932

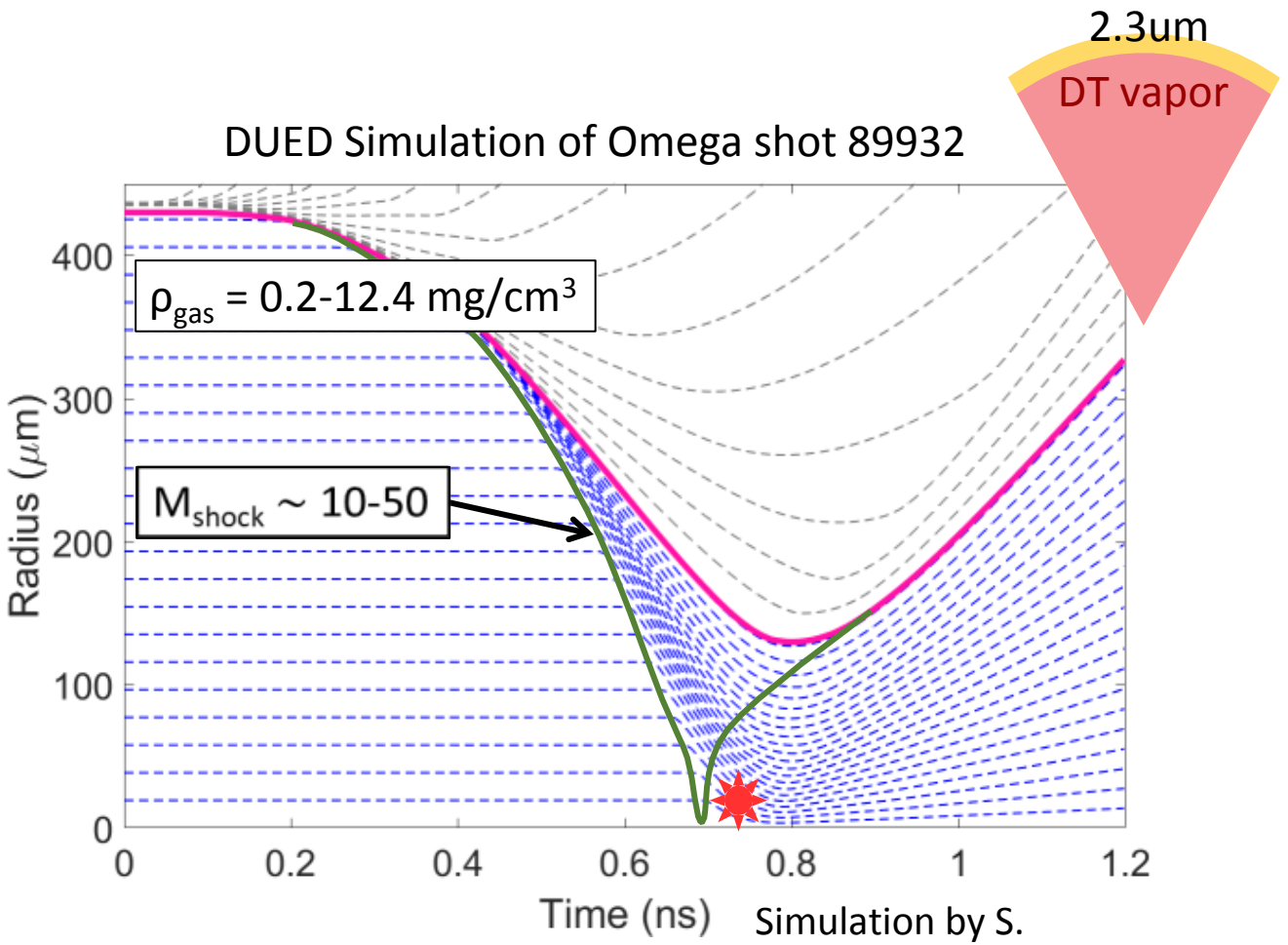

Simulation by S. Atzeni

Simulation of NIF Hot-spot ignition

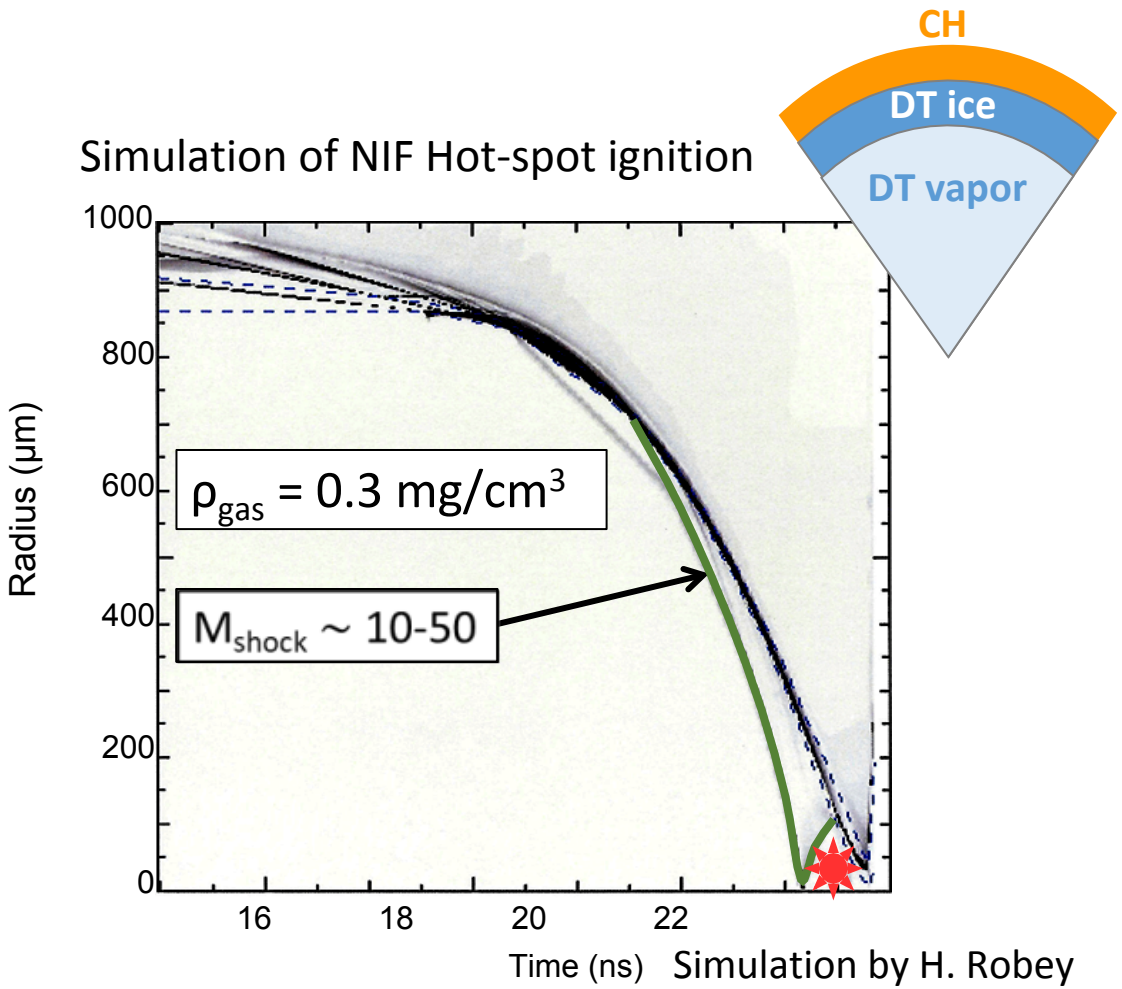

Simulation by H. Robey

Thin shell shock driven implosions generate a shock convergence phase with similar conditions to ignition implosions

DUED Simulation of Omega shot 89932

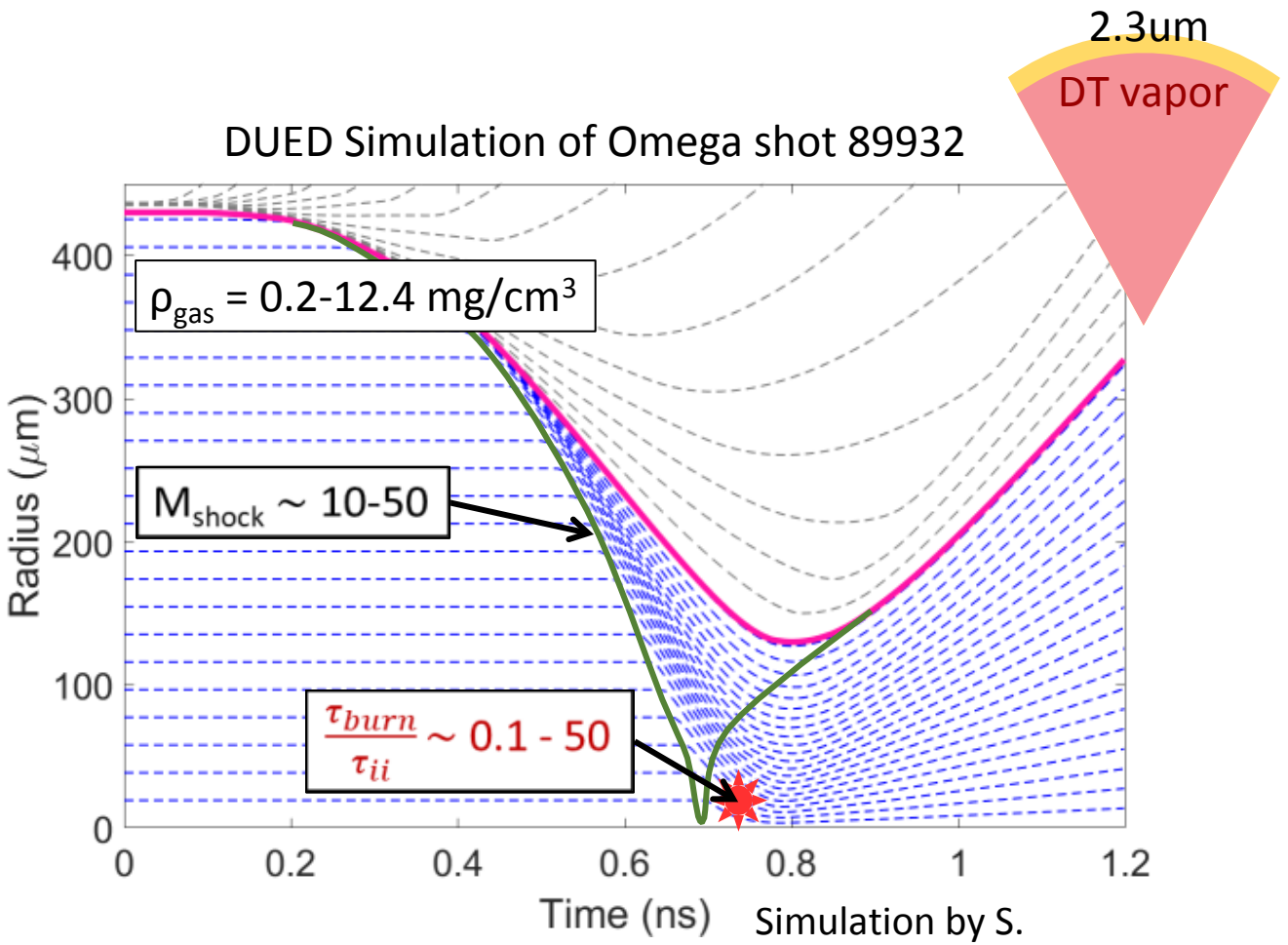

Simulation by S. Atzeni

Simulation of NIF Hot-spot ignition

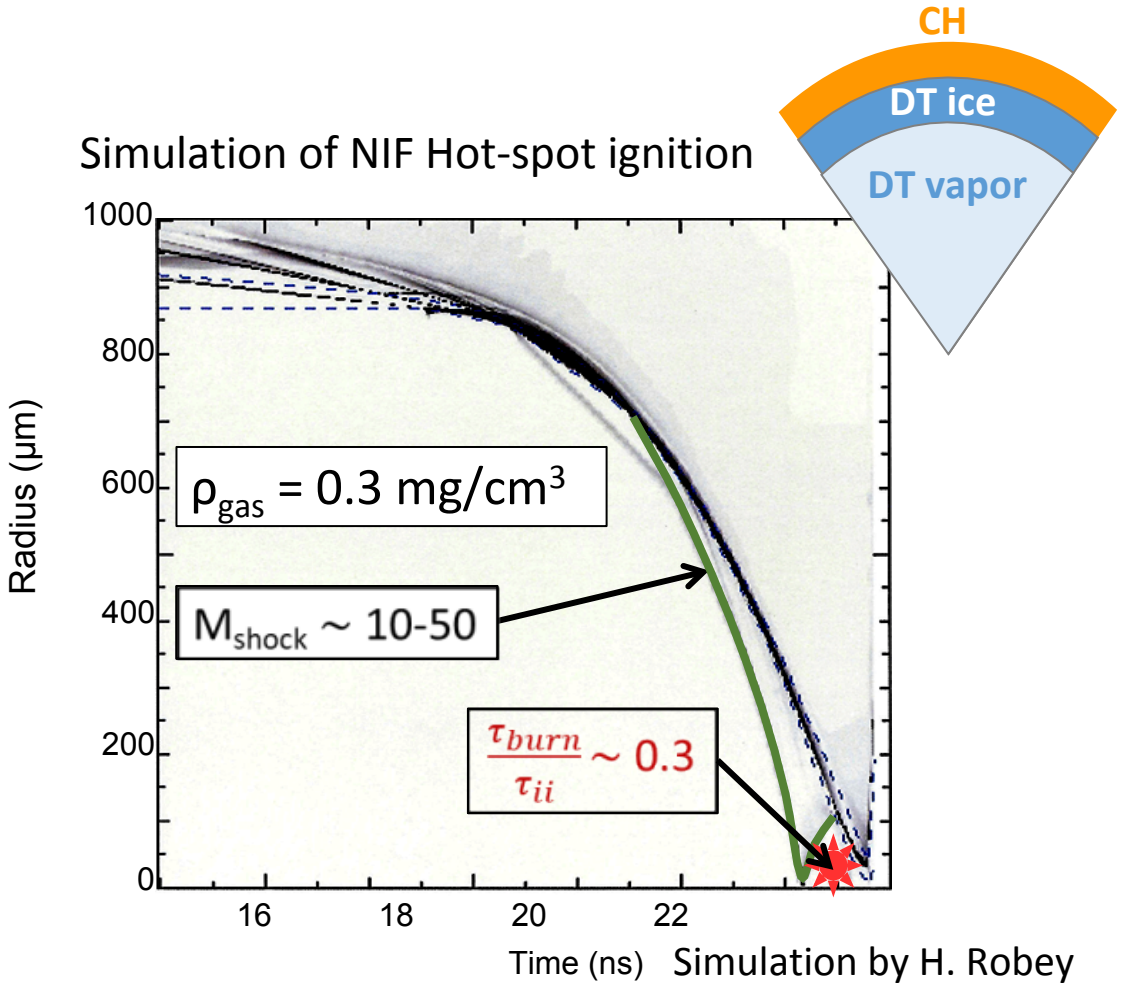

Simulation by H. Robey

Thin shell shock driven implosions generate a shock convergence phase with similar conditions to ignition implosions

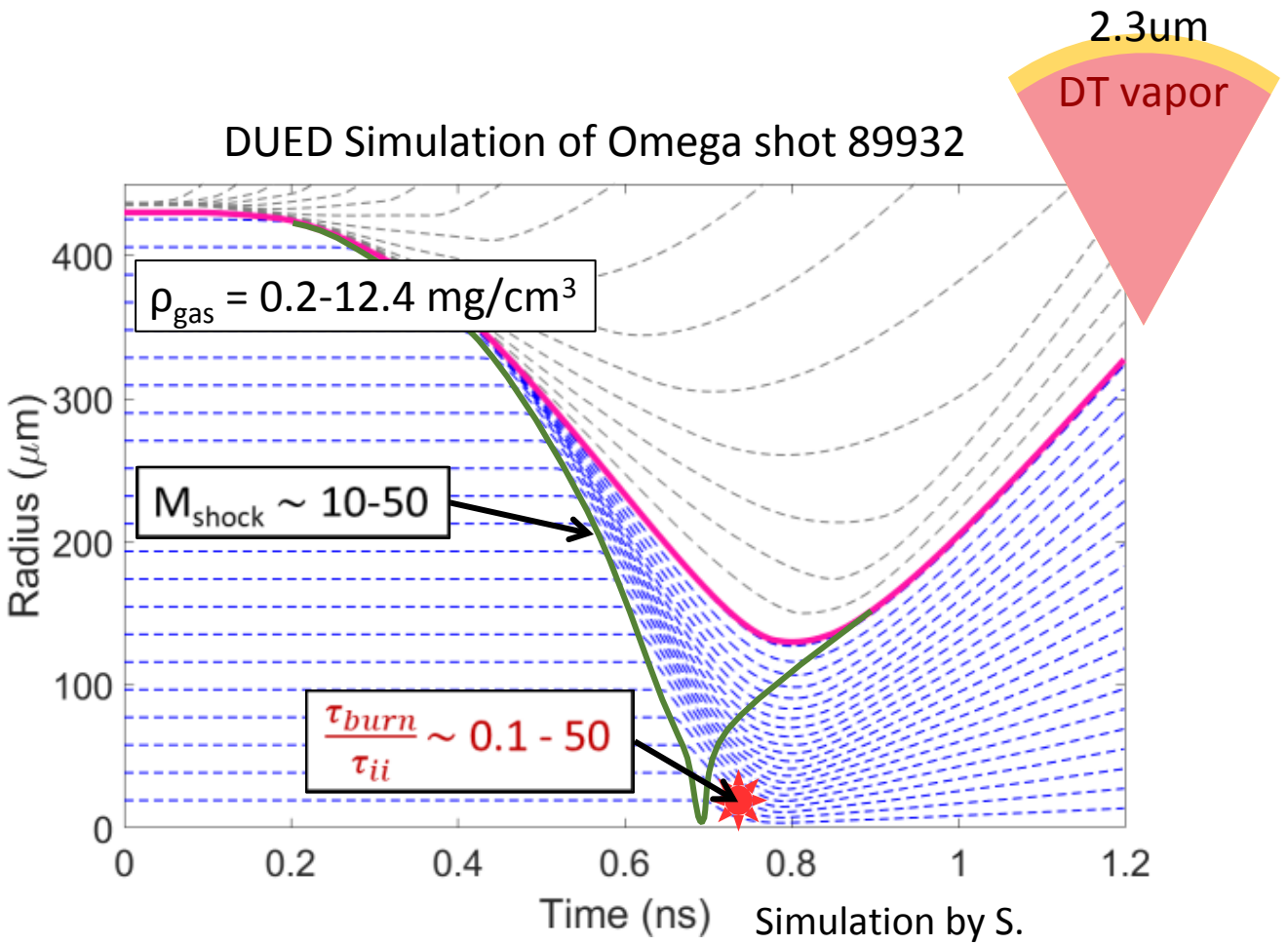

Simulation by S. Atzeni

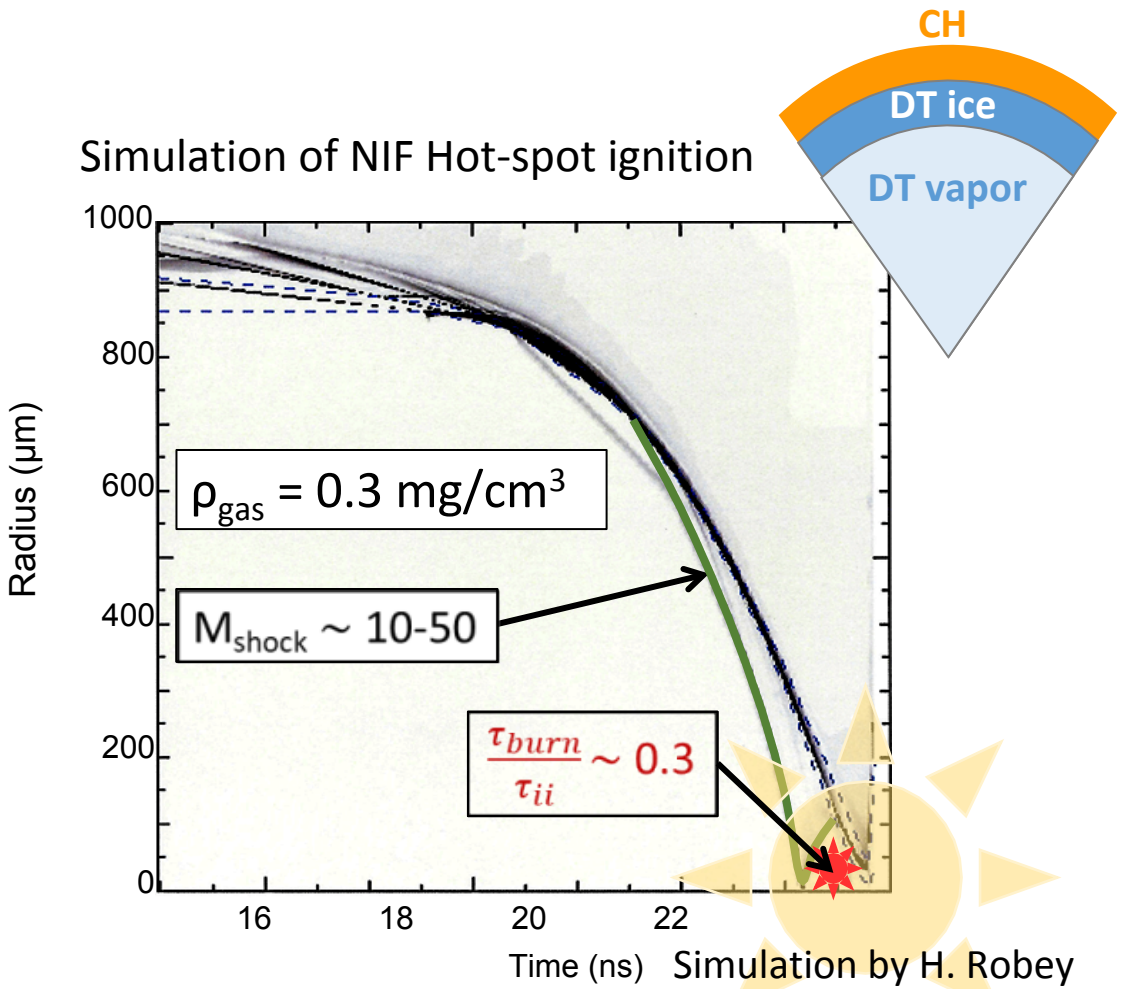

Simulation by H. Robey

This phase is difficult to study in ignition-relevant implosions in which the subsequent compression phase dominates the nuclear and X-ray observables.

Outline

- Experimental Platform
- Measured T_{DDn} and T_{DTn}
- The mass dependence of ion shock coupling
- Impacts on ion viscosity
- Test of the impact of non-Maxwellian distributions
- Comparison to iFP Fokker-Planck

There is separation between the NTOF measured T_{DTn} and T_{DDn}, which increases with decreasing fill density

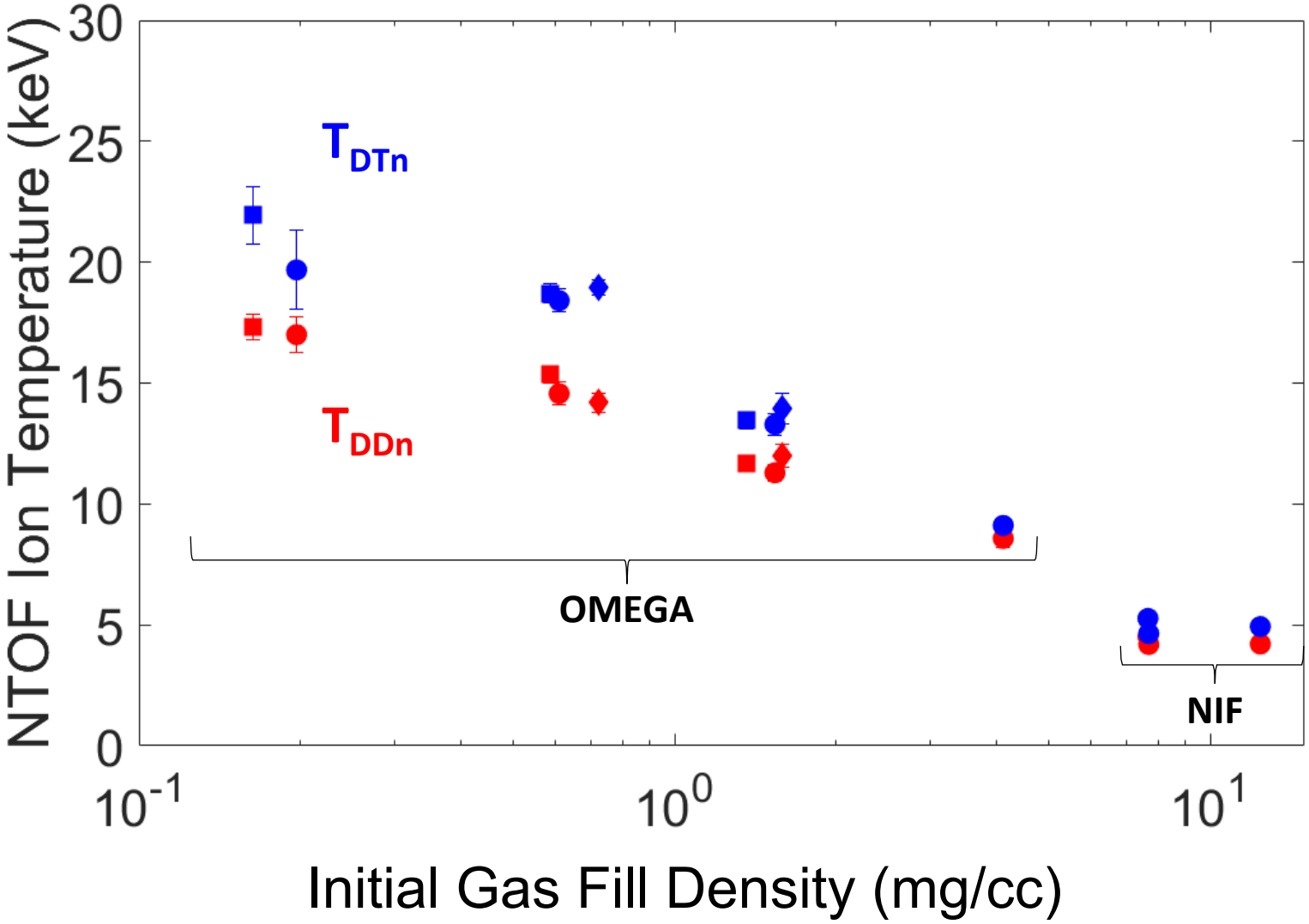

The DTn and DDn ion temperatures are inferred from the widths of the fusion product spectra as measured with NTOFs.

There is separation between the NTOF measured T_{DTn} and T_{DDn}, which increases with decreasing fill density

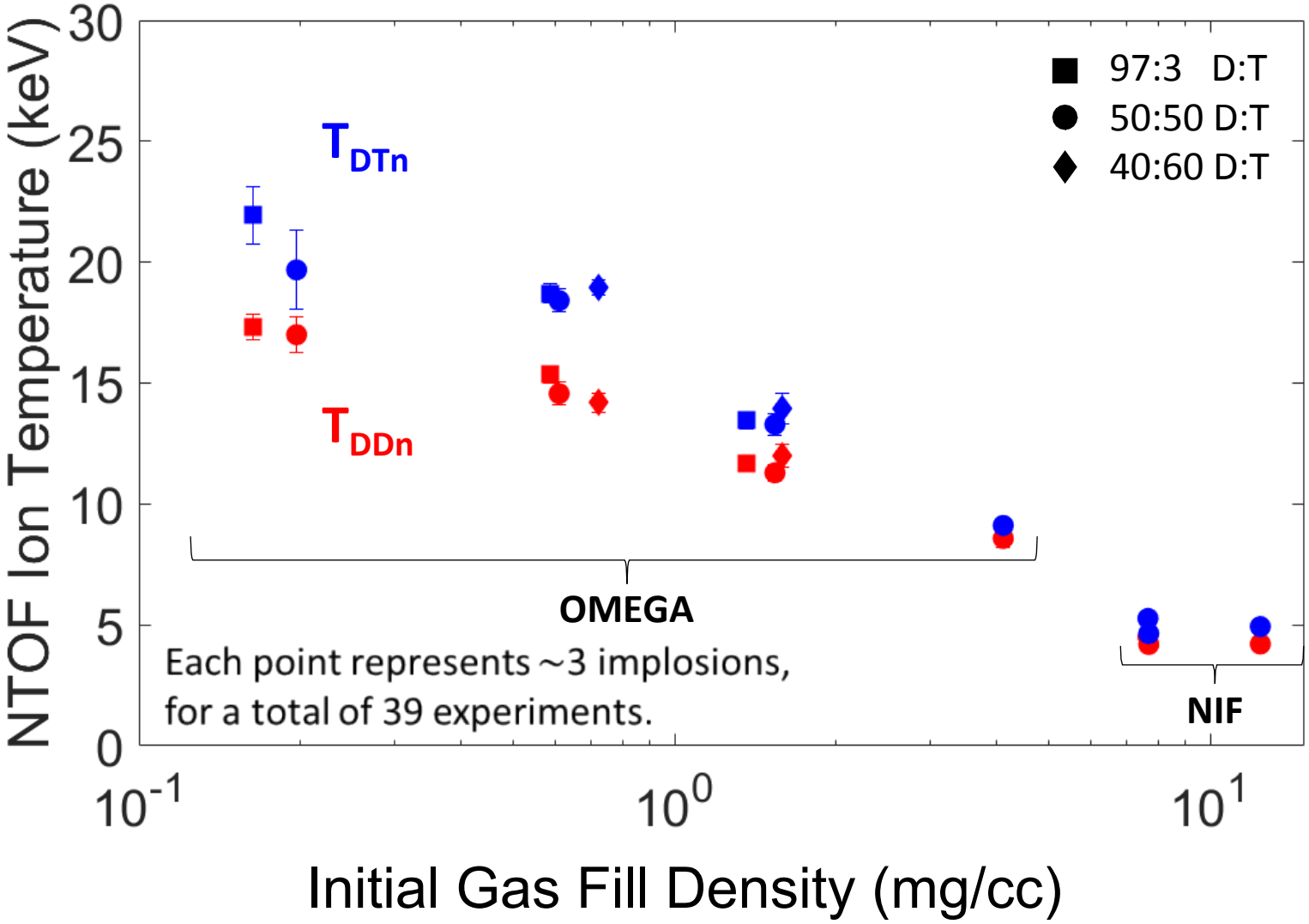

The DTn and DDn ion temperatures are inferred from the widths of the fusion product spectra as measured with NTOFs.

Outline

- Experimental Platform
- Measured T_{DDn} and T_{DTn}
- The mass dependence of ion shock coupling
- Impacts on ion viscosity
- Test of the impact of non-Maxwellian distributions
- Comparison to iFP Fokker-Planck

The apparent D and T ion temperatures can be inferred from the measured DTn and DDn temperatures

$$T_{DTn} = \frac{m_T T_T + m_D T_D}{m_T + m_D}$$

$$T_T = T_{DTn} + \frac{m_D}{m_T}(T_{DTn} - T_{DDn})$$

For the NIF data, a higher order model taking into account temperature variation is used.

Kabadi et al., Phys. Plasmas 28, 022701 (2021).

The apparent D and T ion temperatures can be inferred from the measured DTn and DDn temperatures

$$T_{DTn} = \frac{m_T T_T + m_D T_D}{m_T + m_D}$$

$$T_T = T_{DTn} + \frac{m_D}{m_T}(T_{DTn} - T_{DDn})$$

For the NIF data, a higher order model taking into account temperature variation is used.

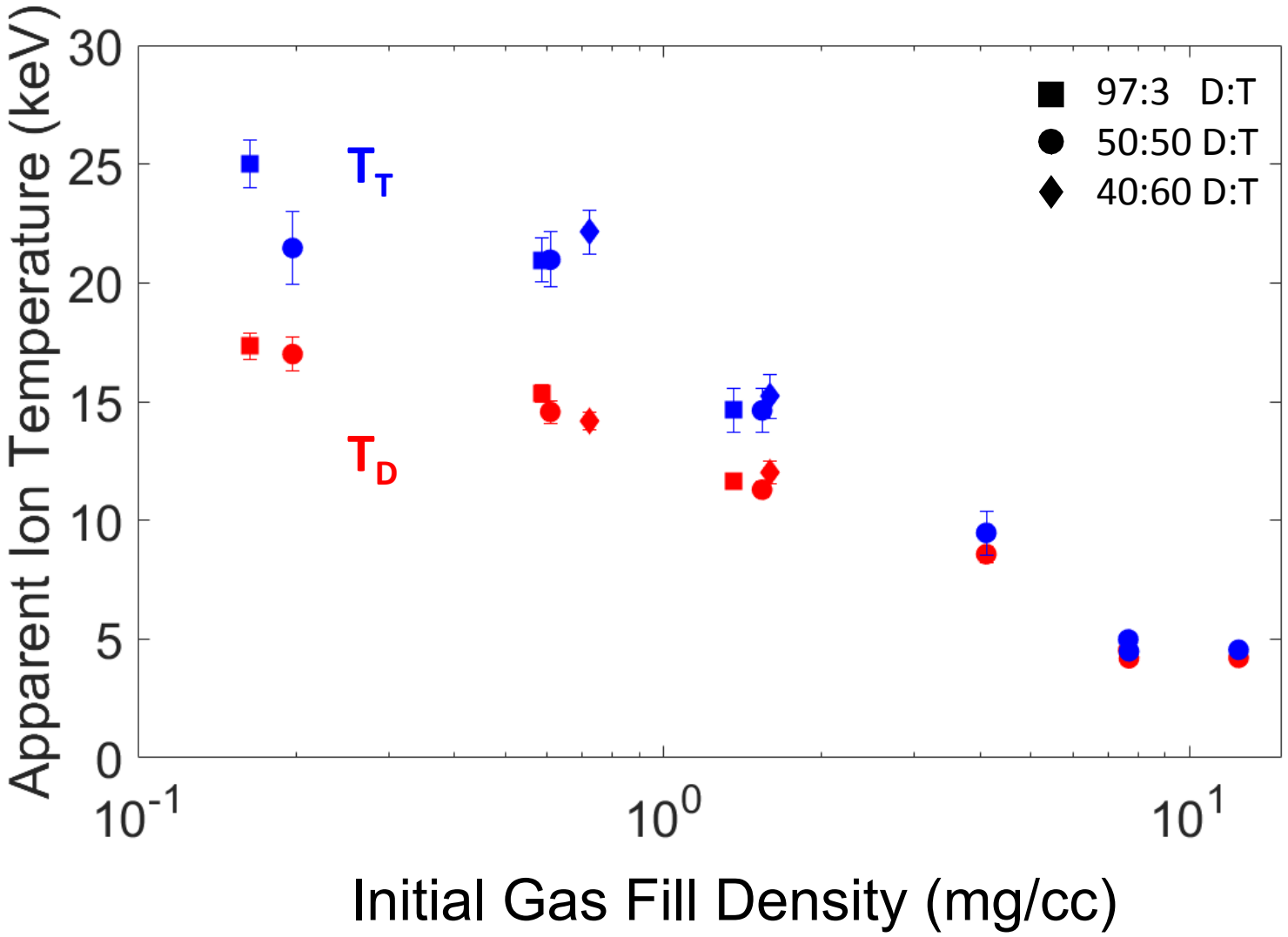

 Kabadi et al., Phys. Plasmas 28, 022701 (2021).

In these implosions the ion-ion equilibration time (τ_{ii}) can be long,

T separation due to shock coupling

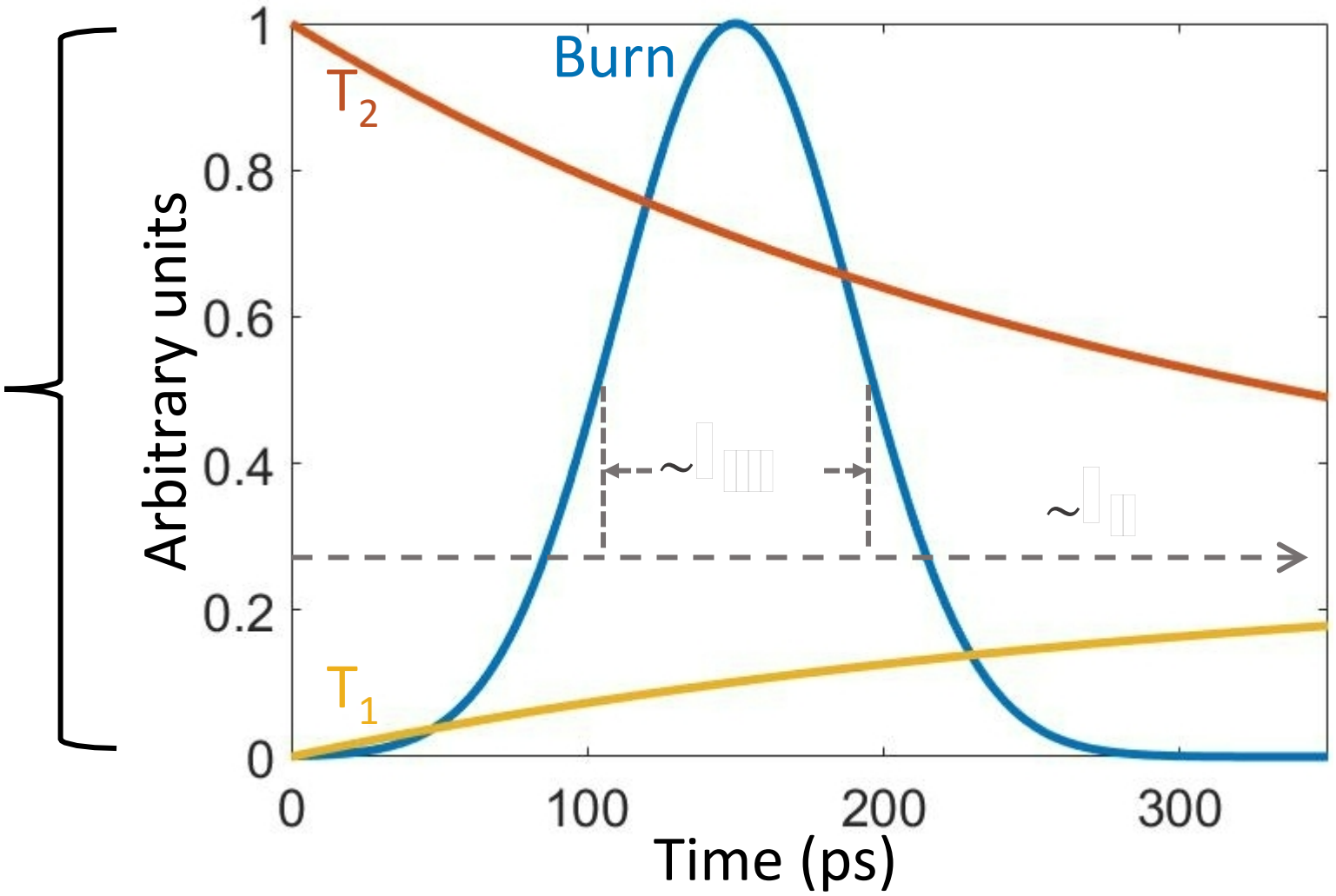

In these implosions the ion-ion equilibration time (τ_{ii}) can be long,

T separation due to shock coupling

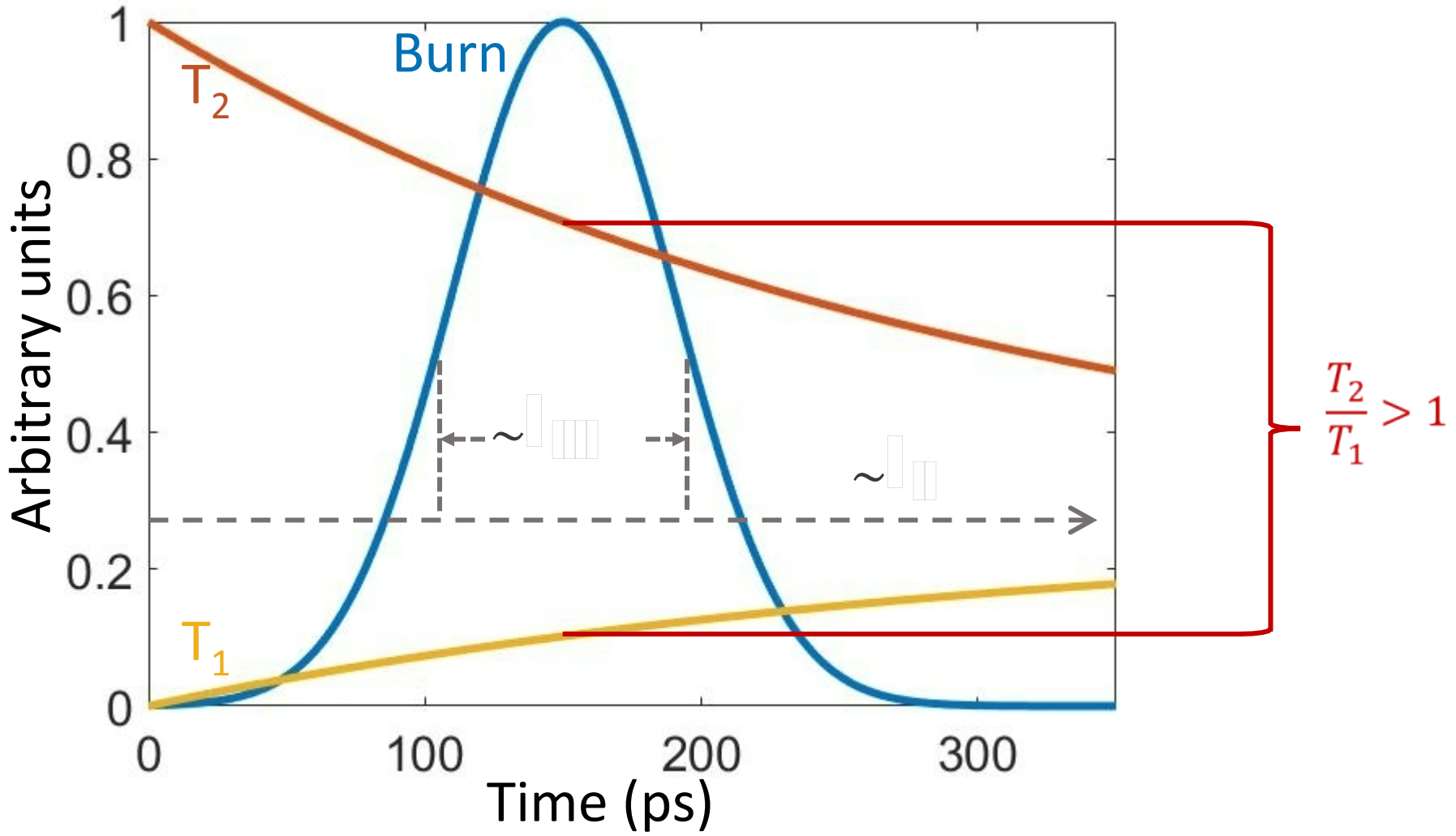

$\frac{T_2}{T_1}$ can be greater than 1 in situations where $\tau_N \equiv \frac{\tau_{burn}}{\tau_{ii}} \lesssim 1$.

Using hydrodynamic approximations, an expected equilibration trend has been derived

$$\tau_{12} = 5.6 \times 10^{18} \frac{(m_1 T_2 + m_2 T_1)^{3/2}}{Z_1^2 Z_2^2 (m_1 m_2)^{1/2} n_2 \lambda_{12}} sec. \qquad \tau_{ii} = [\frac{1}{\tau_{12}} + \frac{1}{\tau_{21}}]^{-1}$$

$$\frac{dT_1}{dt} = \frac{1}{\tau_{12}}(T_2 - T_1). \qquad \frac{dT_2}{dt} = \frac{1}{\tau_{21}}(T_1 - T_2).$$

A. S. Richardson. 2019 NRL plasma formulary. page 72,

Using hydrodynamic approximations, an expected equilibration trend has been derived

$$\tau_{12} = 5.6 \times 10^{18} \frac{(m_1 T_2 + m_2 T_1)^{3/2}}{Z_1^2 Z_2^2 (m_1 m_2)^{1/2} n_2 \lambda_{12}} sec. \qquad \tau_{ii} = [\frac{1}{\tau_{12}} + \frac{1}{\tau_{21}}]^{-1}$$

$$\frac{dT_1}{dt} = \frac{1}{\tau_{12}}(T_2 - T_1). \qquad \frac{dT_2}{dt} = \frac{1}{\tau_{21}}(T_1 - T_2).$$

$$\frac{d}{dt}\frac{T_2}{T_1} = -\frac{1}{\tau_{12}}(\frac{T_2}{T_1})^2 + (\frac{1}{\tau_{12}} - \frac{1}{\tau_{21}})\frac{T_2}{T_1} + \frac{1}{\tau_{21}}.$$

A. S. Richardson. 2019 NRL plasma formulary. page 72,

Using hydrodynamic approximations, an expected equilibration trend has been derived

$$\tau_{12} = 5.6 \times 10^{18} \frac{(m_1 T_2 + m_2 T_1)^{3/2}}{Z_1^2 Z_2^2 (m_1 m_2)^{1/2} n_2 \lambda_{12}} sec. \qquad \tau_{ii} = [\frac{1}{\tau_{12}} + \frac{1}{\tau_{21}}]^{-1}$$

$$\frac{dT_1}{dt} = \frac{1}{\tau_{12}}(T_2 - T_1). \qquad \frac{dT_2}{dt} = \frac{1}{\tau_{21}}(T_1 - T_2).$$

$$\frac{d}{dt}\frac{T_2}{T_1} = -\frac{1}{\tau_{12}}(\frac{T_2}{T_1})^2 + (\frac{1}{\tau_{12}} - \frac{1}{\tau_{21}})\frac{T_2}{T_1} + \frac{1}{\tau_{21}}.$$

$$\frac{T_2}{T_1} = \tanh\left(\frac{1}{2}\frac{t}{\tau_{ii}} + \operatorname{atanh}(R_0)\right), \qquad R_0 = \left.\frac{T_2}{T_1}\right|_{t=0}$$

For each specific implosion we will average and take $\frac{t}{\tau_{ii}} \approx \tau_N = \frac{\tau_{burn}}{\tau_{ii}}$

Rygg et al. Phys. Rev. E 80, 026403 (2009)

A. S. Richardson. 2019 NRL plasma formulary. page 72,

An initial temperature ratio of 1.5 is inferred from the data confirming long standing theory that shocks couple proportional to mass in multi-ion plasmas

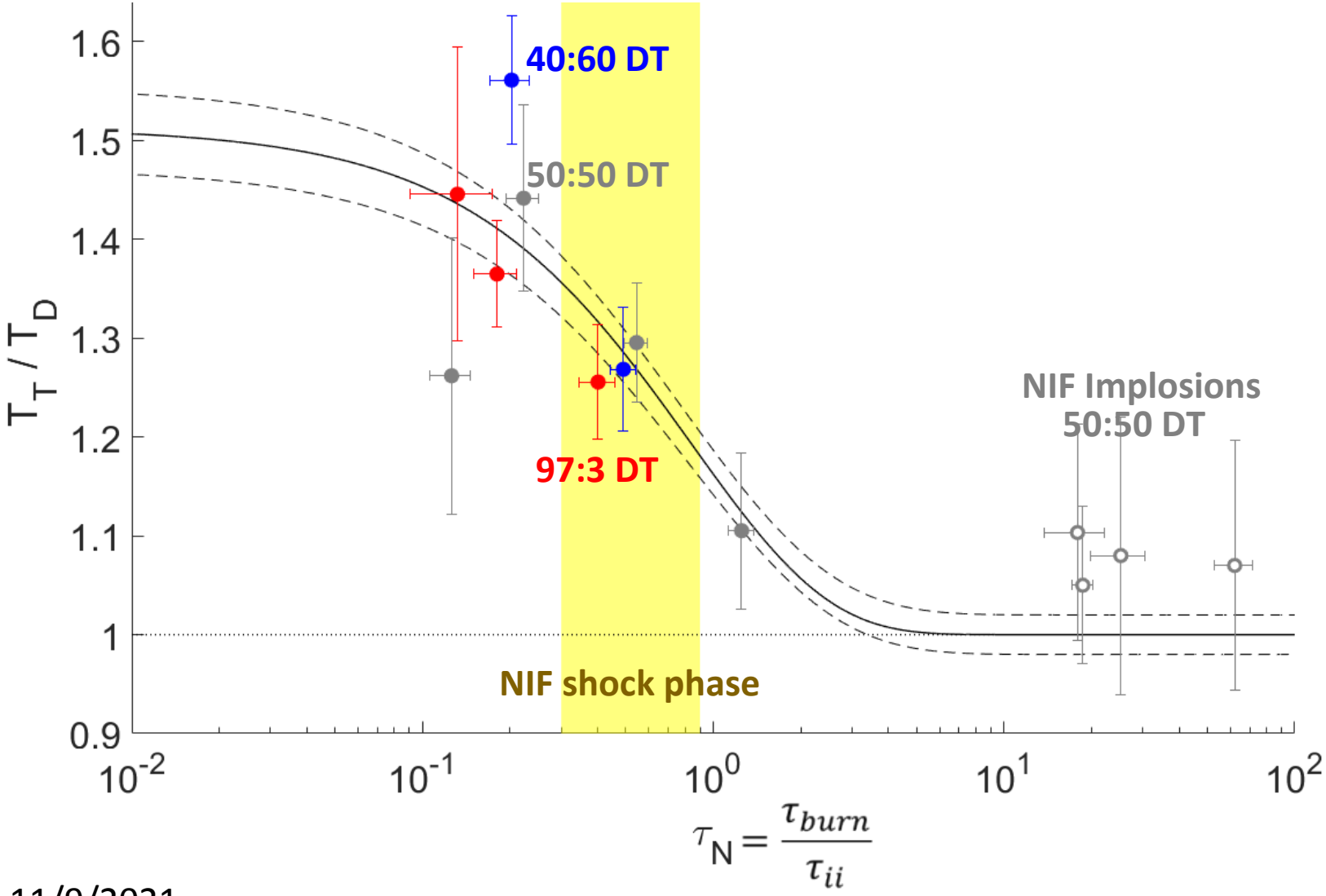

An initial temperature ratio of 1.5 is inferred from the data confirming long standing theory that shocks couple proportional to mass in multi-ion plasmas

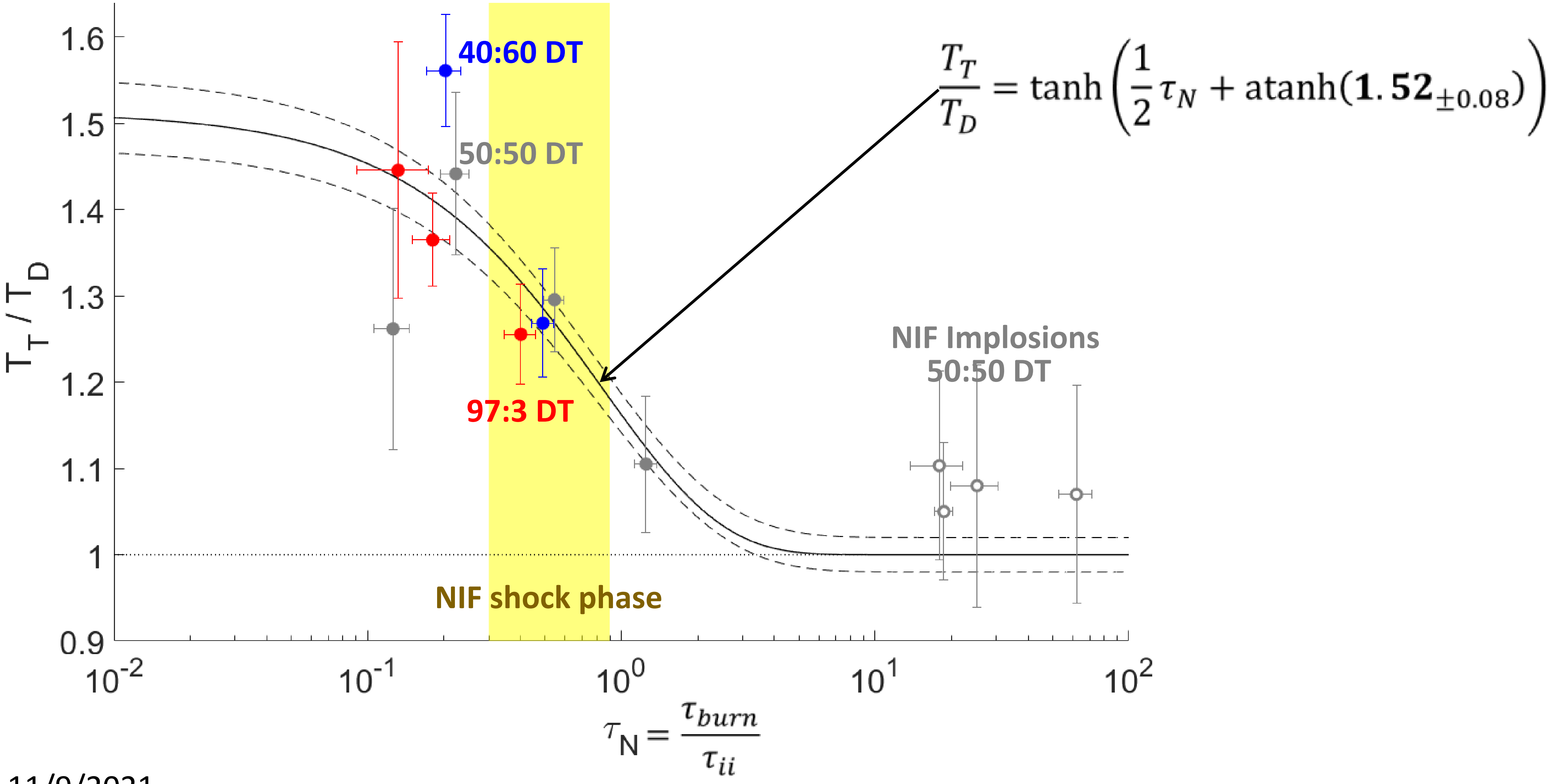

An initial temperature ratio of 1.5 is inferred from the data confirming long standing theory that shocks couple proportional to mass in multi-ion plasmas

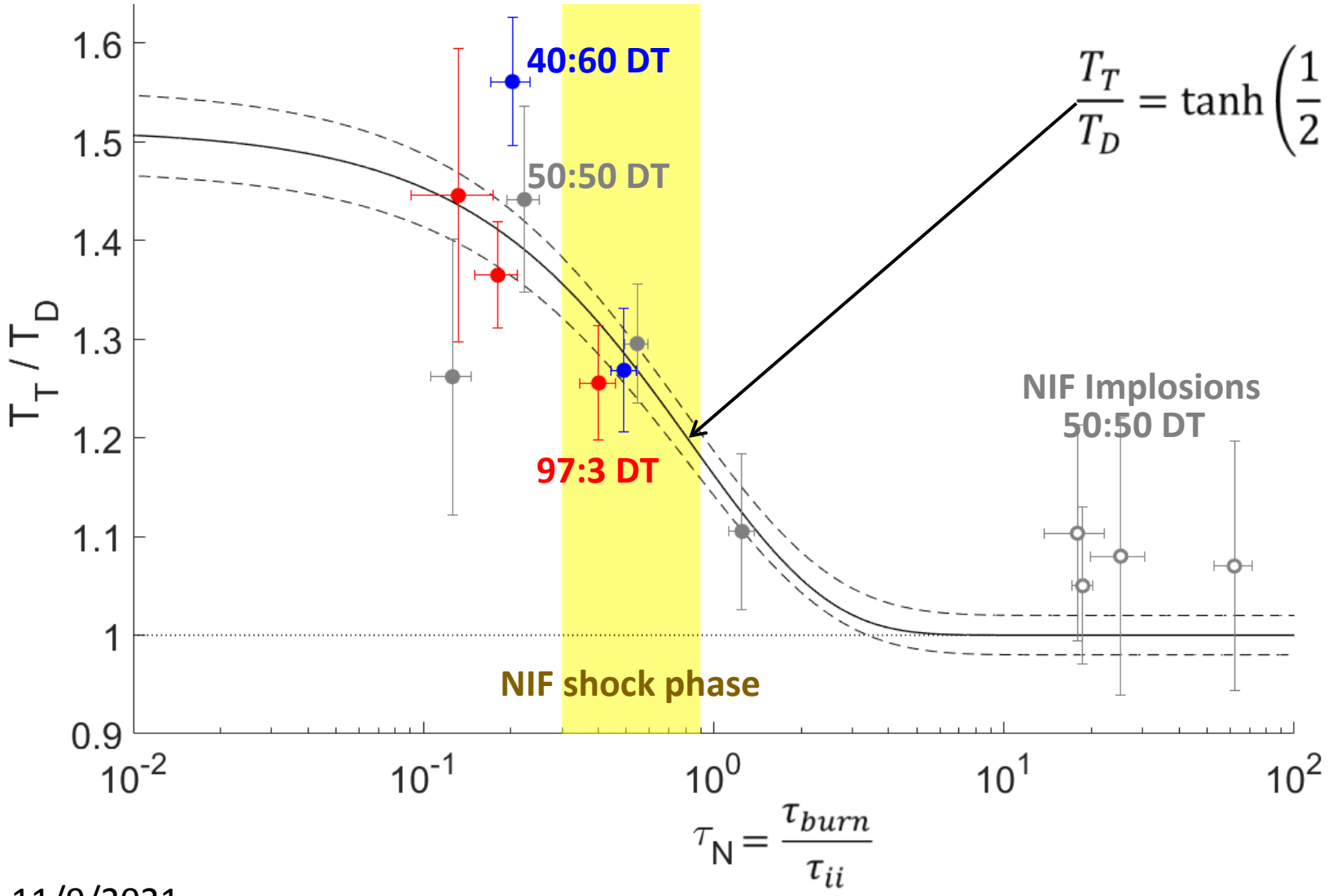

$$\frac{T_T}{T_D} = \tanh\left(\frac{1}{2}\tau_N + \operatorname{atanh}(\mathbf{1.52}_{\pm 0.08})\right)$$

$$T_i \propto m_i.$$

Kabadi et al., Phys. Rev. E **104**, L013201 (2021)

An initial temperature ratio of 1.5 is inferred from the data confirming long standing theory that shocks couple proportional to mass in multi-ion plasmas

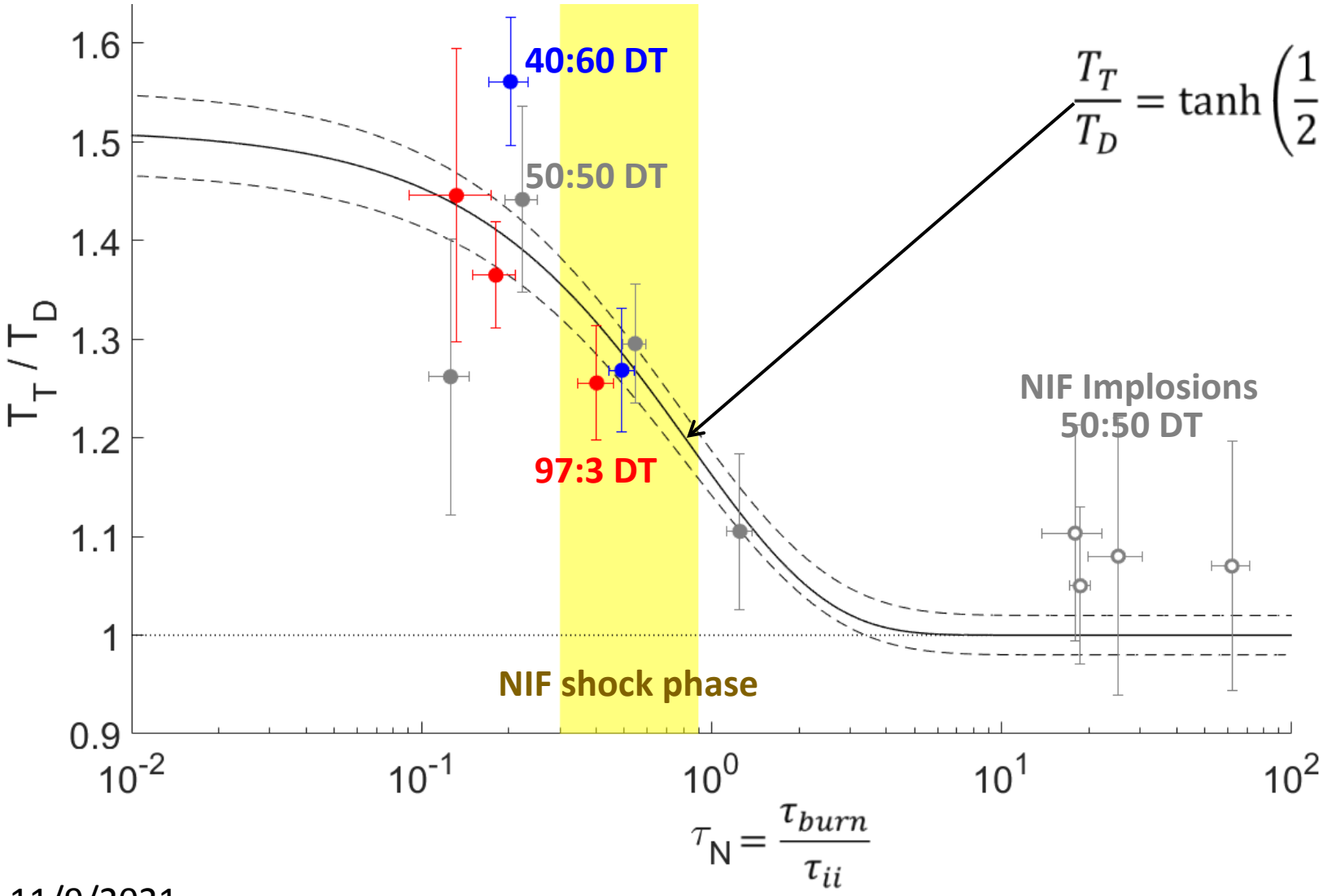

This is the first lab-based measurement of this mass dependence corroborating recent astrophysical findings published in Nature Astronomy*

Miceli et. al. *Nature Astronomy* 3, no. 3 (March 2019): 236–41.

Outline

- Experimental Platform
- Measured T_{DDn} and T_{DTn}
- The mass dependence of ion shock coupling
- Impacts on ion viscosity
- Test of the impact of non-Maxwellian distributions
- Comparison to iFP Fokker-Planck

With multiple ion temperatures, calculation of the ion viscosity with average ion properties is incorrect

$$\mu = 1.01\text{E-}15 \frac{T_i^{5/2} A^{1/2}}{Z^4 \ln\Lambda} \text{ g cm}^{-1} \text{ s}^{-1}$$

Incorrectly modeling the ion viscosity during the shock convergence phase will result in wrong initial conditions for the subsequent compression.

S. I. Braginskii, Rev. Plas. Phys. 205-311 (2006).

With multiple ion temperatures, calculation of the ion viscosity with average ion properties is incorrect

$$\mu = 1.01\text{E-}15 \frac{T_i^{5/2} A^{1/2}}{Z^4 \ln\Lambda} \text{ g cm}^{-1} \text{ s}^{-1}$$

Fill density mg/cc	τ_N	T ratio	T_{DTn} keV	μ average ion g cm^{-1} s^{-1}	μ multi ion g cm^{-1} s^{-1}	% error
4	1.1	1.1	8	3.1E-14	3.7E-14	-16%

Incorrectly modeling the ion viscosity during the shock convergence phase will result in wrong initial conditions for the subsequent compression.

S. I. Braginskii, Rev. Plas. Phys. 205-311 (2006).

With multiple ion temperatures, calculation of the ion viscosity with average ion properties is incorrect

$$\mu = 1.01\text{E-}15 \frac{T_i^{5/2} A^{1/2}}{Z^4 \ln\Lambda} \text{ g cm}^{-1} \text{ s}^{-1}$$

Fill density mg/cc	τ_N	T ratio	T_{DTn} keV	μ average ion g cm^{-1} s^{-1}	μ multi ion g cm^{-1} s^{-1}	% error
4	1.1	1.1	8	3.1E-14	3.7E-14	-16%
0.2	0.1	1.45	21	1.6E-13	2.8E-13	-42%

Incorrectly modeling the ion viscosity during the shock convergence phase will result in wrong initial conditions for the subsequent compression.

S. I. Braginskii, Rev. Plas. Phys. 205-311 (2006).

Outline

- Experimental Platform
- Measured T_{DDn} and T_{DTn}
- The mass dependence of ion shock coupling
- Impacts on ion viscosity
- Test of the impact of non-Maxwellian distributions
- Comparison to iFP Fokker-Planck

Many of these implosions are in a regime where non-Maxwellian distribution functions are likely

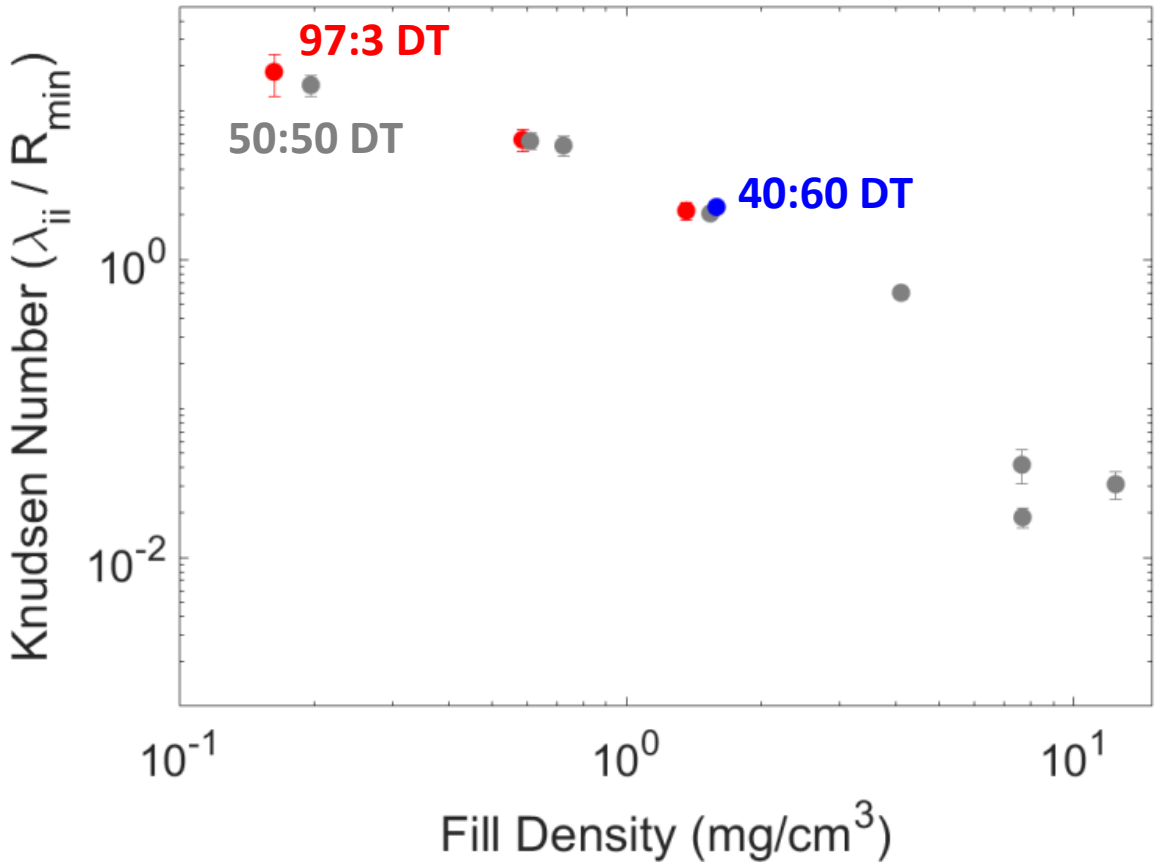

This data set spans nearly 3 orders of magnitude in collisionality

M.J. Rosenberg et al., Phys. Plasmas 22, 062702 (2015).

Many of these implosions are in a regime where non-Maxwellian distribution functions are likely

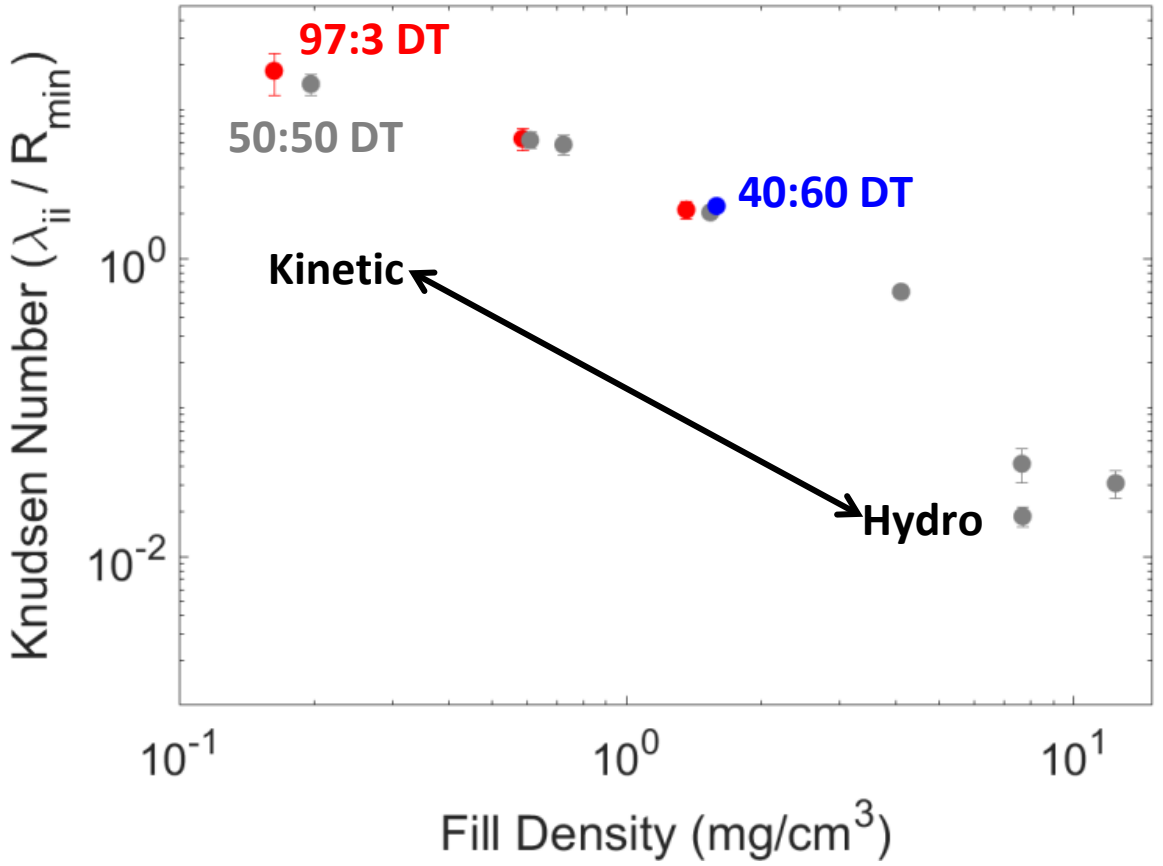

This data set spans nearly 3 orders of magnitude in collisionality

M.J. Rosenberg et al., Phys. Plasmas 22, 062702 (2015).

To test the impact of non-Maxwellian distribution functions on the inferred temperature ratio, a series of Monte-Carlo calculations were performed

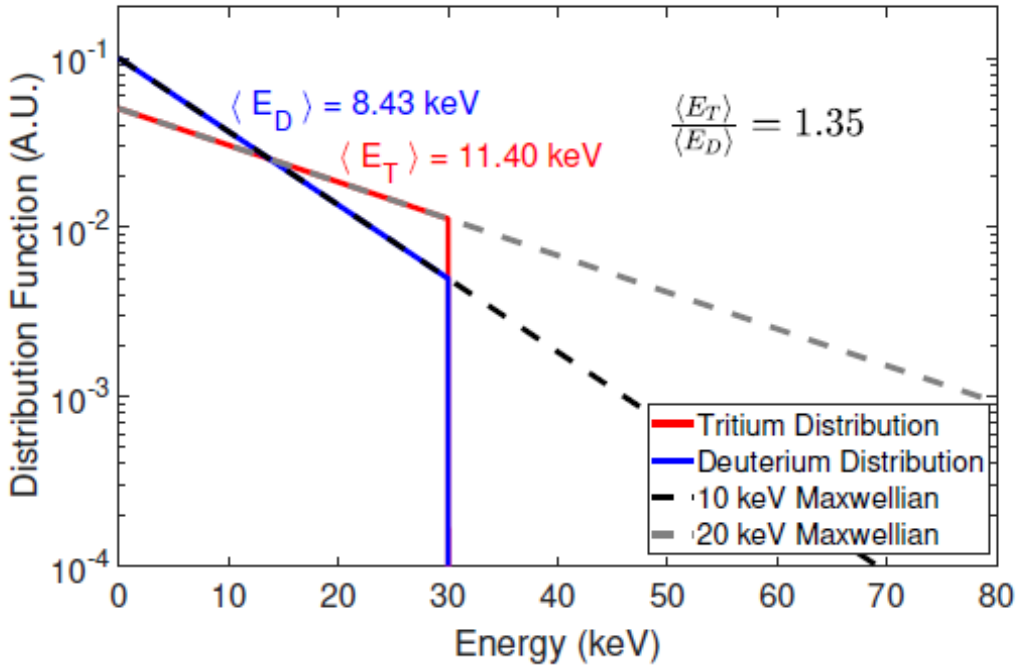

For a Maxwellian, the mean energy ratio and the temperature ratio are identical. For non-Maxwellians we need to test if this holds.

To test the impact of non-Maxwellian distribution functions on the inferred temperature ratio, a series of Monte-Carlo calculations were performed

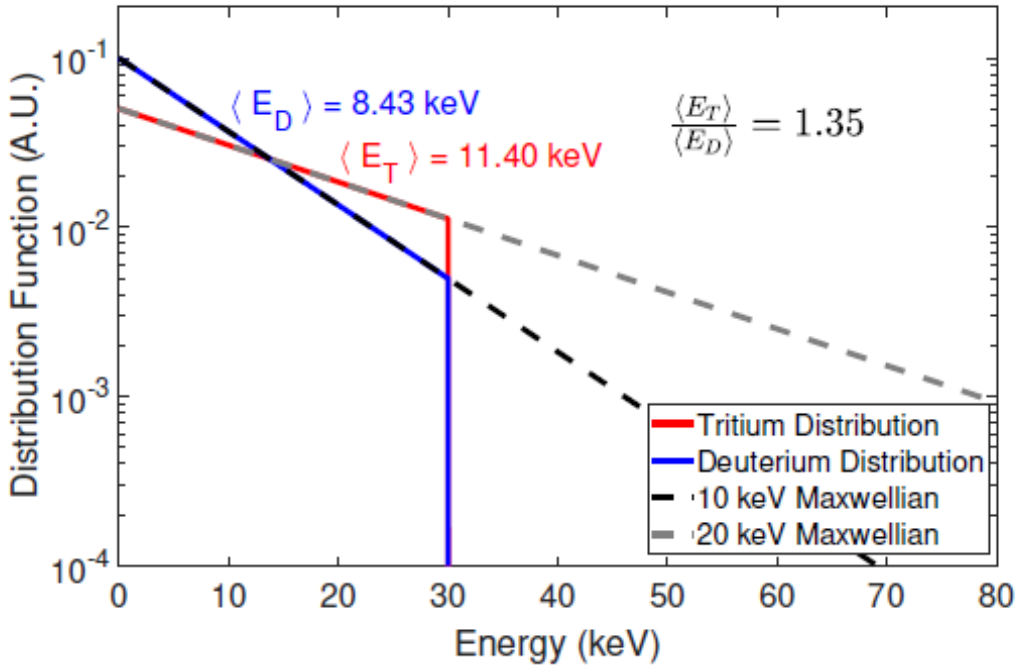

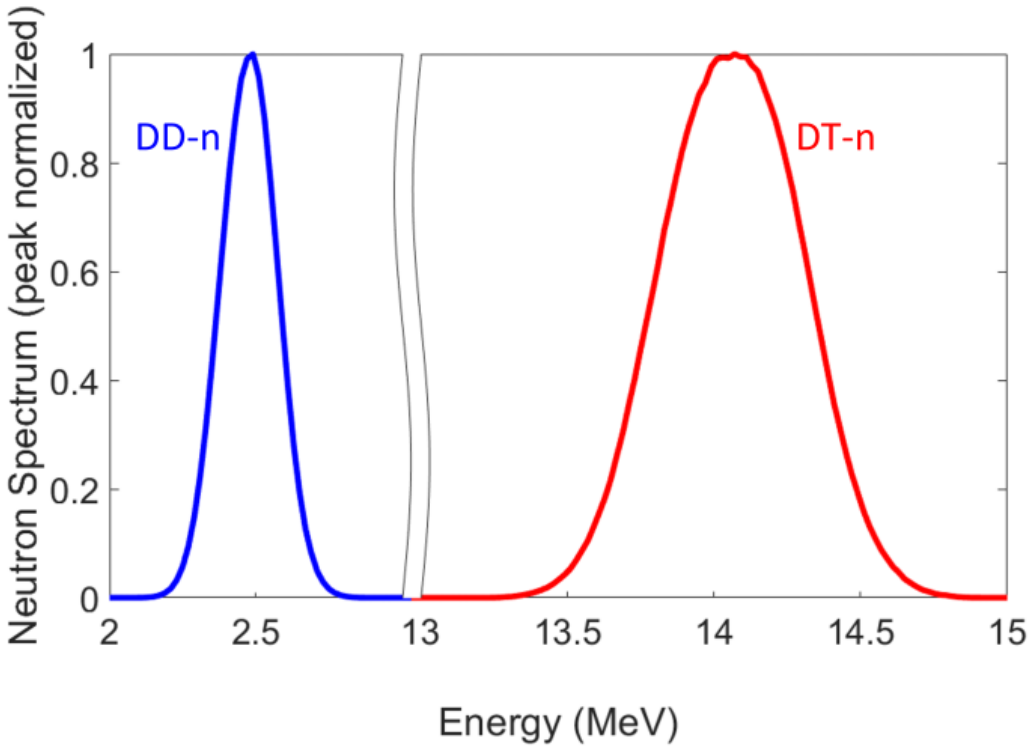

For a Maxwellian, the mean energy ratio and the temperature ratio are identical. For non-Maxwellians we need to test if this holds.

To test the impact of non-Maxwellian distribution functions on the inferred temperature ratio, a series of Monte-Carlo calculations were performed

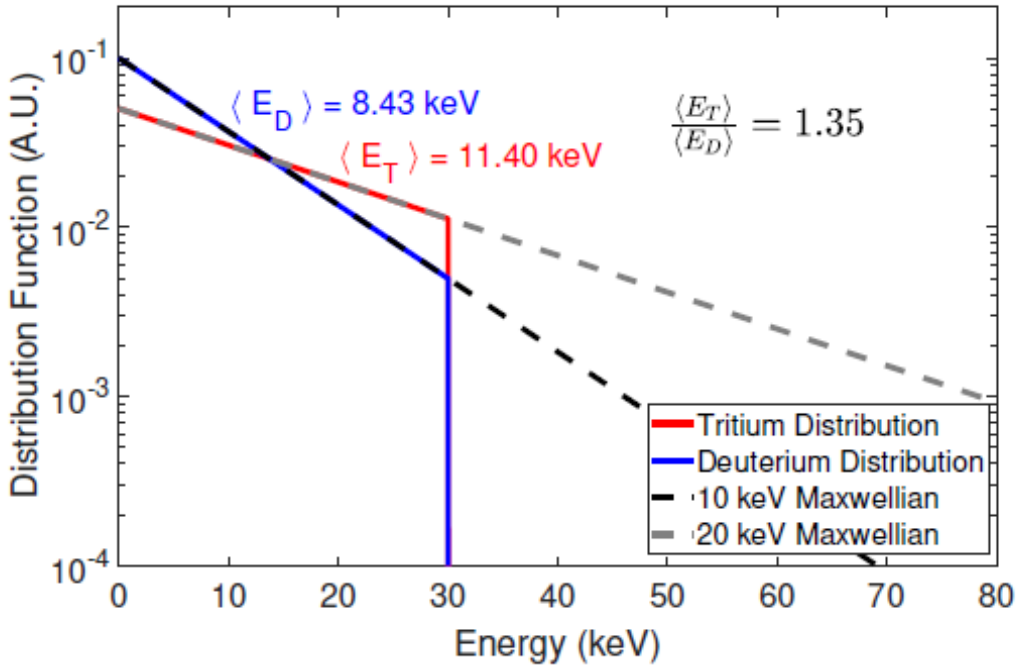

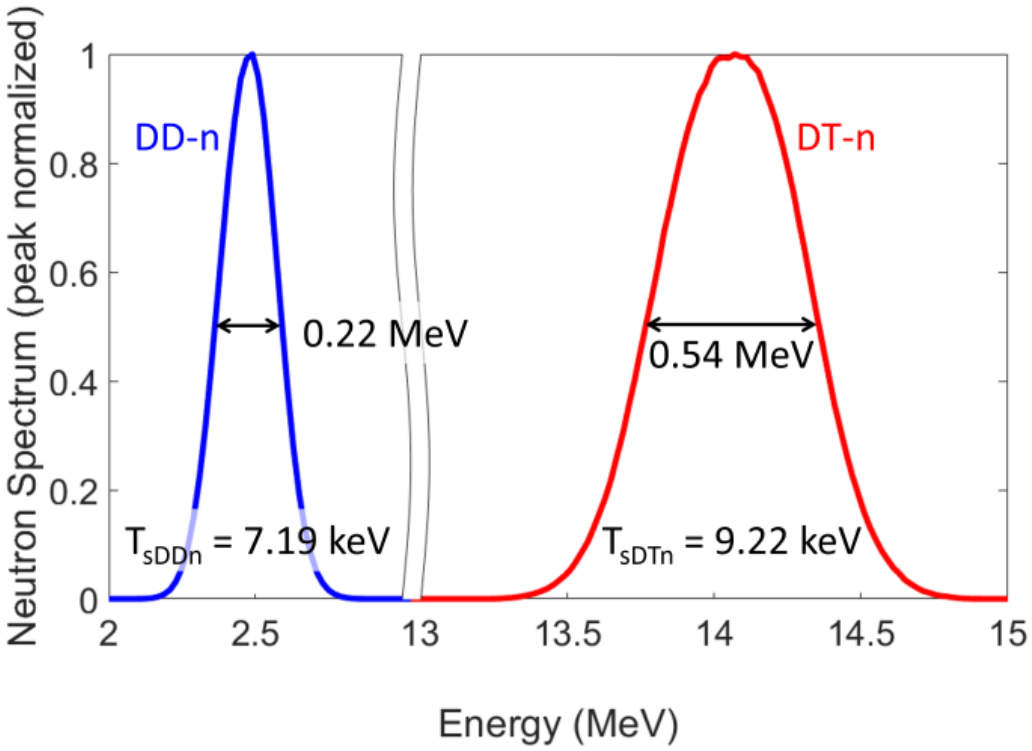

For a Maxwellian, the mean energy ratio and the temperature ratio are identical. For non-Maxwellians we need to test if this holds.

To test the impact of non-Maxwellian distribution functions on the inferred temperature ratio, a series of Monte-Carlo calculations were performed

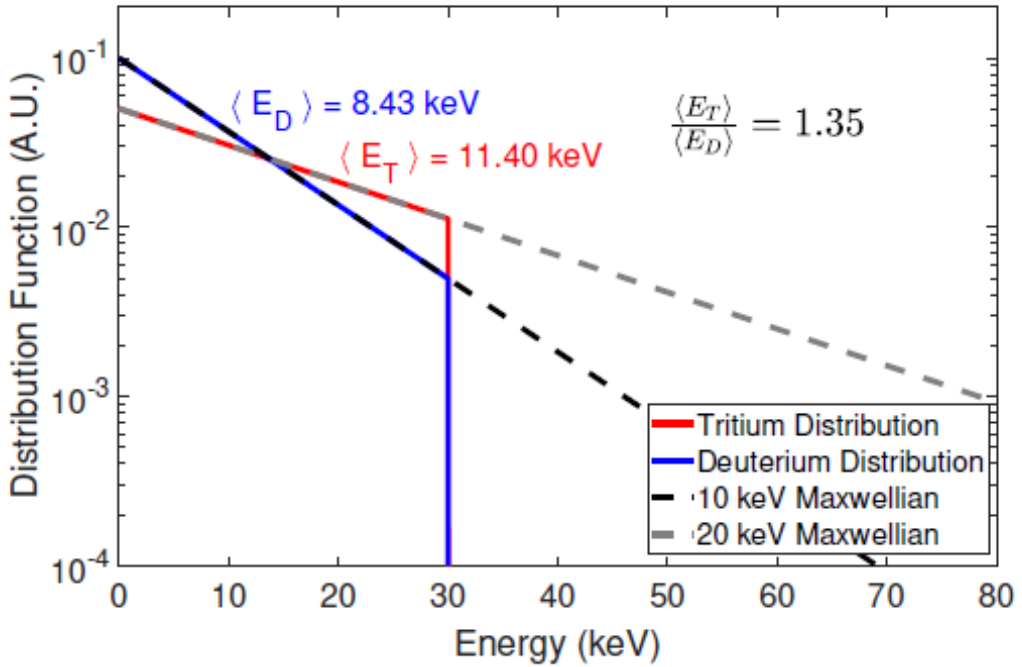

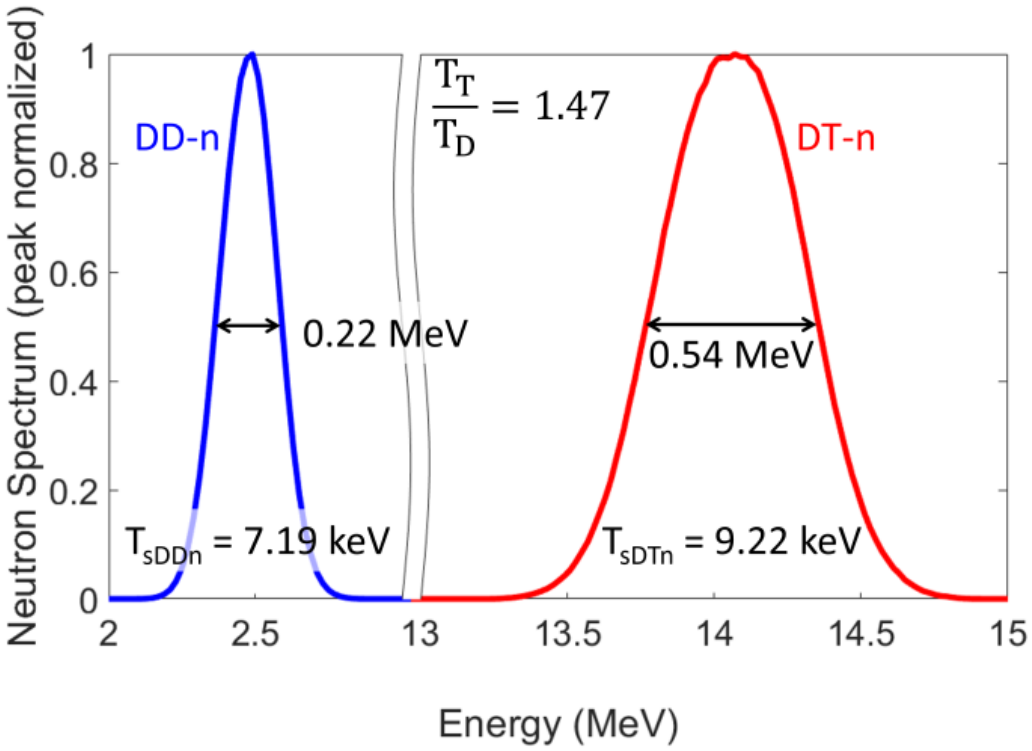

For a Maxwellian, the mean energy ratio and the temperature ratio are identical. For non-Maxwellians we need to test if this holds.

The error incurred by assuming the apparent temperature ratio is the mean energy ratio is less than ~20% for all the distributions tested

Examples of the tested distributions

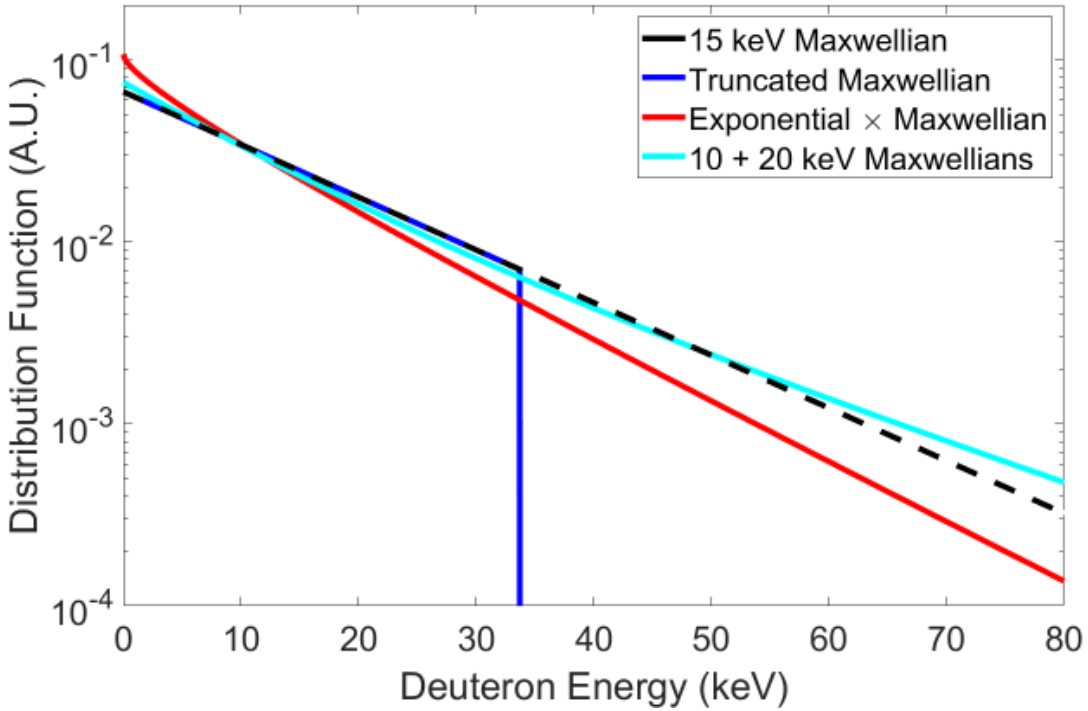

The error incurred by assuming the apparent temperature ratio is the mean energy ratio is less than ~20% for all the distributions tested

Examples of the tested distributions

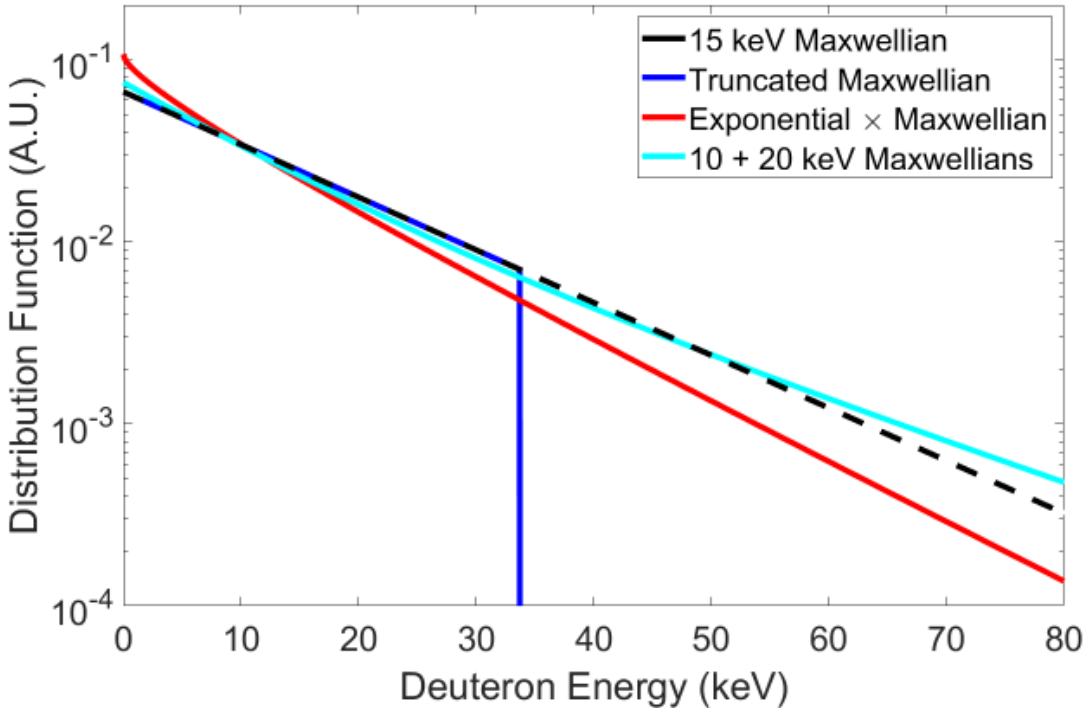

Error in assuming the apparent ion temperature ratio is the mean energy ratio

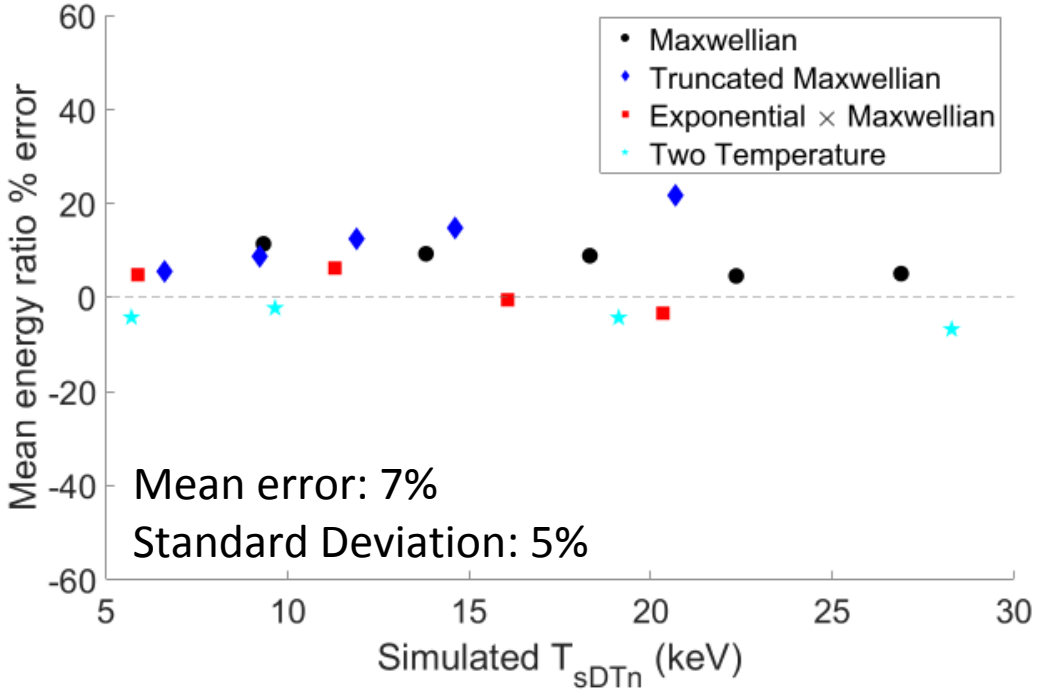

There is large error on the absolute temperature, but when taking a ratio of apparent D and T ion temperatures the error is reduced.

Outline

- Experimental Platform
- Measured T_{DDn} and T_{DTn}
- The mass dependence of ion shock coupling
- Impacts on ion viscosity
- Test of the impact of non-Maxwellian distributions
- Comparison to iFP Fokker-Planck

The implicit Fokker-Planck (iFP) code does an excellent job reproducing the measured DTn and DDn yields for fill densities >0.5 mg/cc

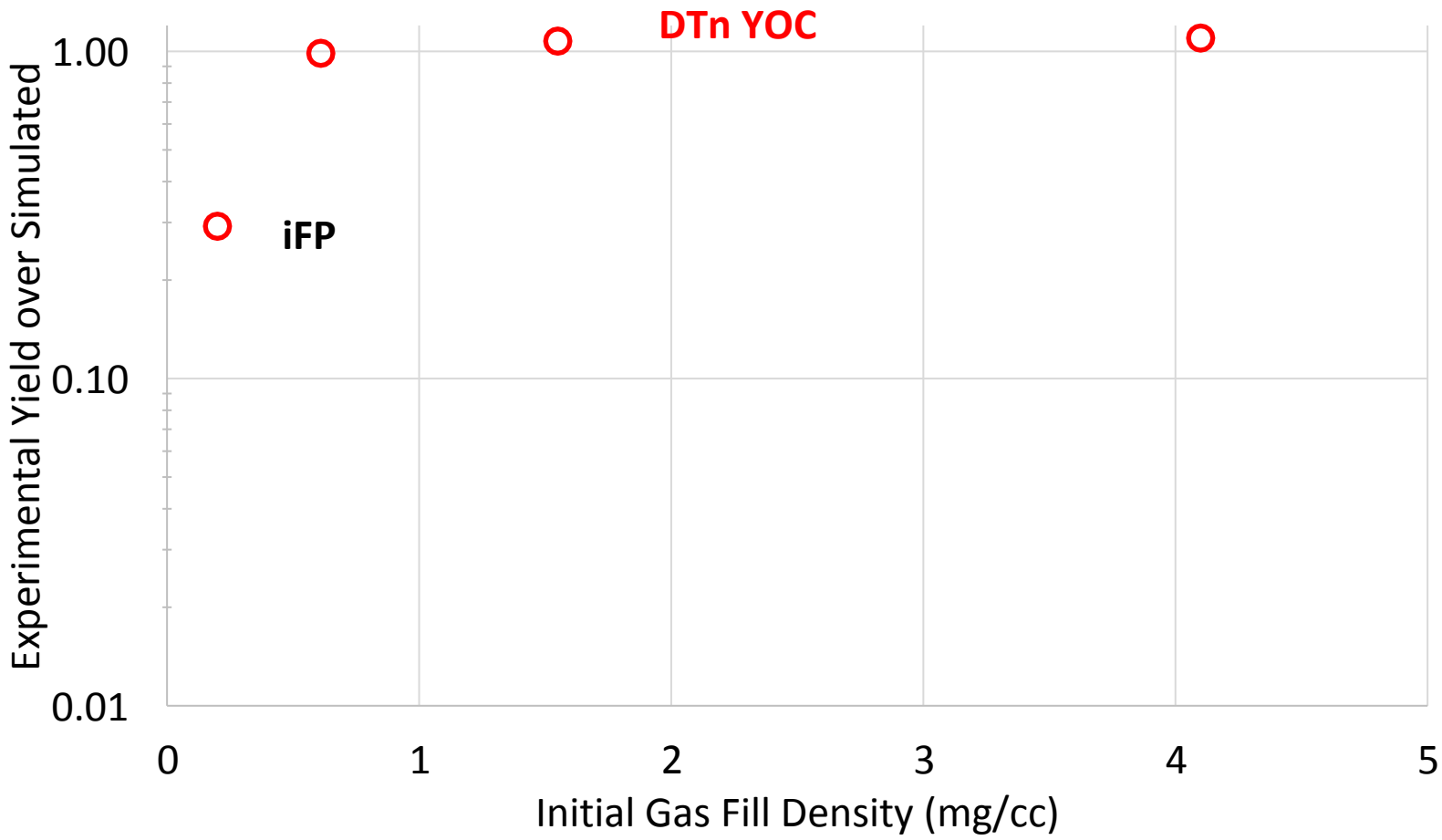

iFP is a 1D2V VFP code using nonlinear implicit time-stepping and an adaptative phase-space grid

W. T. Taitano, et al., Phys. of Plasm. 25(5) 056310 (2018).

The implicit Fokker-Planck (iFP) code does an excellent job reproducing the measured DTn and DDn yields for fill densities >0.5 mg/cc

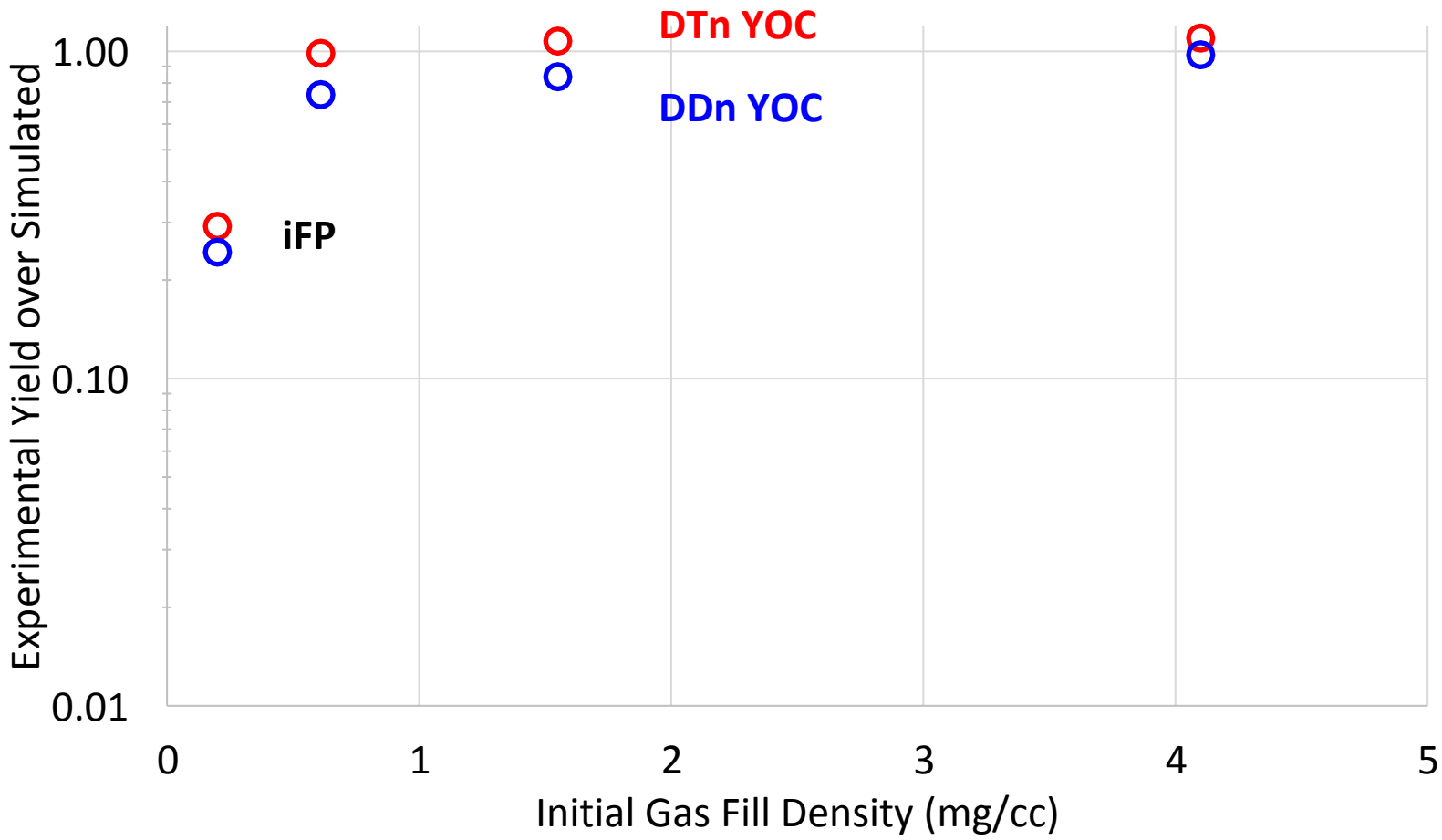

iFP is a 1D2V VFP code using nonlinear implicit time-stepping and an adaptative phase-space grid

W. T. Taitano, et al., Phys. of Plasm. 25(5) 056310 (2018).

iFP does an excellent job reproducing the measured DTn and DDn yields for fill densities >0.5 mg/cc

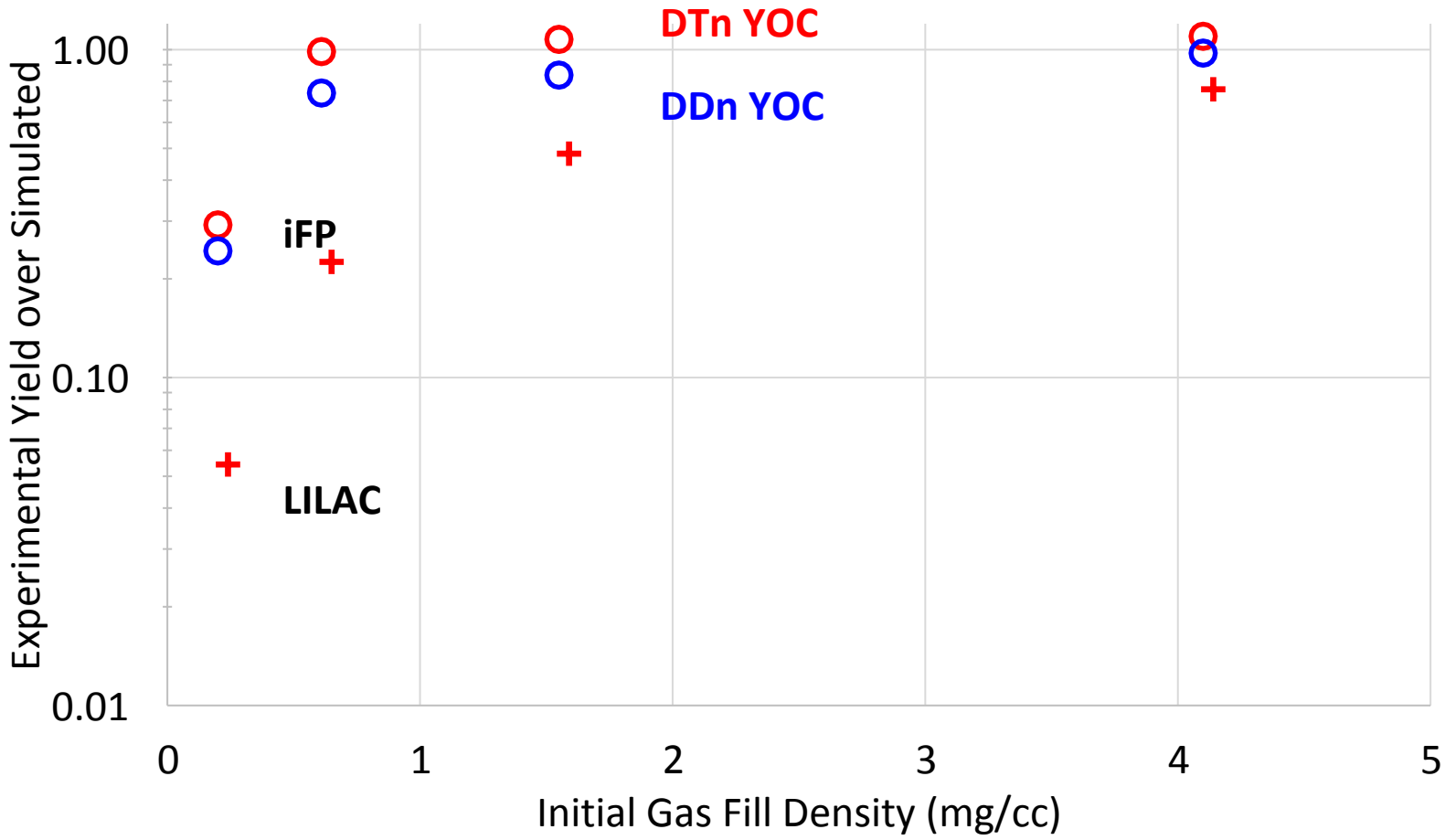

iFP does not include a laser package, so the simulations are driven using boundary conditions from LILAC hydrodynamic simulations. LILAC overpredicts the yields at all fill densities tested.

W. T. Taitano, et al., Phys. of Plasm. 25(5) 056310 (2018).

iFP does an excellent job reproducing the measured DTn and DDn yields for fill densities >0.5 mg/cc

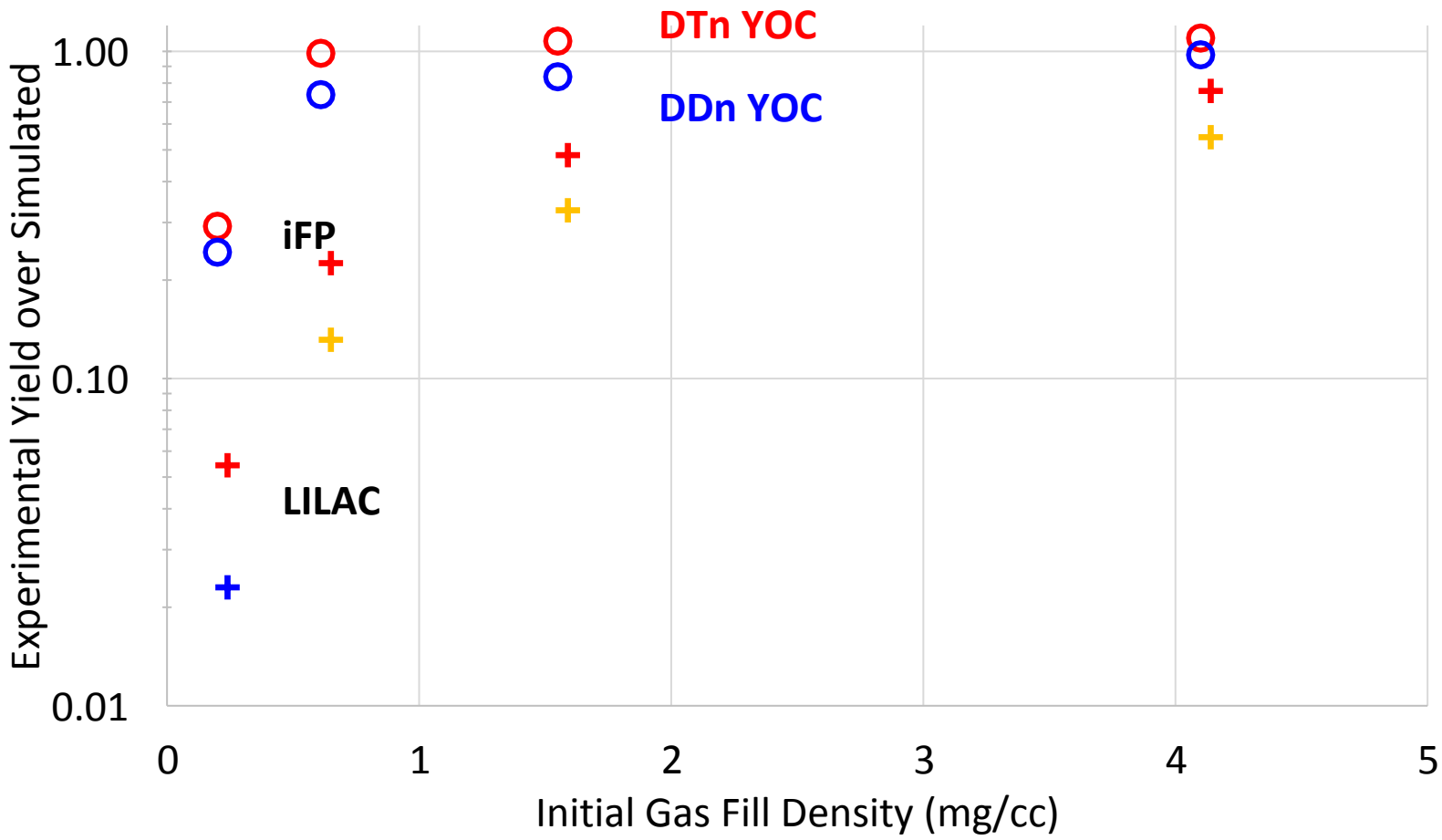

iFP does not include a laser package, so the simulations are driven using boundary conditions from LILAC hydrodynamic simulations. LILAC overpredicts the yields at all fill densities tested.

W. T. Taitano, et al., Phys. of Plasm. 25(5) 056310 (2018).

iFP does an excellent job reproducing the measured DTn and DDn yields for fill densities >0.5 mg/cc

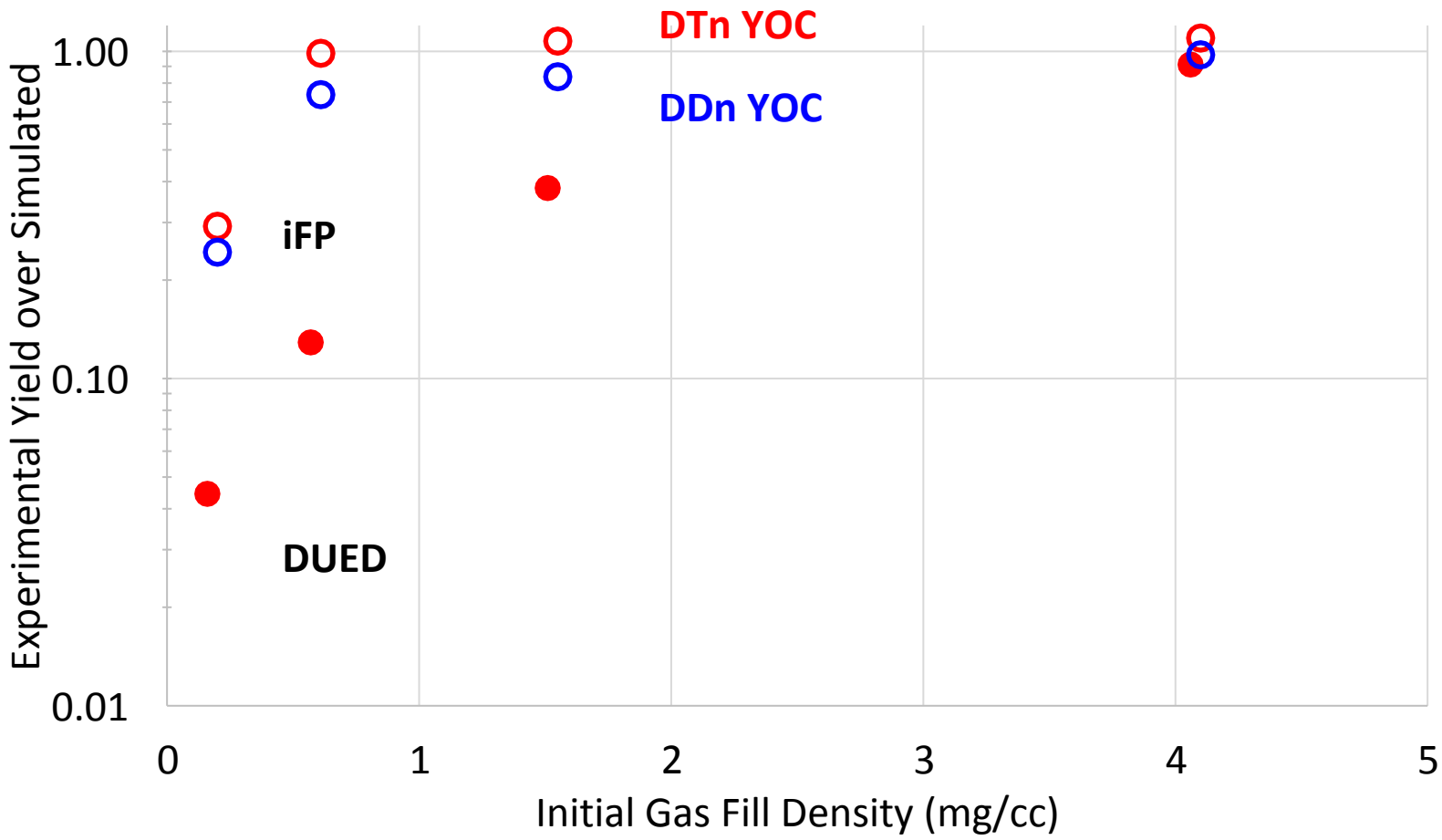

The hydro code DUED, which includes real ion viscosity, nearly reproduces the measured yields for ~4 mg/cc fill density, but fails at densities < 2 mg/cc

W. T. Taitano, et al., Phys. of Plasm. 25(5) 056310 (2018).

iFP does an excellent job reproducing the measured DTn and DDn yields for fill densities >0.5 mg/cc

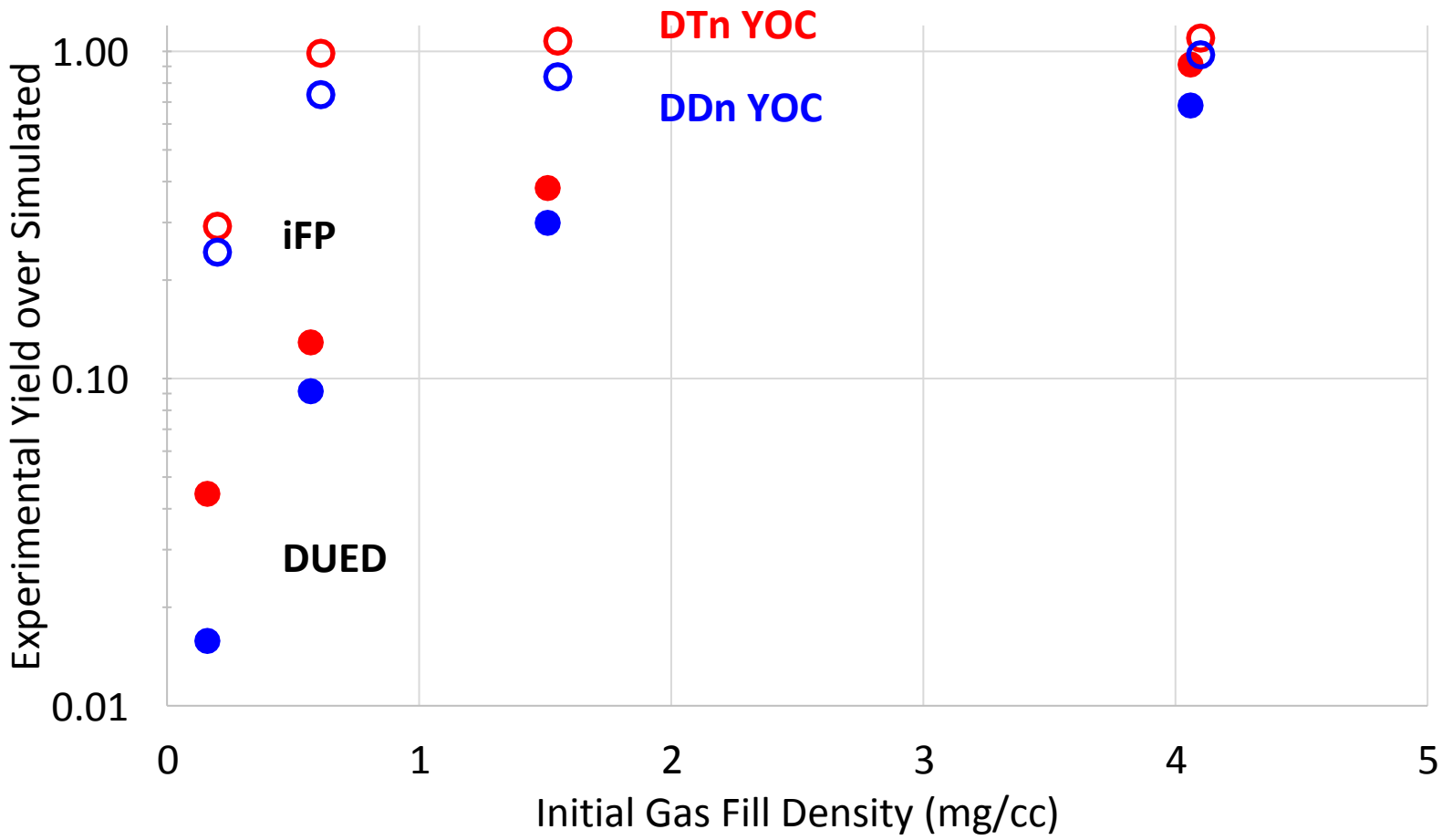

The hydro code DUED, which includes real ion viscosity, nearly reproduces the measured yields for ~4 mg/cc fill density, but fails at densities < 2 mg/cc

W. T. Taitano, et al., Phys. of Plasm. 25(5) 056310 (2018).

iFP simulation of the 4 mg/cc fill density implosion shows slight kinetic features in the D and T distribution functions

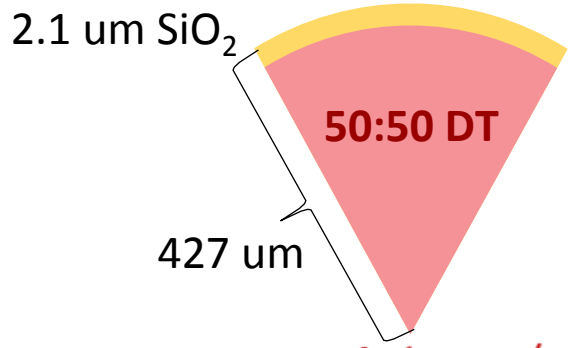

$\rho_0 = 4.1\ mg/cc$

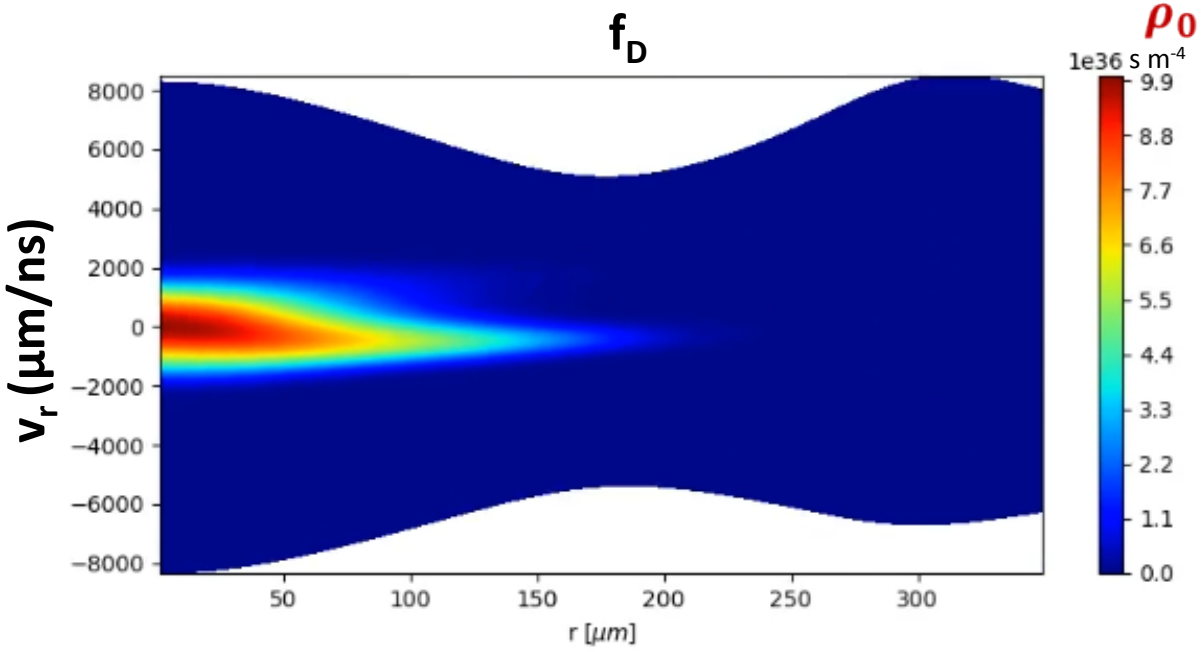

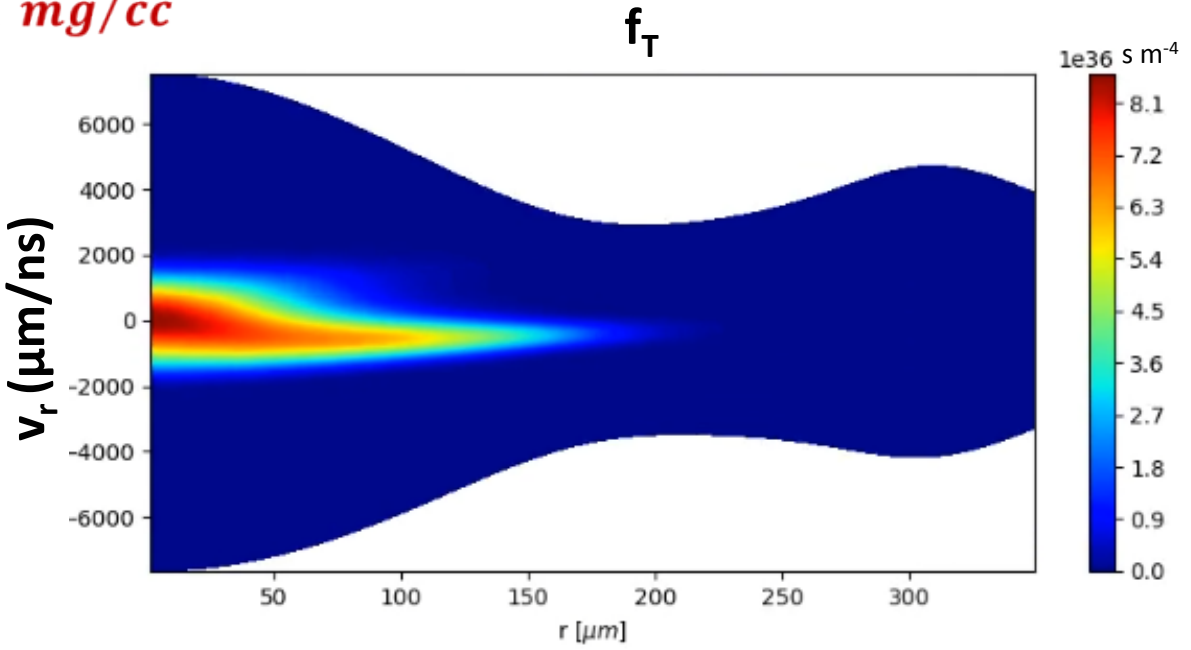

These are the bang time distribution functions integrated over the orthogonal velocity coordinate.

iFP simulation of the 4 mg/cc fill density implosion shows slight kinetic features in the D and T distribution functions

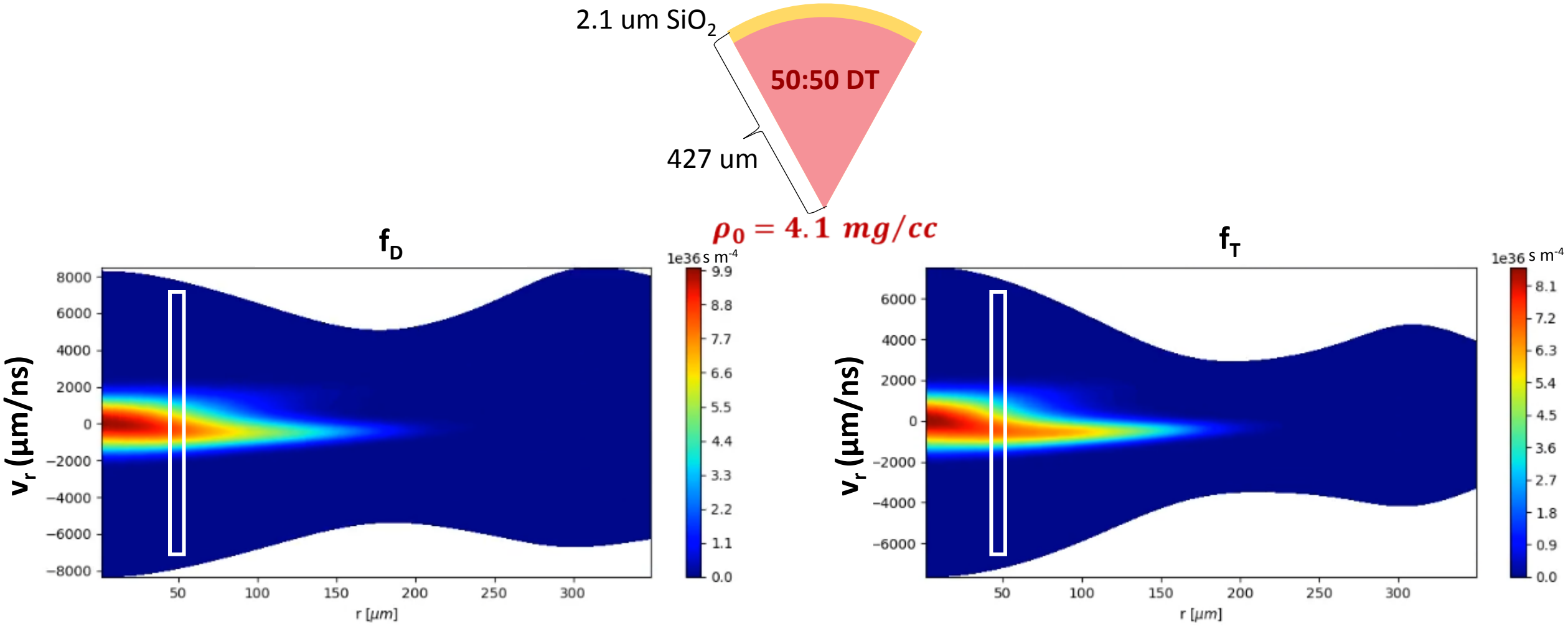

These are the bang time distribution functions integrated over the orthogonal velocity coordinate.

iFP simulation of the 4 mg/cc fill density implosion shows slight kinetic features in the D and T distribution functions

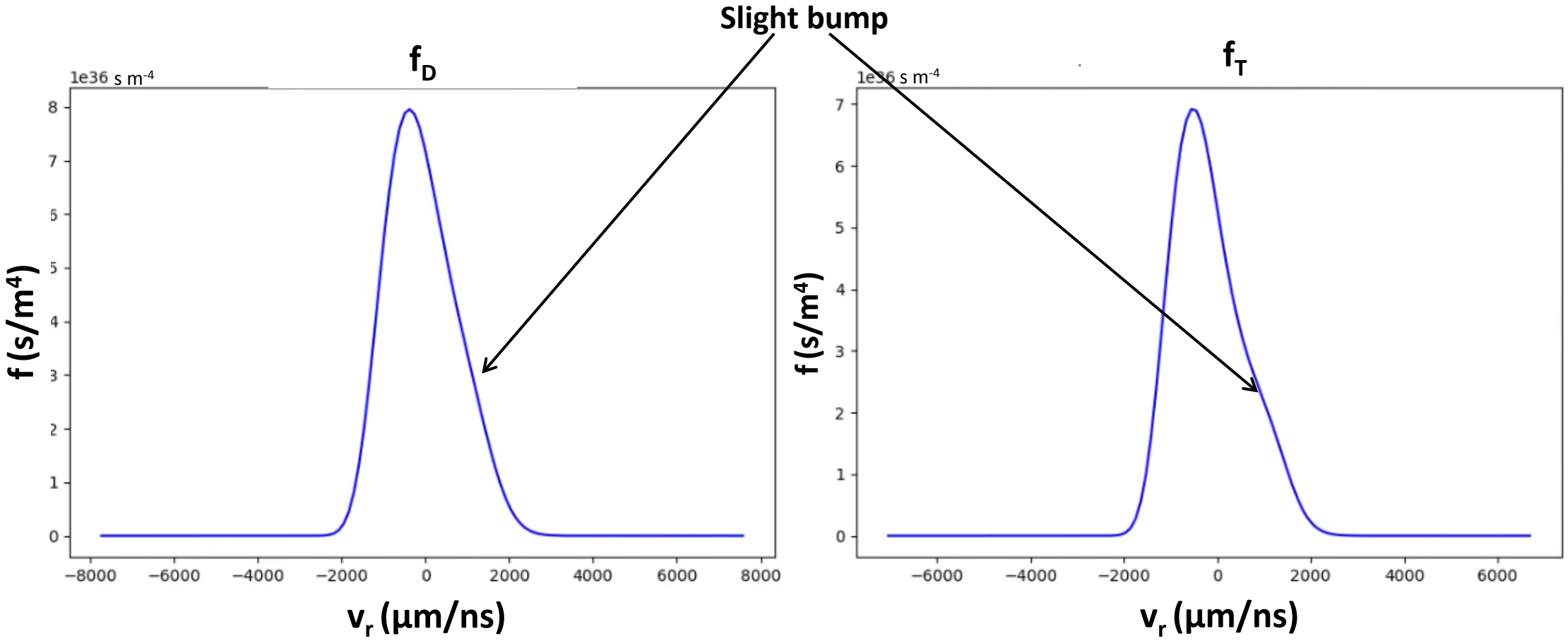

For clarity line-outs at the radius of maximal DTn emission are shown

iFP simulation of the 0.2 mg/cc fill density implosion shows two distinct ion populations

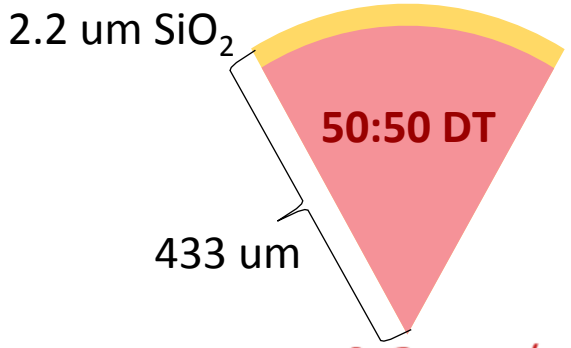

$\rho_0 = 0.2\ mg/cc$

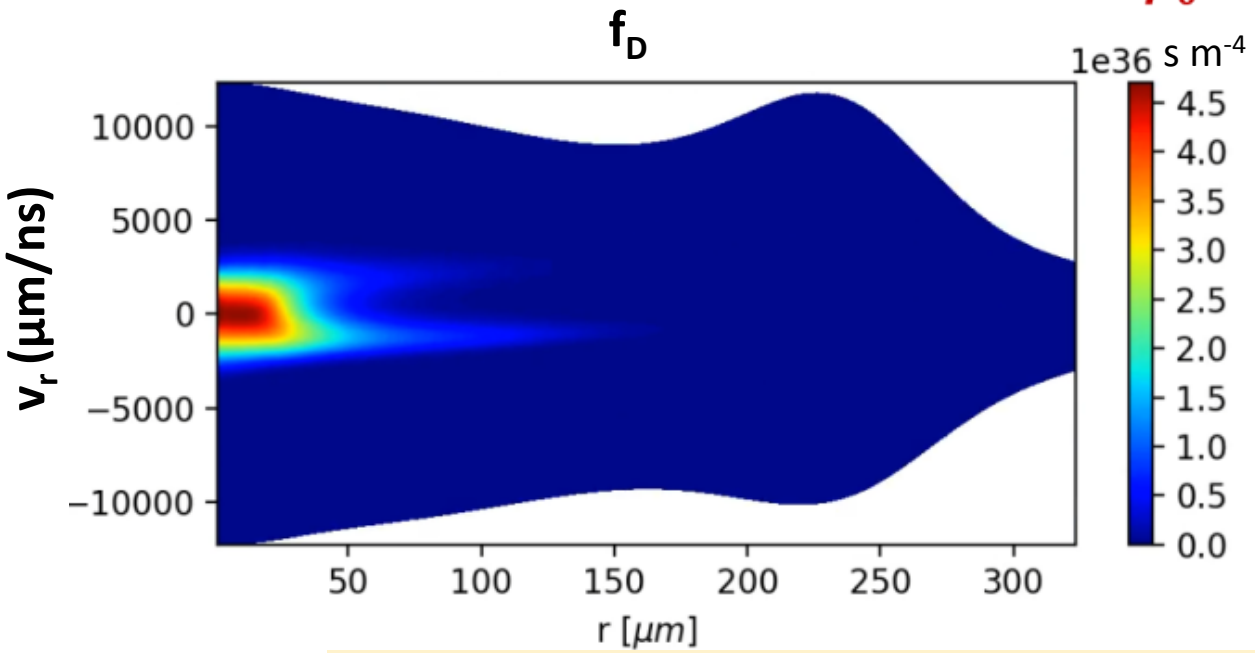

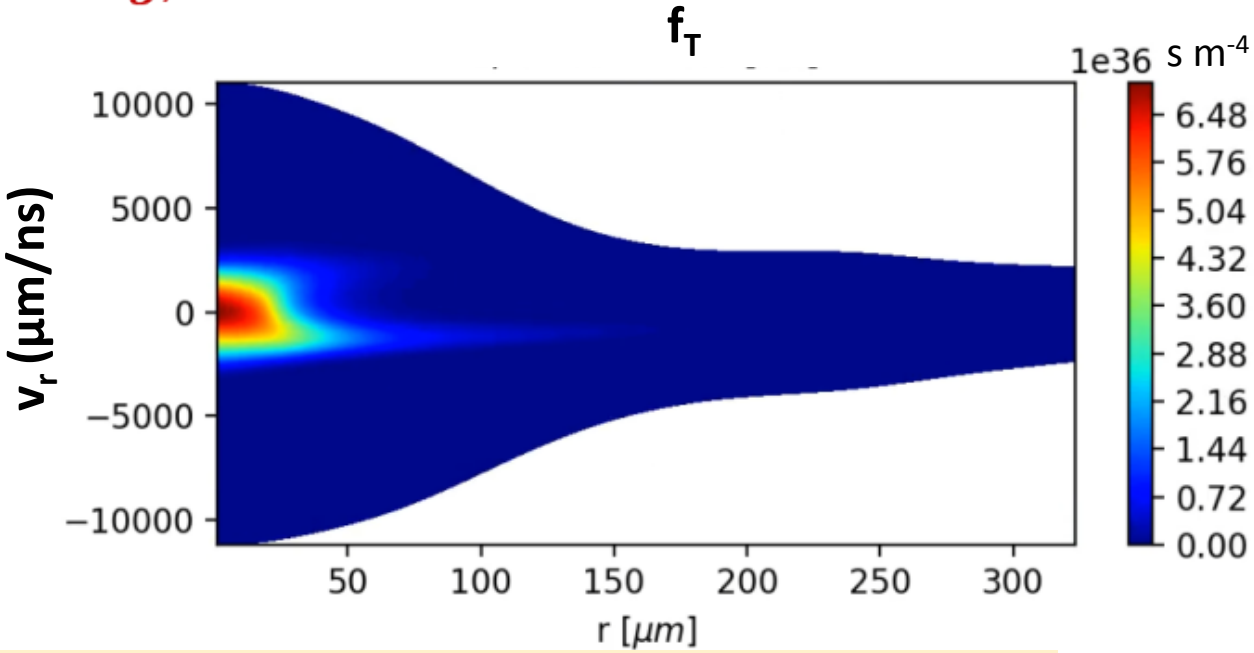

These are the bang time distribution functions integrated over the orthogonal velocity coordinate.

iFP simulation of the 0.2 mg/cc fill density implosion shows two distinct ion populations

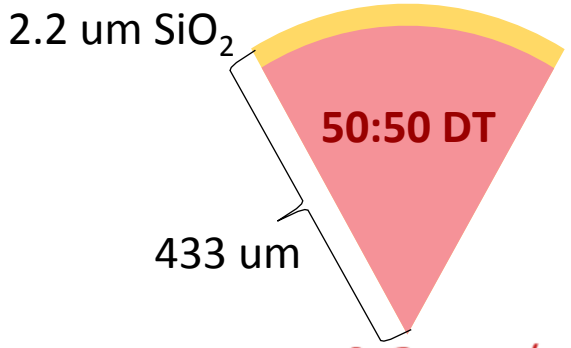

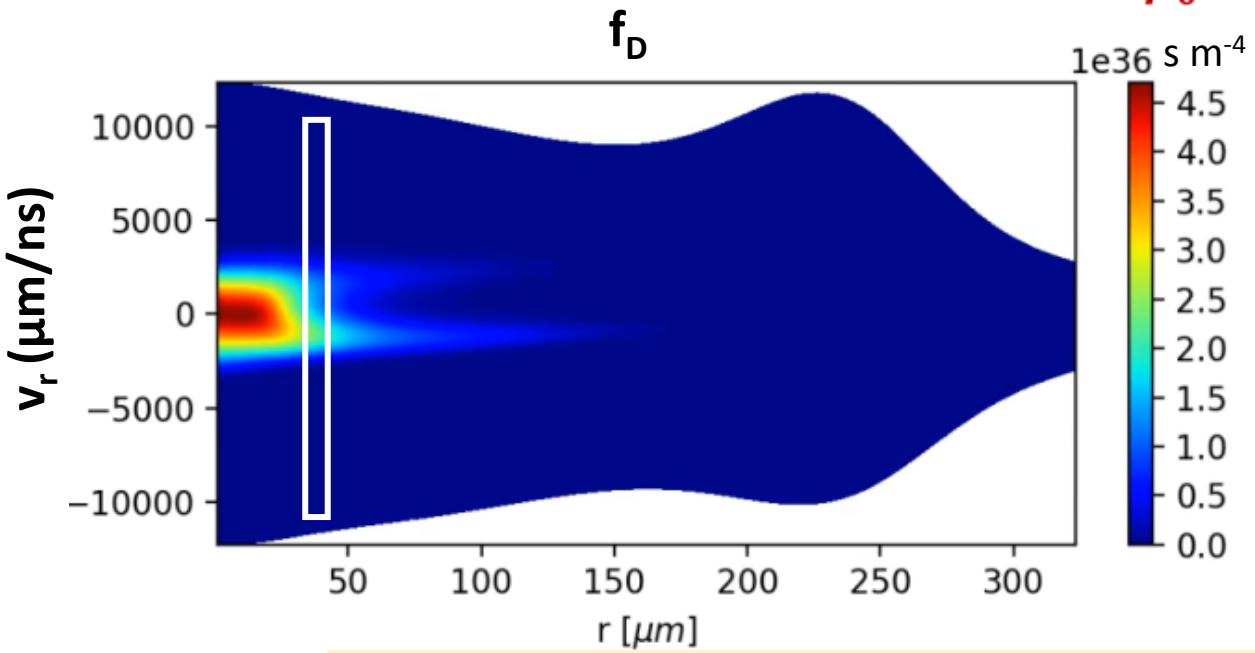

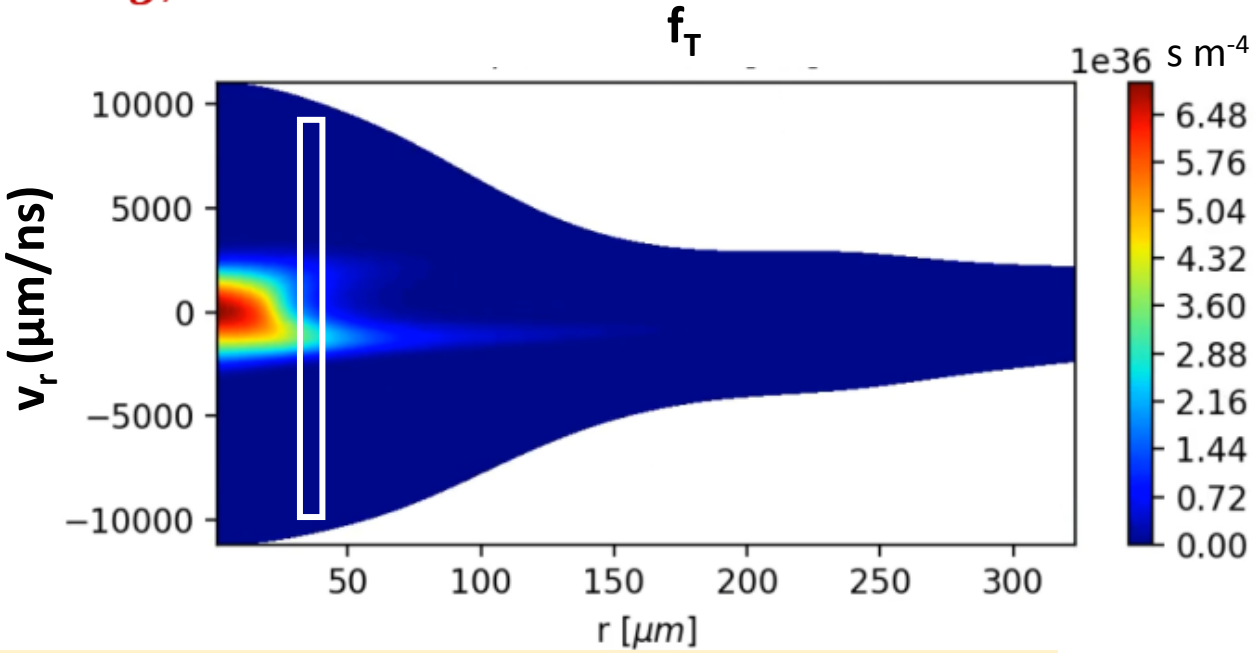

These are the bang time distribution functions integrated over the orthogonal velocity coordinate.

iFP simulation of the 0.2 mg/cc fill density implosion shows two distinct ion populations

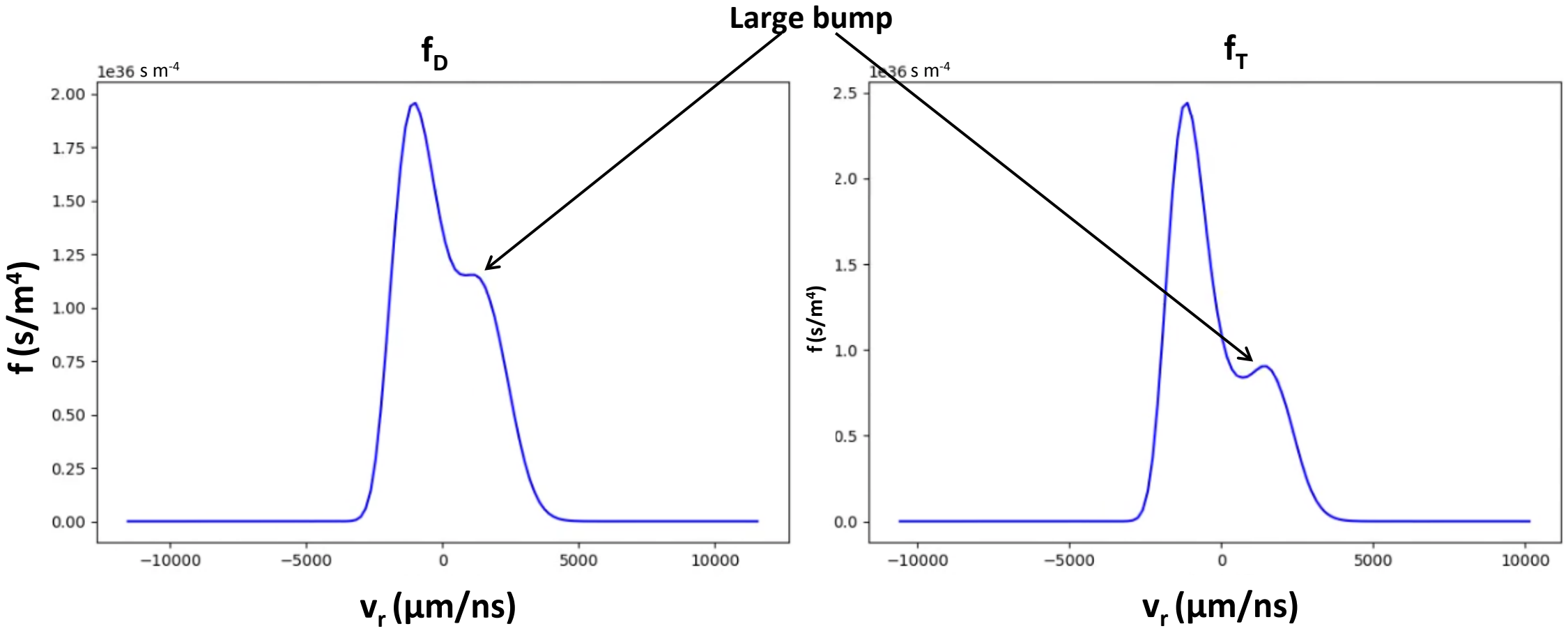

For clarity line-outs at the radius of maximal DTn emission are shown

The apparent temperature ratio computed from the iFP 1D2V distribution functions is close to the true mean energy ratio

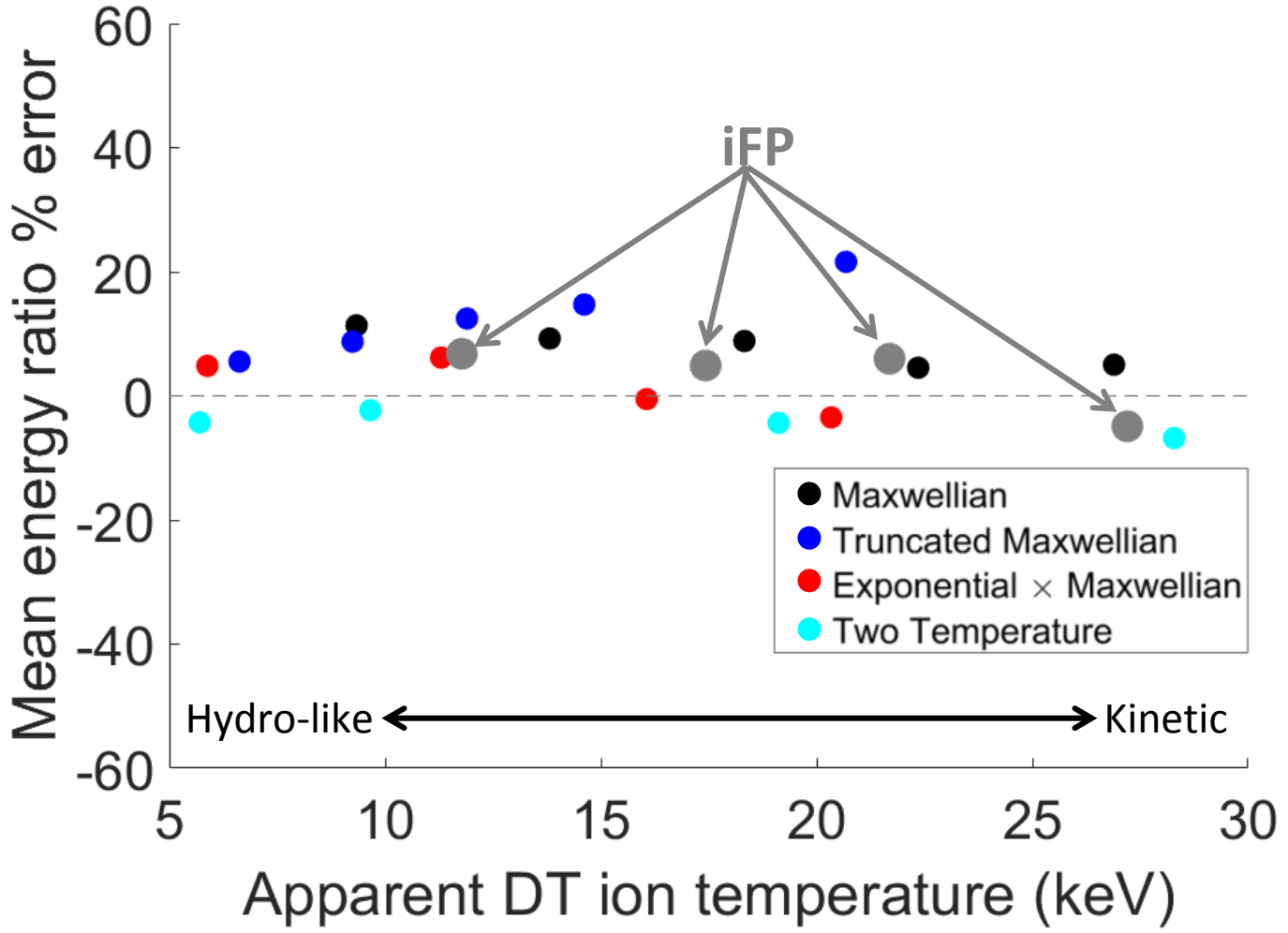

Future work

- Understand why hydro theory does a good job predicting the equilibration trend for highly kinetic conditions

- Design experiments to measure the impacts of thermal decoupling during shock convergence on the subsequent compression

The observed difference between T_{DTn} and T_{DDn} is explained by shock coupling proportional to mass, and equilibration consistent with hydro theory.

- This is the first direct lab-based experimental measurement of shocks coupling directly proportional to mass in multi-ion plasmas, verifying a long standing prediction.

- For NIF ignition implosions, during the shock convergence phase the D and T ions are out of thermal equilibrium which greatly impacts the ion viscosity.

- iFP simulations indicate that this result is robust, even in the highly kinetic regime.

Questions?

The Brysk form for the temperature mass weighting is only accurate for DT implosions when the temperature ratio is not too large

$$T_{DTn} = \frac{m_T T_T + m_D T_D}{m_T + m_D}$$

$$T_T = T_{DTn} + \frac{m_D}{m_T}(T_{DTn} - T_{DDn})$$

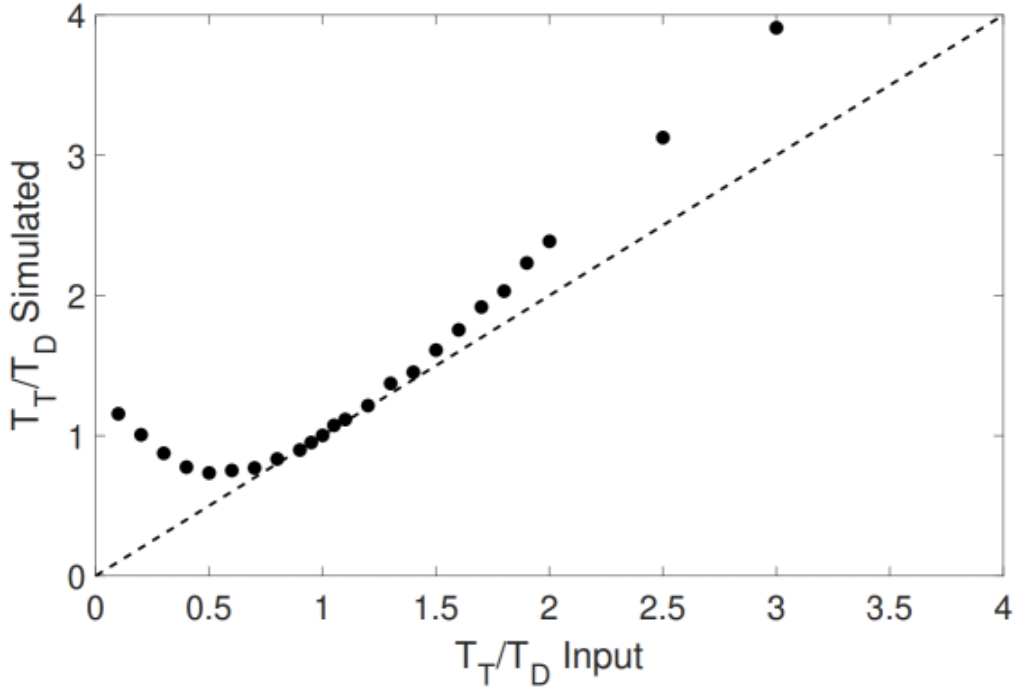

Figure 4. Black points show the temperature ratios inferred from Monte Carlo simulated neutron spectra plotted versus the input temperature ratio. The dashed black line is a reference showing equality between input and simulated values.

Species separation was previously observed in D^3He gas-filled shock driven implosions

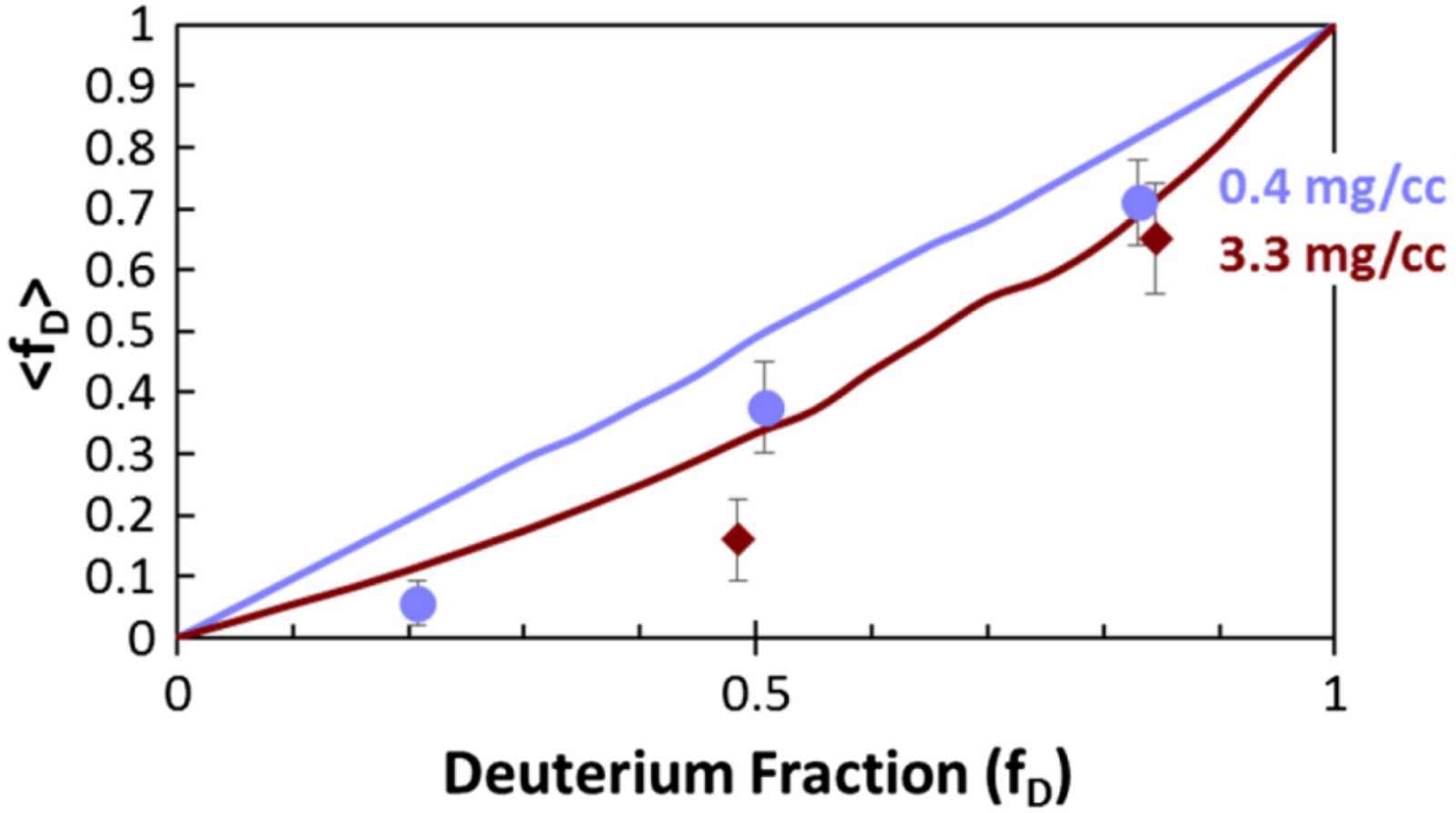

These experiments used the same OMEGA platform and consistently inferred suppression of the D content in the core during nuclear emission.

Rinderknecht et. al. Phys. Rev. Lett. **114**, 025001

The level of species separation can be inferred from the combined yields and ion temperatures taking into account profiles to second order

DT – flat reactivity ratio – Uniform model –

$$< f_D >= \frac{\frac{Y_{DDn}}{Y_{DTn}}}{\frac{Y_{DDn}}{Y_{DTn}} + \frac{1}{2}\frac{\sigma v_{DDn}(T_{rDD})}{\sigma v_{DTn}(T_{rDT})}}$$

$$\frac{< f_D >}{< f_{^3He} >} = 2R_o \frac{Y_{DDn}}{Y_{D^3Hep}}[1 + \frac{1}{4}\frac{\delta^2 R_o}{\delta T^2}\frac{T_{sD^3Hep} - BT_{sDDn}}{B\frac{\delta R_o}{\delta T}}]$$

D^3He – steep reactivity ratio – second order model* –

$$B = \frac{m_{^3He} + m_D * \frac{T_{^3He}}{T_D}}{m_D + m_{^3He}}$$

From f_D the mass concentration of the light species (c) can be computed as $$c = \frac{2 * f_D}{2 * f_D + 3 * (1 - f_D)}$$

*Requires use of temperature ratio trend inferred from DT data

One potential source of species separation is multi-ion diffusion within the sharp gradients of the shock front

The diffusion equation can be written as:

$$\rho \frac{Dc}{Dt} = -\nabla \cdot i$$

- c is the light species mass concentration ($\frac{\rho_l}{\rho}$)
- i is the drift velocity of the light species relative to the center of mass

$$i = \rho_l (u_l - u)$$

$$= -\rho D(\nabla c + k_p \nabla log P_i + k_{Ti} \nabla log T_i + k_{Te} \nabla log T_e + k_E \frac{e}{T_i} \nabla \Phi)$$

using $\nabla \Phi \approx \frac{\nabla P_e}{e\, n_e}$ and the ideal gas equation:

$$= -\rho D(\nabla c + k_p \nabla log P_i + k_{Ti} \nabla log T_i + k_{Te} \nabla log T_e + k_E \nabla log P_e)$$

Separation driven by gradients in T, and P is compared to homogenization driven by classical diffusion to estimate the concentration gradient

The strength of the separation can be estimated as:

$$L_s = \frac{i}{\rho_l} * \tau_{shock} = (u_l - u) * \tau_{shock}$$

$$= -\frac{D}{c}\frac{(k_p + k_{Ti} + k_{Te} + k_E)}{\Delta_{shock}} * \frac{\Delta_{shock}}{v_{shock}}$$

$$\boxed{L_s = -\frac{D}{c}\frac{(k_p + k_{Ti} + k_{Te} + k_E)}{v_{shock}}}$$

Separation driven by gradients in T, and P is compared to homogenization driven by classical diffusion to estimate the concentration gradient

The strength of homogenization can be estimated as:

$$L_r = (u_l - u) * \tau_{imp} = -\frac{D}{c}\frac{R_0}{v_{shock}}\nabla c$$

Separation driven by gradients in T, and P is compared to homogenization driven by classical diffusion to estimate the concentration gradient

$$= -\frac{D}{c}\frac{R_0}{v_{shock}}\nabla c \qquad L_s = -\frac{D}{c}\frac{(k_p + k_{Ti} + k_{Te} + k_E)}{v_{shock}}$$

$$\nabla c = \frac{k_p + k_{Ti} + k_{Te} + k_E}{R_0}$$

$$\Delta c = \nabla c * R_{min} = (k_p + k_{Ti} + k_{Te} + k_E)\frac{R_{min}}{R_0}$$

$$\Delta c = \frac{k_p + k_{Ti} + k_{Te} + k_E}{CR} = \frac{\Sigma k}{CR}$$

The inferred level of species separation is correlated with the estimated value, but consistently lower

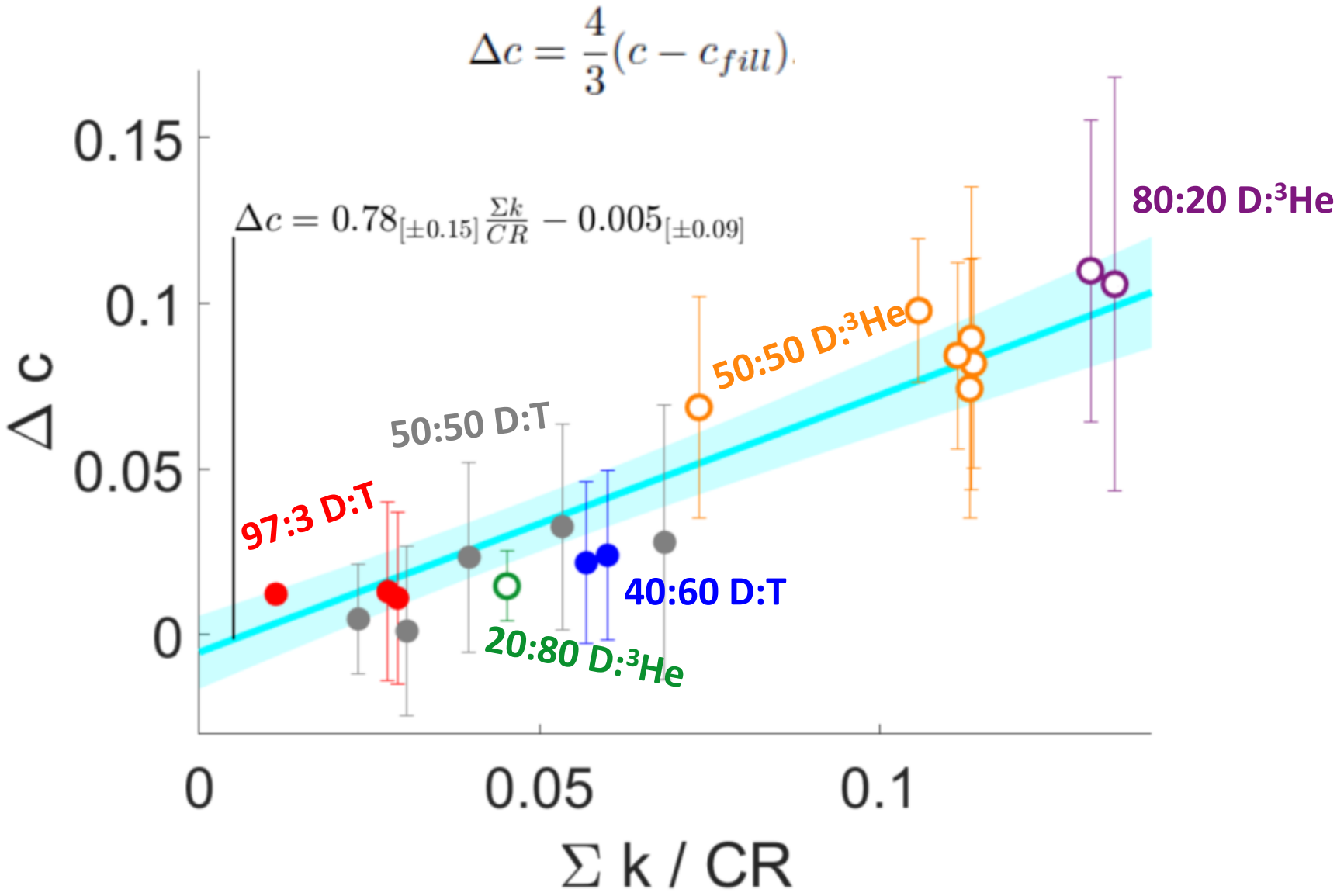

Path forward

- Multi-ion hydro simulations with PHORCE (VT)

- Experiments investigating the impact of disequilibrium in the shock convergence phase on the subsequent compression phase
  - Experiments have been completed, data analysis is ongoing

Other things

Previous measurements with the Particle X-ray Temporal Diagnostic were used to implicate time-resolved multi-ion effects during shock emission

The PXTD was used to measure the DTn, D^3Hep, and DDn bang times simultaneously on experiments with “hydro equivalent” fill ratios.

The cause of the emission time difference is determined by measuring the relative emission timing with varying D fraction in hydro equivalent implosions

fD (0.57-0.97)

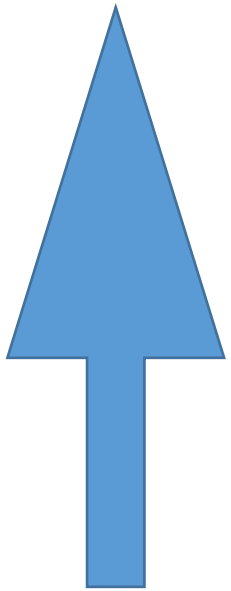

Increasing D fraction

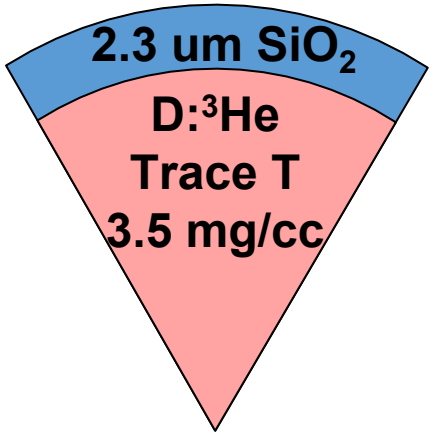

The cause of the emission time difference is determined by measuring the relative emission timing with varying D fraction in hydro equivalent implosions

fD (0.57-0.97)

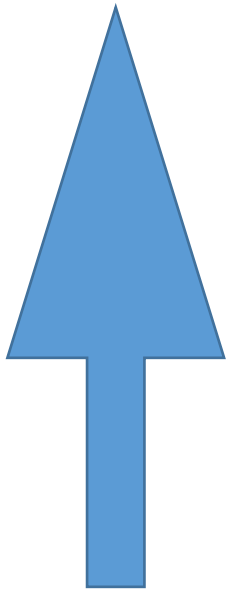

Increasing D fraction

N_k (0.2-1)

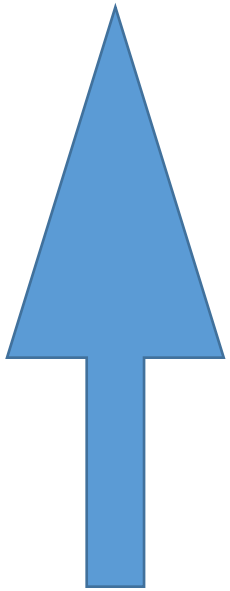

Increases the N_k making kinetic effects stronger

The cause of the emission time difference is determined by measuring the relative emission timing with varying D fraction in hydro equivalent implosions

fD (0.57-0.97)

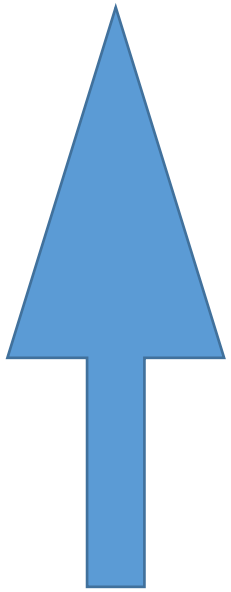

Increasing D fraction

N_k (0.2-1)

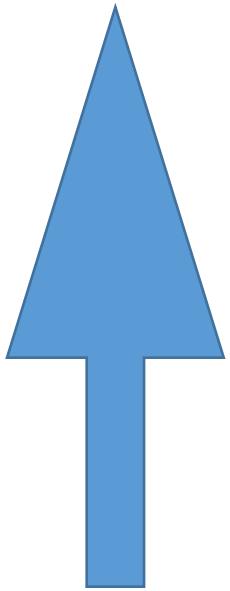

Increases the N_k making kinetic effects stronger

$\sum K$ /CR (3-4)

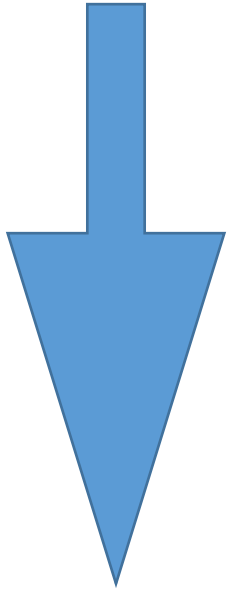

Decreases $\sum K$ /CR and species separation

The cause of the emission time difference is determined by measuring the relative emission timing with varying D fraction in hydro equivalent implosions

fD (0.57-0.97)

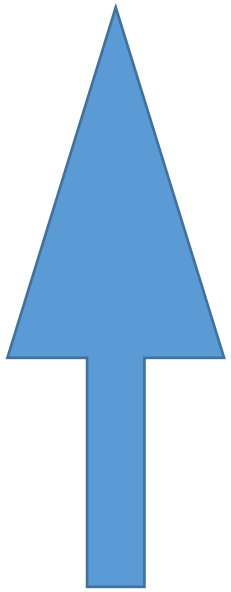

Increasing D fraction

N_k (0.2-1)

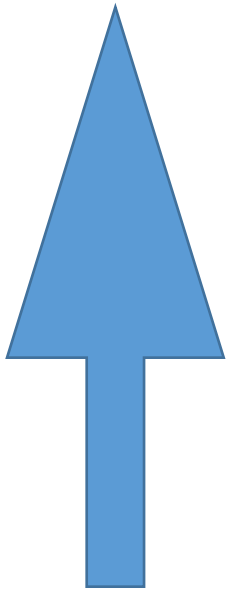

Increases the N_k making kinetic effects stronger

$\sum K / CR$ (3-4)

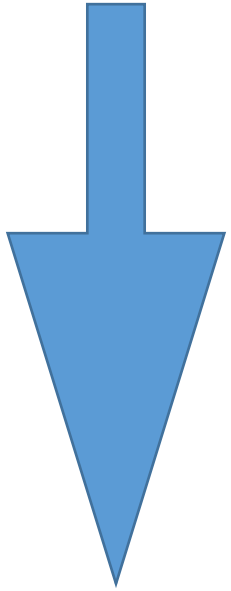

Decreases $\sum K / CR$ and species separation

τ_N (3-4)

τ_N is large and stays similar

The cause of the emission time difference is determined by measuring the relative emission timing with varying D fraction in hydro equivalent implosions

fD (0.57-0.97)

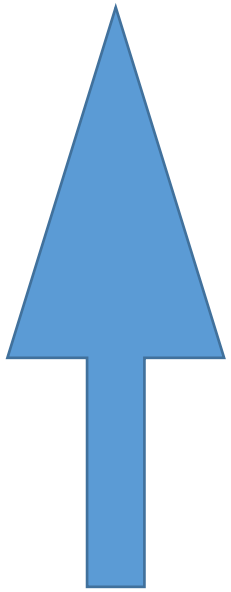

Increasing D fraction

N_k (0.2-1)

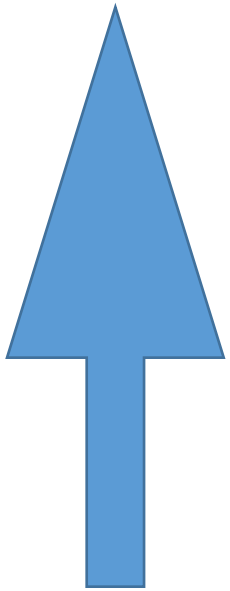

Increases the N_k making kinetic effects stronger

$\sum K / CR$ (3-4)

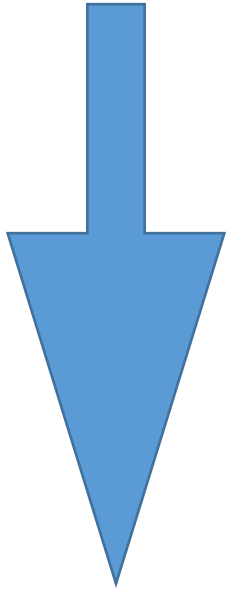

Decreases $\sum K / CR$ and species separation

τ_N (3-4)

τ_N is large and stays similar

Rho (3.5 mg/cc)

Rho is held constant to maintain hydro-equivalence

The cause of the emission time difference is determined by measuring the relative emission timing with varying D fraction in hydro equivalent implosions

fD (0.57-0.97)

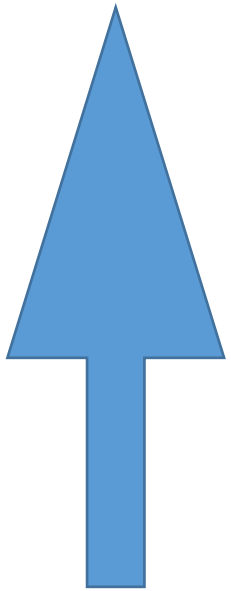

Increasing D fraction

N_k (0.2-1)

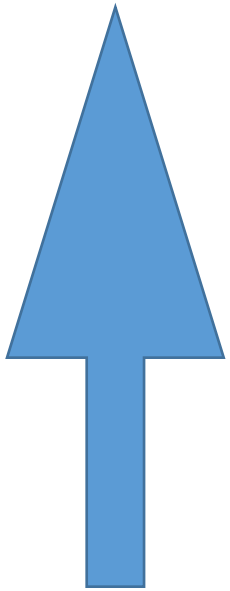

Increases the N_k making kinetic effects stronger

$\sum K$ /CR (3-4)

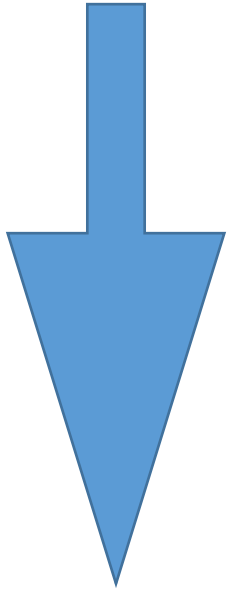

Decreases $\sum K$ /CR and species separation

τ_N (3-4)

τ_N is large and stays similar

Rho (3.5 mg/cc)

Rho is held constant to maintain hydro-equivalence

If the delta bang time increases with fD it is likely kinetic effects, if the bang time decreases with fD species separation is likely dominant, if it does not change then it could be a hydro effect.

On these experiments the DDn, DTn, and D^{3}Hep emission histories were simultaneously measured on PXTD

Example data from shot 98968

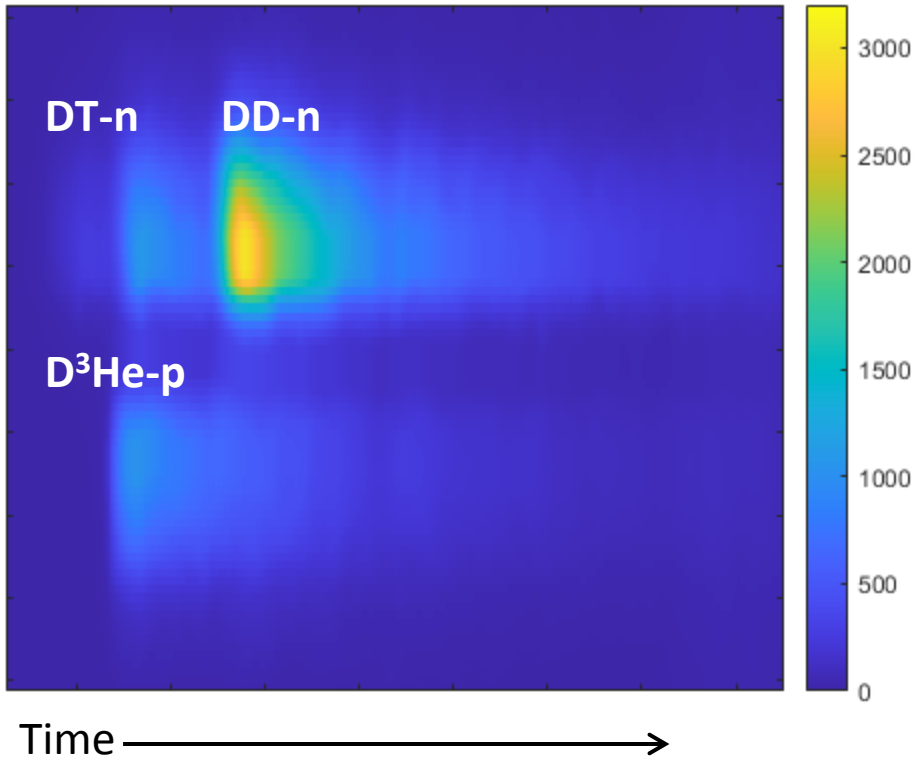

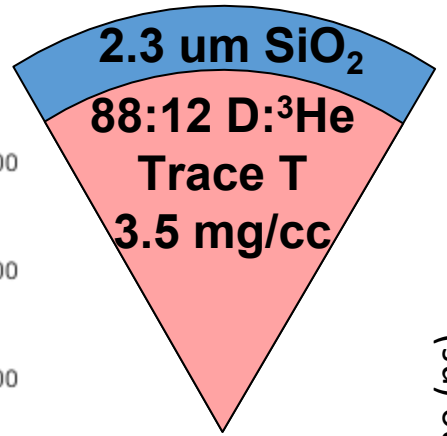

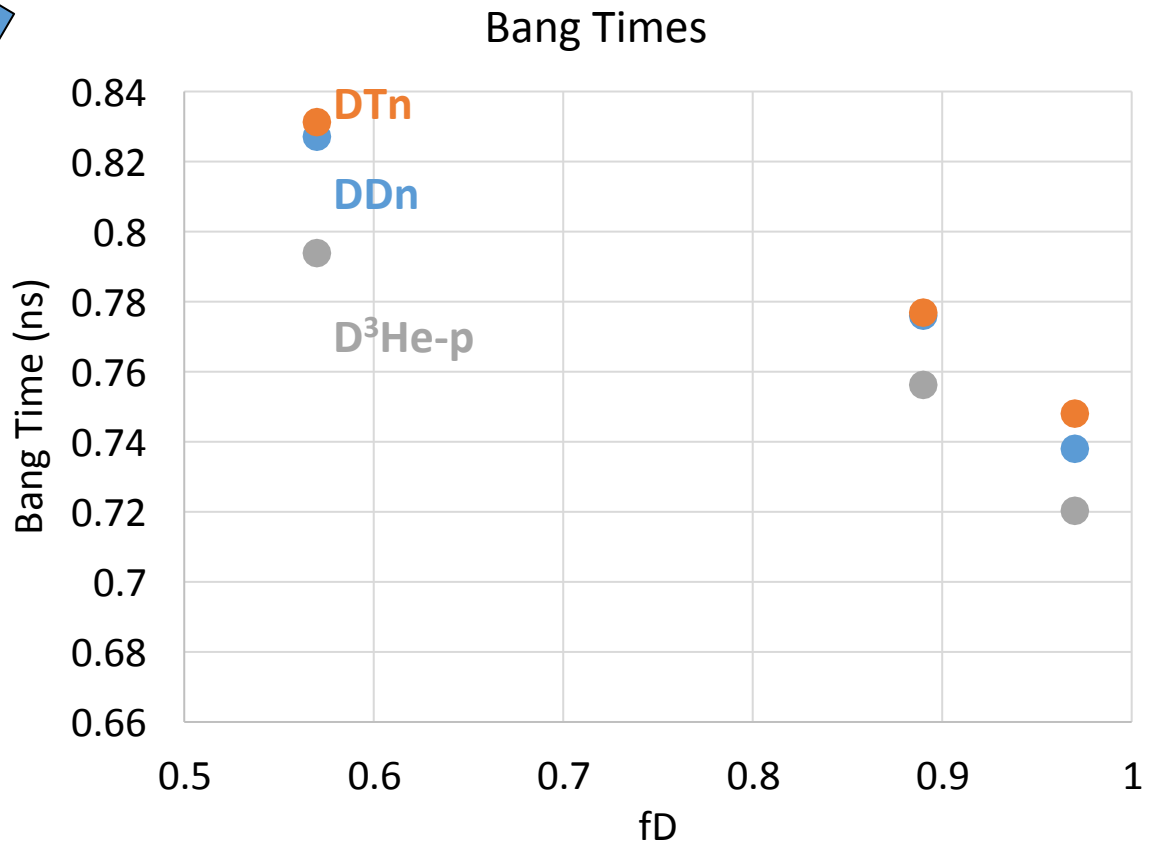

The measured bang time differentials are consistent with a constant value, indicating that hydrodynamics is most likely responsible

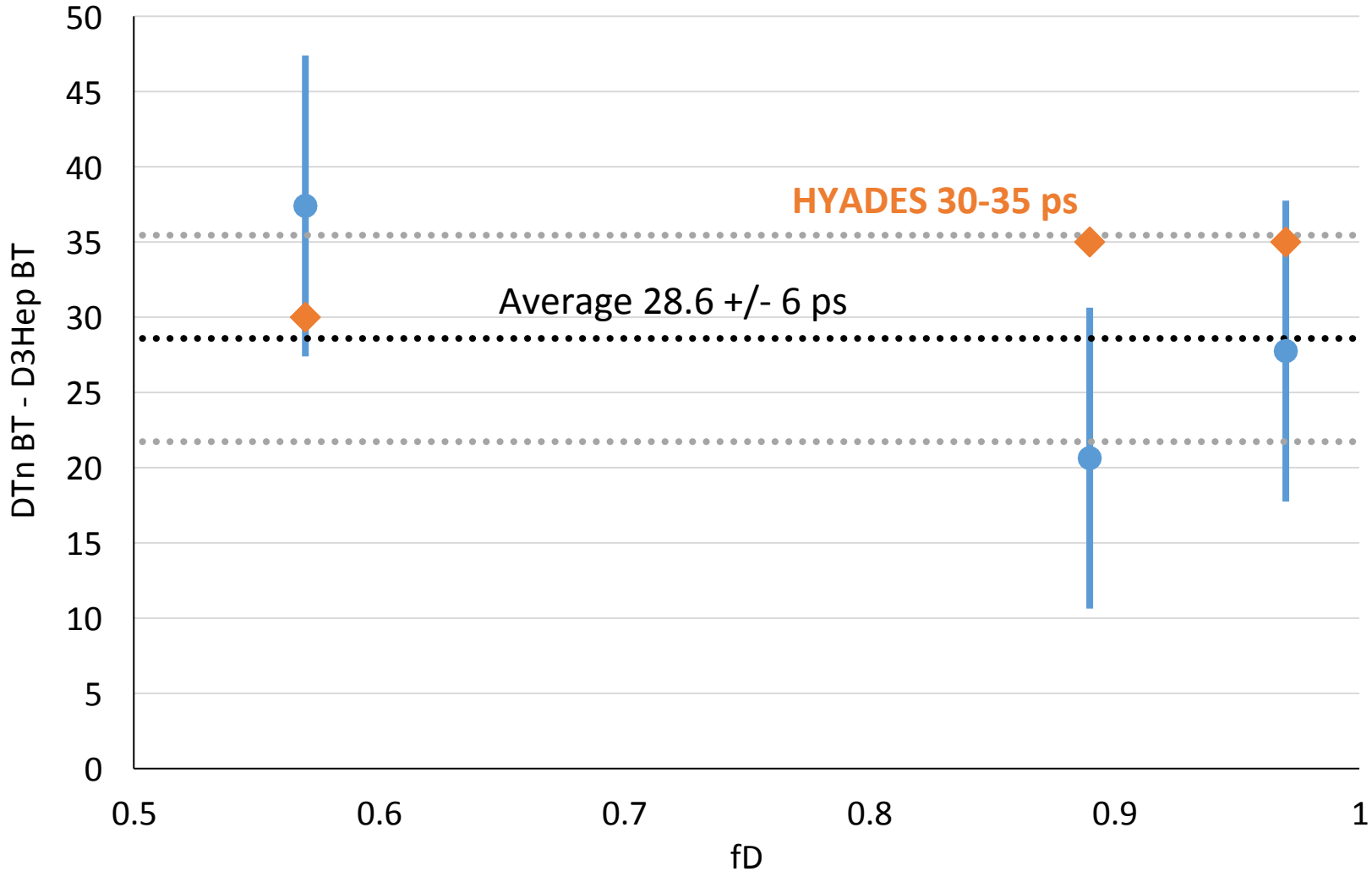

The D^3Hep emission is weighted closer to shock rebound when the central temperatures are higher, but the heated volume is smaller.

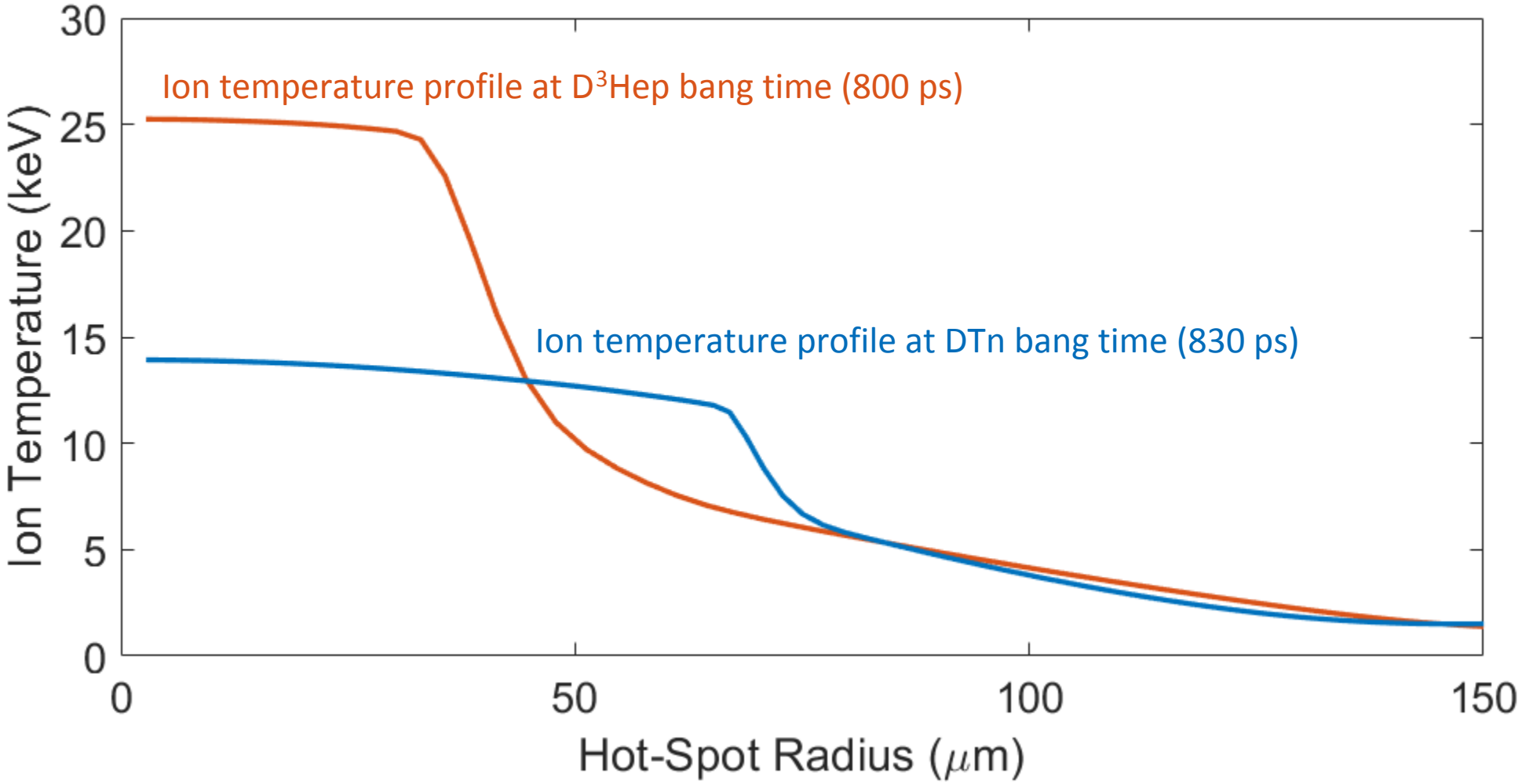

These iFP simulations show dramatically increasing SiO_2 mix with decreasing DT fill density

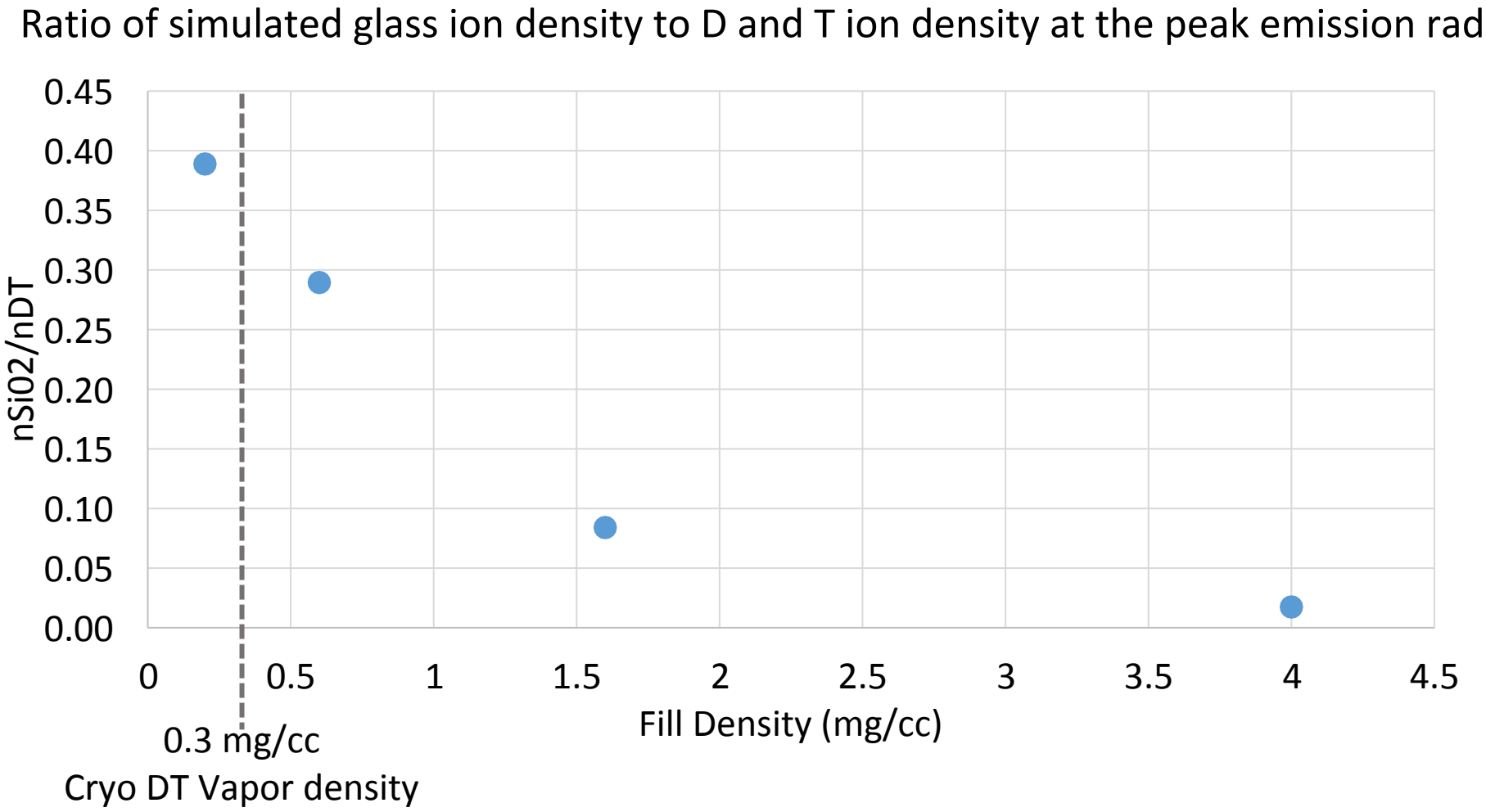

These iFP simulations show dramatically increasing SiO_2 mix with decreasing DT fill density

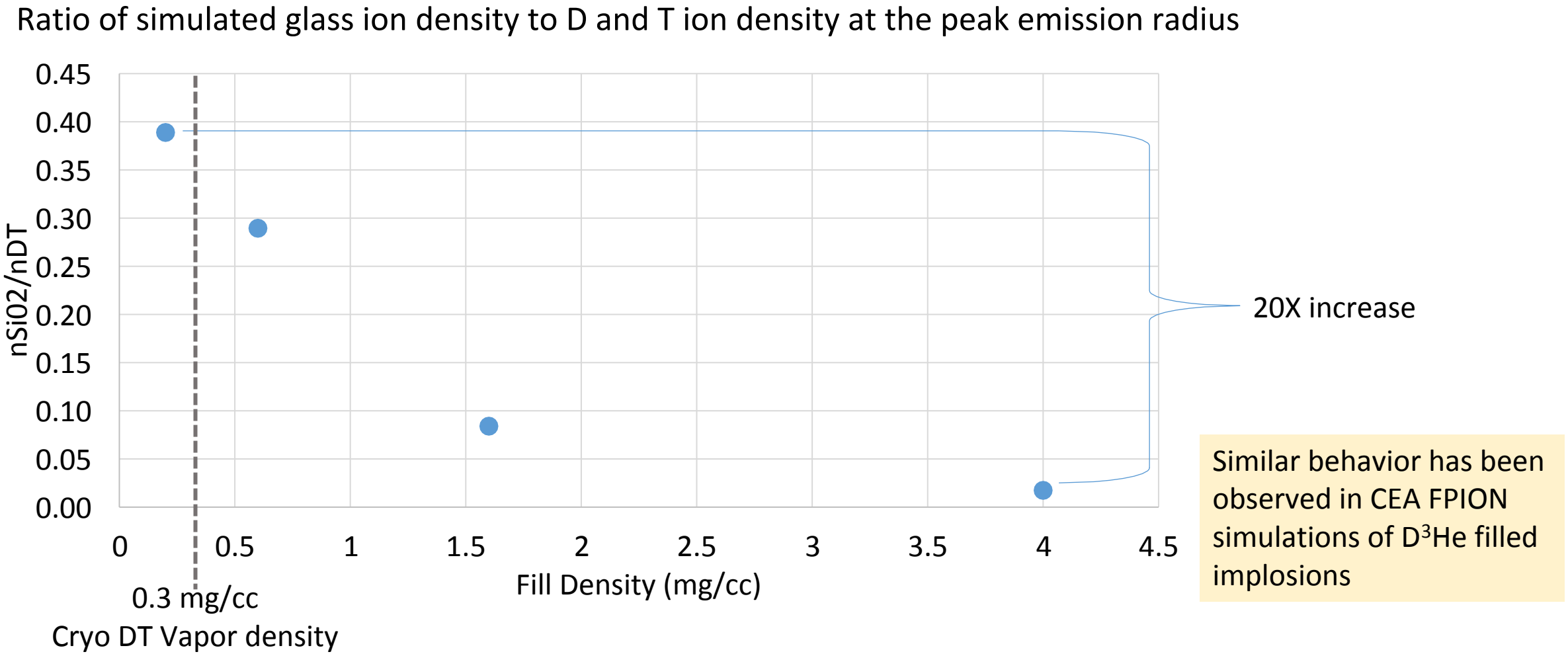

Similar behavior has been observed in CEA FPION simulations of D^3He filled implosions

The iFP simulated ion density profiles at bang time show that the SiO_2 ions dominate the material in the core at low density

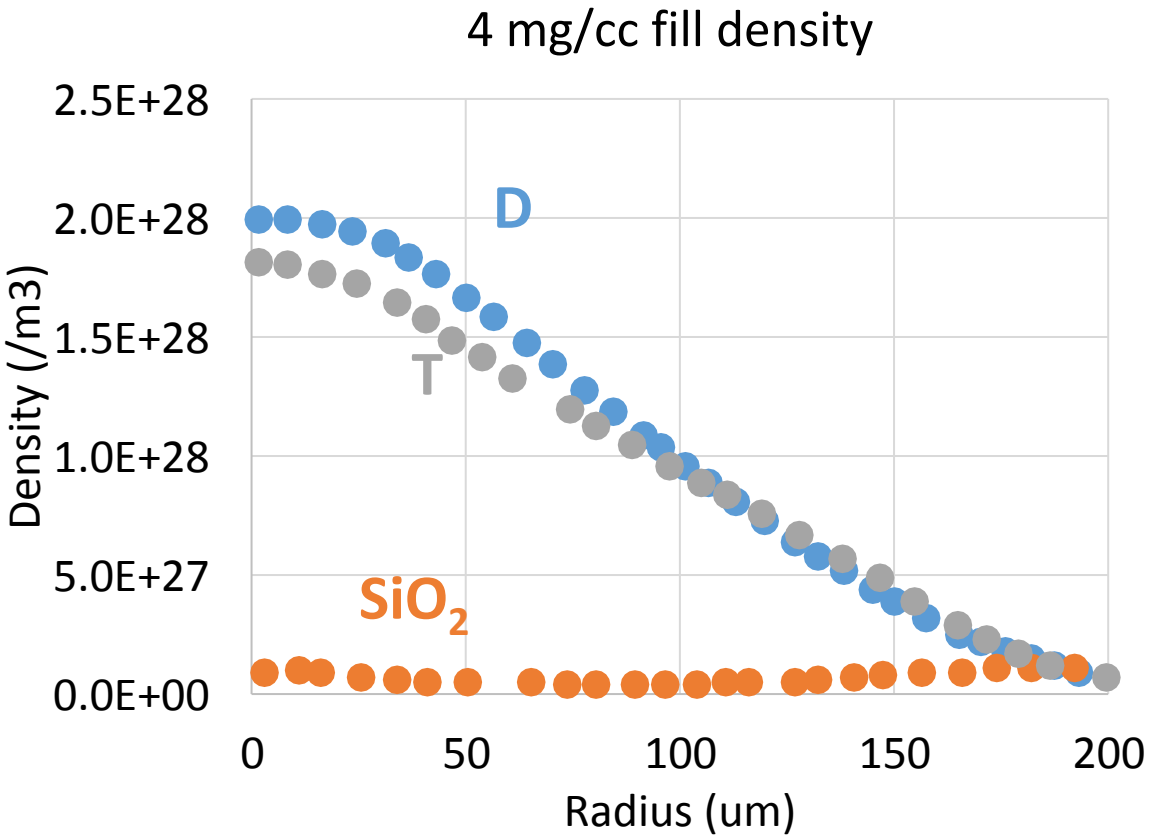

The iFP simulated ion density profiles at bang time show that the SiO_2 ions dominate the material in the core at low density

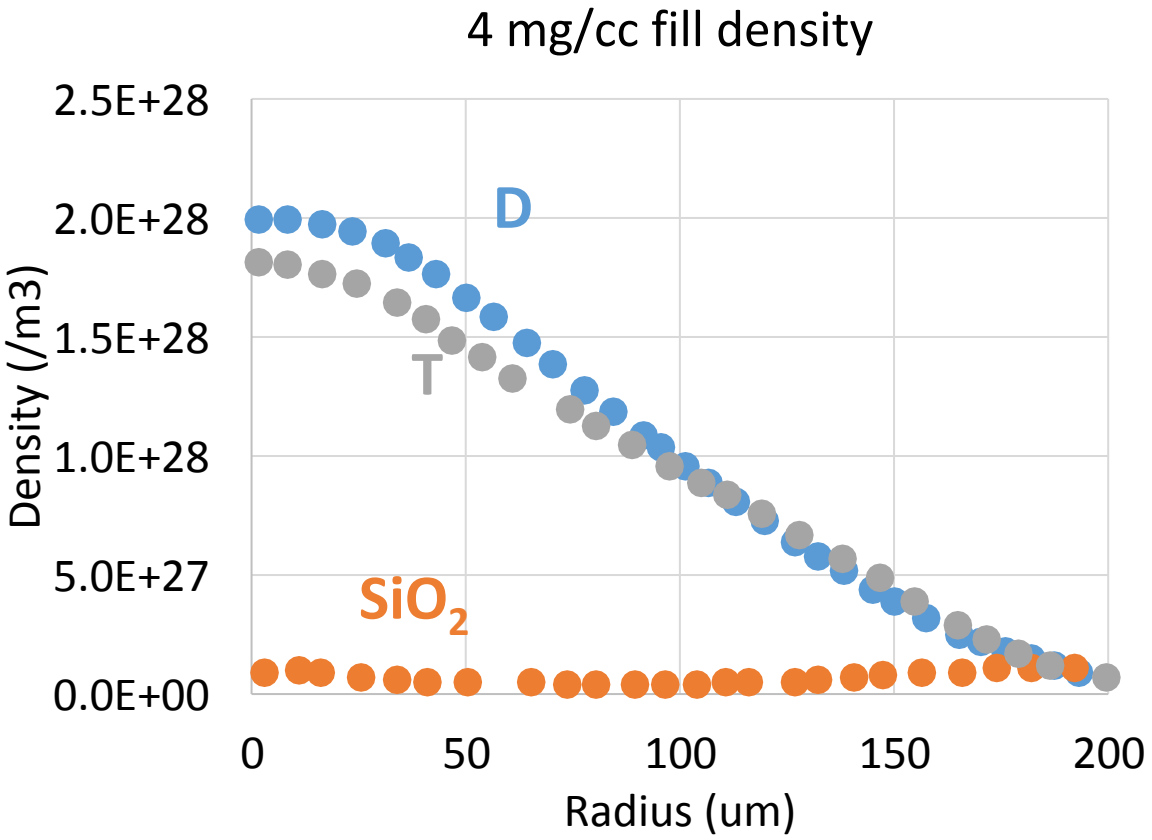

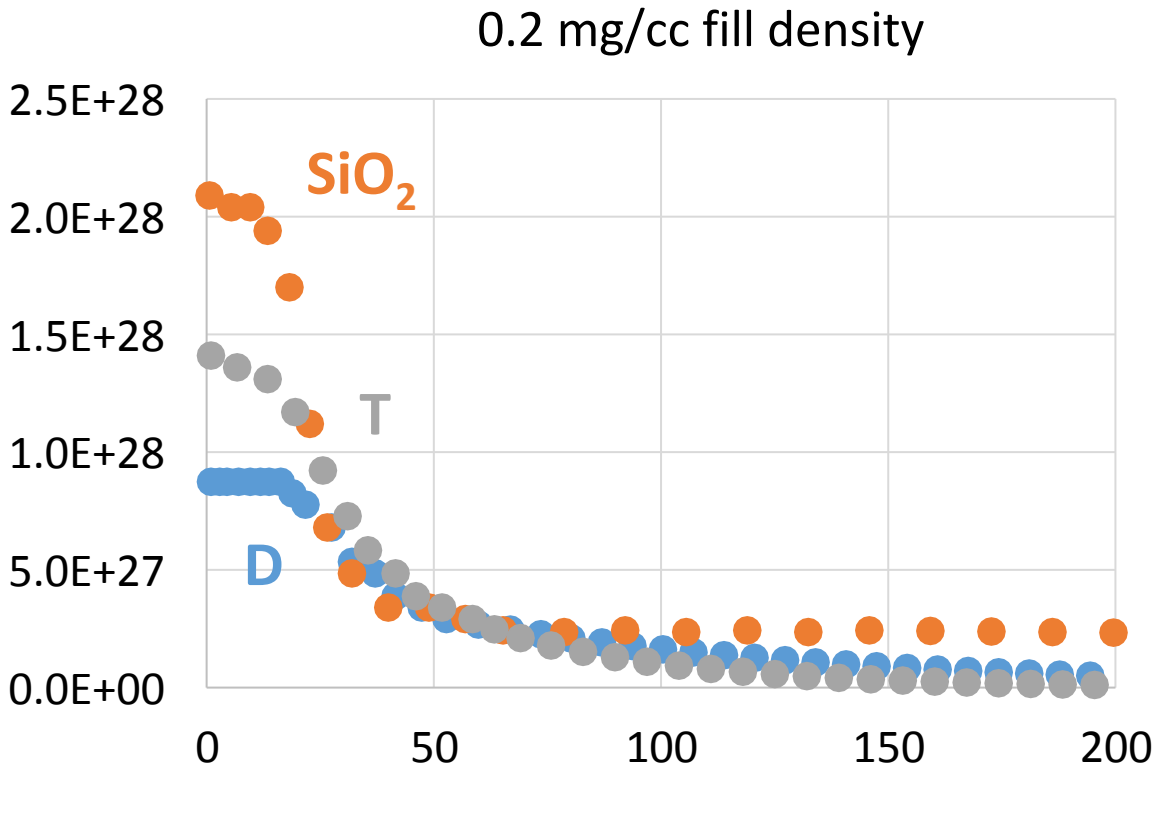

Hans Rinderknecht saw almost identical D3He yield with and without D in the initial 0.5 mg/cc gas fill of CD shell shock driven implosions

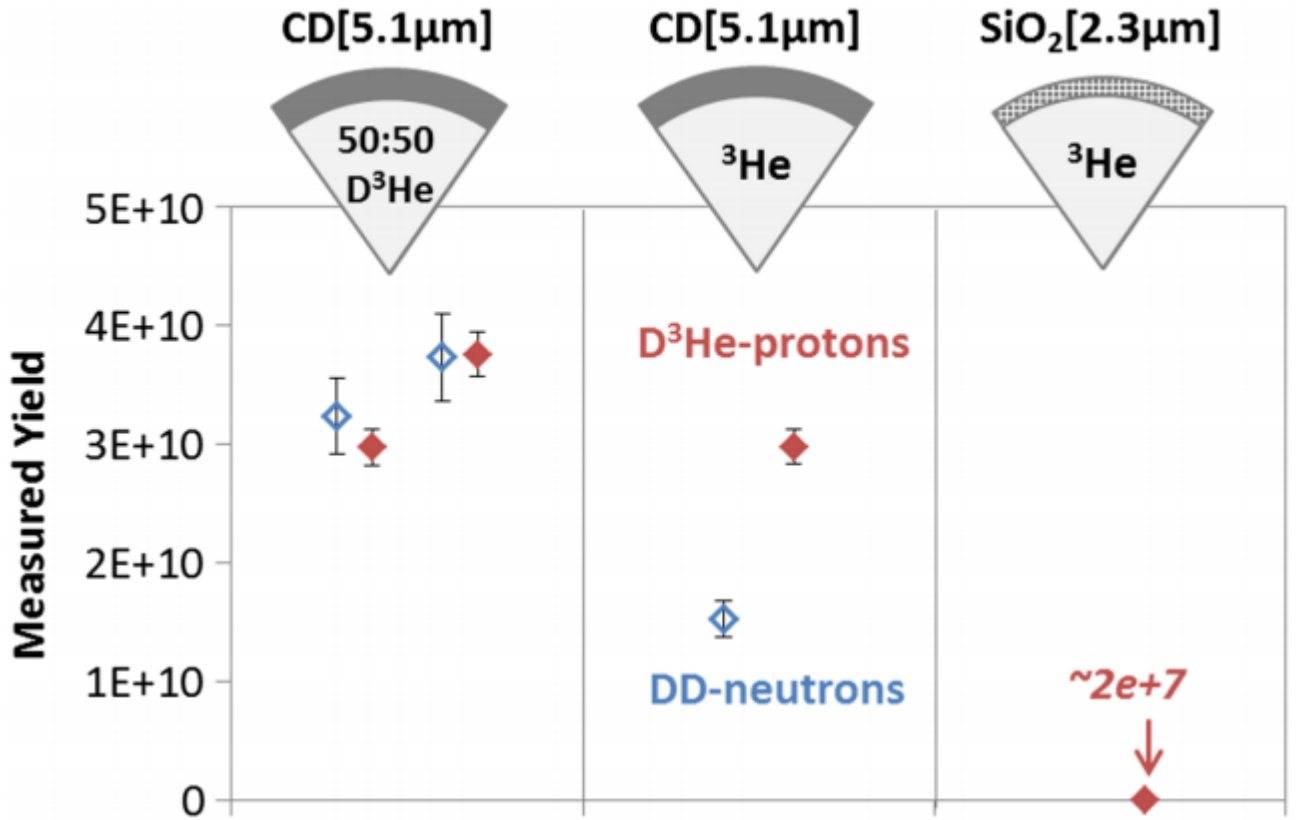

FIG. 1 (color online). Yields of D^3He protons (solid red) recorded from 30 kJ implosions of deuterated plastic shells filled with a 50:50 D^3He mixture are comparable in magnitude to implosions of the same shells filled with pure ^3He. Implosions of glass shells filled with ^3He produce yields 3 orders of magnitude lower, ruling out D_2-gas contamination of the targets as an explanation for this result. The observed D^3He-p yields require shell-deuterium mix into the ^3He fuel to be of the order of 10% the initial ^3He gas density.

PRL 112, 135001 (2014)

Ryan Rygg saw that in compressive implosions the compression yield dominated in the separated reactant implosions.

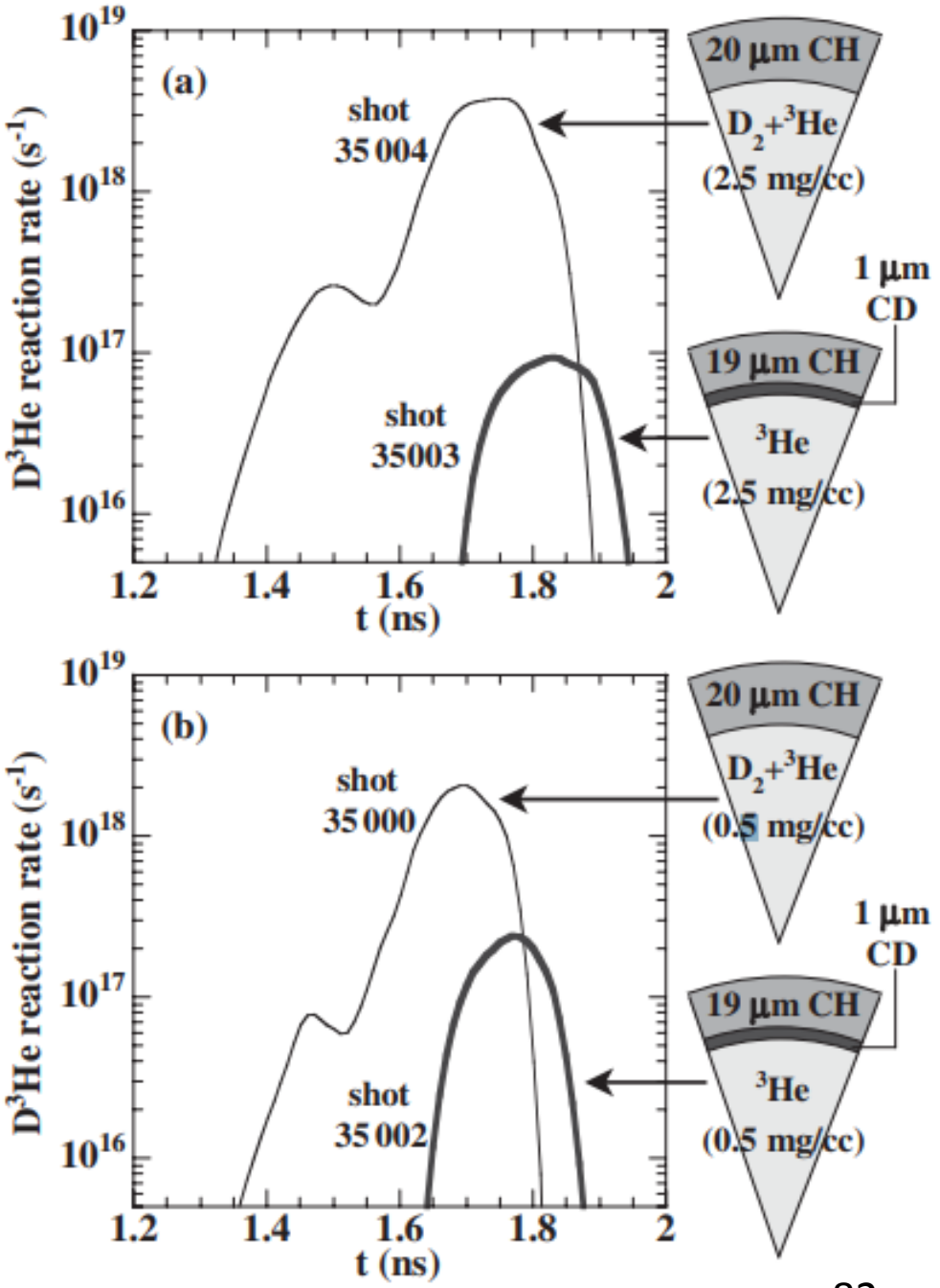

PRL 98, 215002 (2007)

Chikang Li saw that recessing a CD layer in ablatively driven implosions reduces the yield by an order of magnitude.

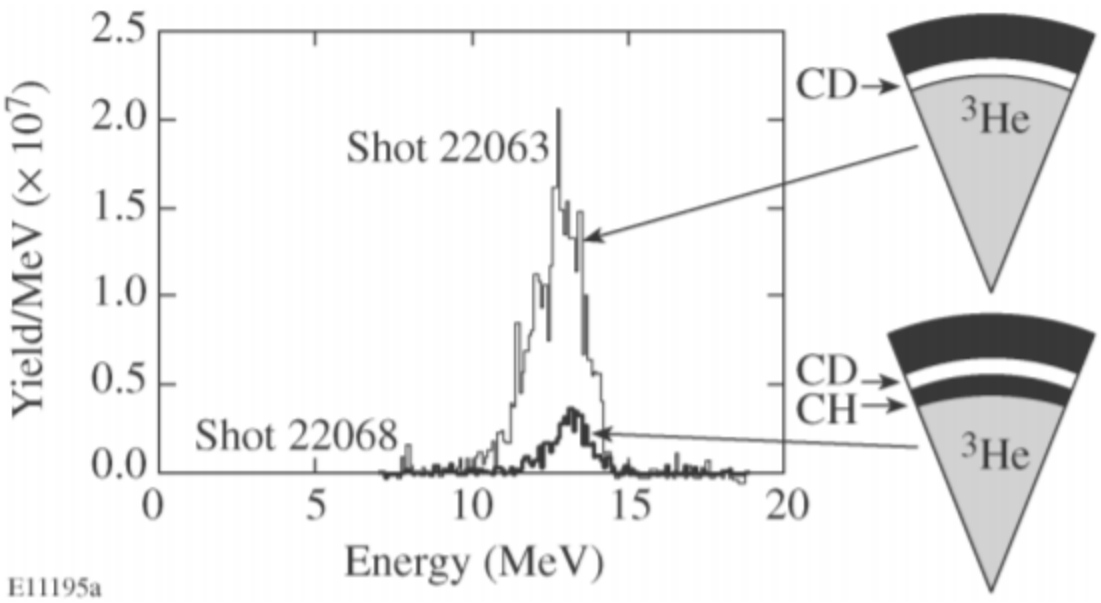

FIG. 1. The structures of two different capsules filled with 4 atm of pure ^{3}He gas, and measured spectra of primary D^{3}He protons from implosions at OMEGA. The ratio of number densities (D to C) is 1.56 in the CD layer.

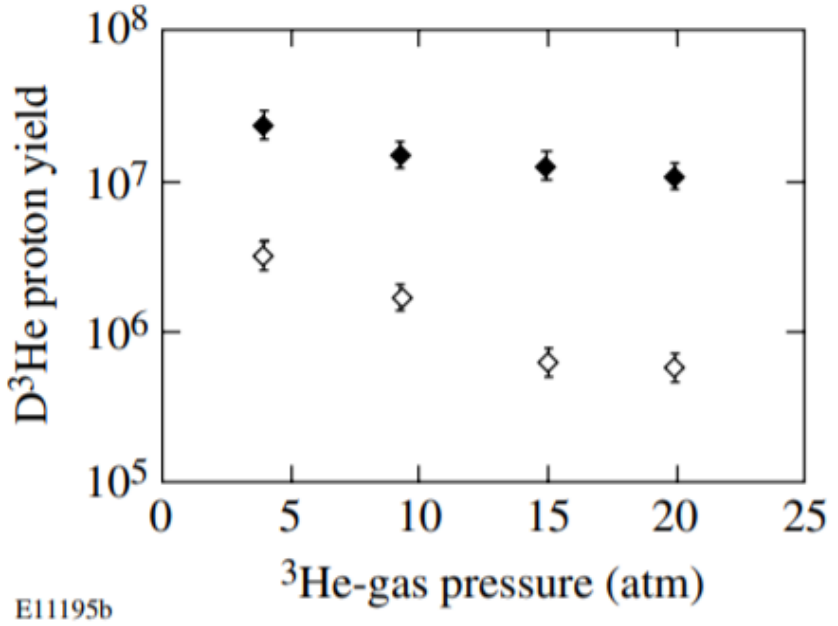

FIG. 2. D^{3}He proton yields plotted as a function of gas-fill pressures for implosions of capsules with ^{3}He fuel and zero- (closed dark diamond) and 1 μm-offset (open diamond) CD layer shells.

PRL 89, 165002 (2002)

Similar results are seen in FPION simulations of D3He-filled implosions

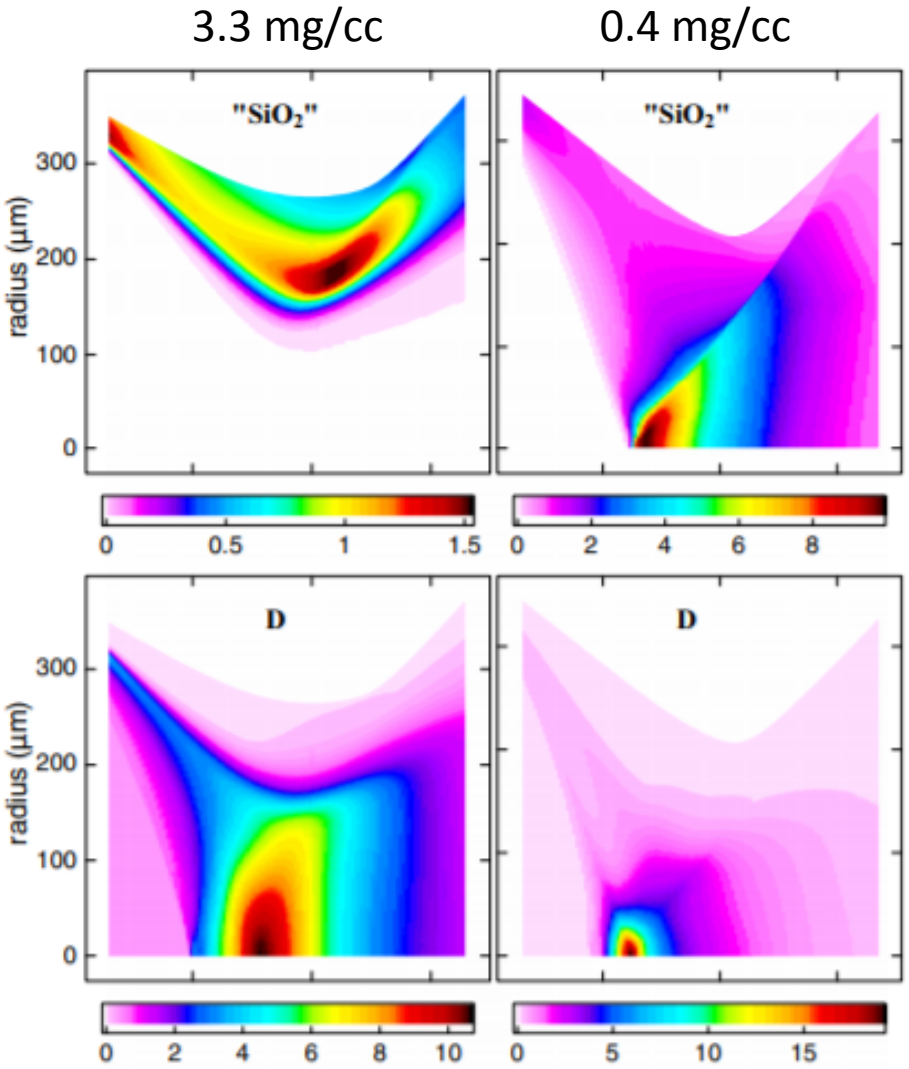

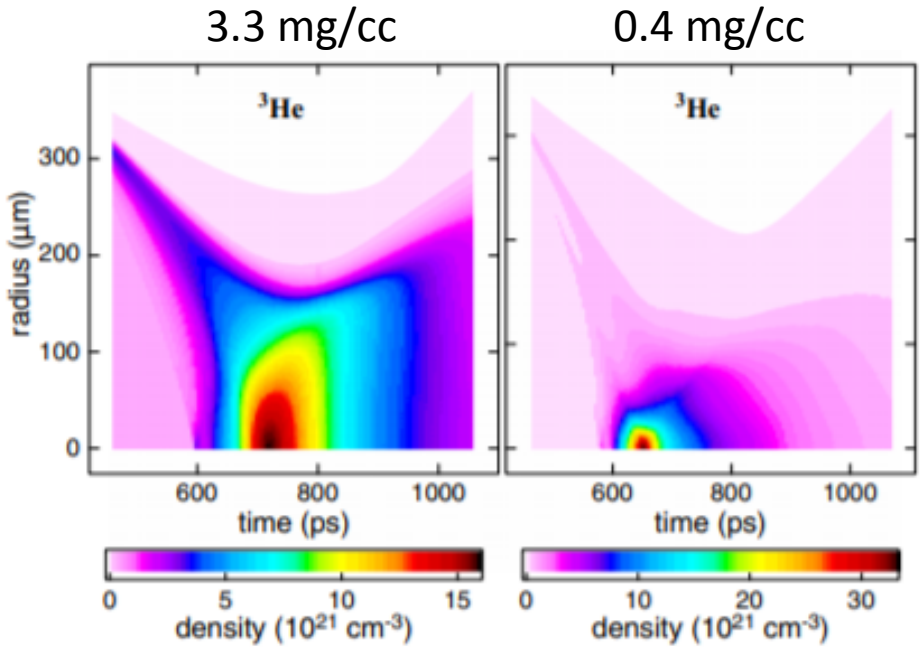

FIG. 1. Space-time evolution of the density for the three species "SiO_2," D, and ^{3}He for the high-density (left column) and low-density (right column) targets.

PRE 98, 031201 (2018)

Mike Rosenberg also saw decreasing YOC with decreasing fill density (and therefore increasing Knudsen number).

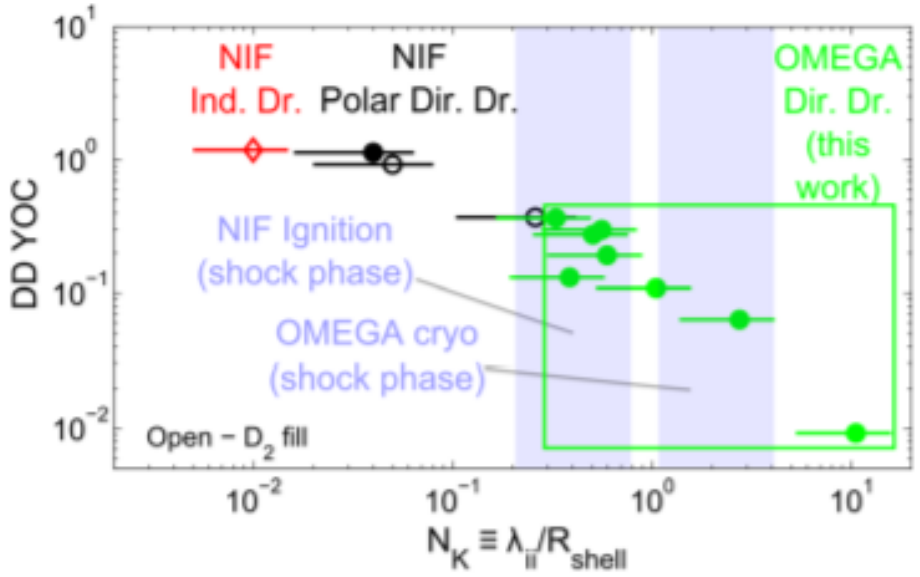

FIG. 1. Ratio of measured DD fusion yields to hydrodynamics-simulated yields (yield over clean, YOC) as a function of the Knudsen number (N_K) for an indirect-drive exploding pusher on NIF (red diamond),[23] three polar-direct-drive (PDD)[24] exploding pushers on NIF,[22] and direct-drive exploding pushers on OMEGA (green circles).[6] Fusion burn profile measurements of the OMEGA experiments are described herein. Filled markers represent D^3He-filled implosions, while open markers denote D_2-filled implosions. Though the drive conditions are quite different, these experiments show a unified picture of the increasing impact of ion kinetic effects as a function of increasing Knudsen number for $N_K \gtrsim 0.1$. A band centered around $N_K = 0.5$ shows the approximate Knudsen number at the center of a NIF ignition-relevant indirect-drive implosion[25] or a NIF polar-direct-drive implosion[24] immediately after shock convergence, while a band centered around $N_K = 2$ shows the approximate Knudsen number after shock convergence at the center of a cryogenic layered implosion on OMEGA.[26] This data were originally presented in Ref. 22. Reproduced with permission from Phys. Plasmas **21**, 122712 (2014).

POP 22, 062702 (2015)

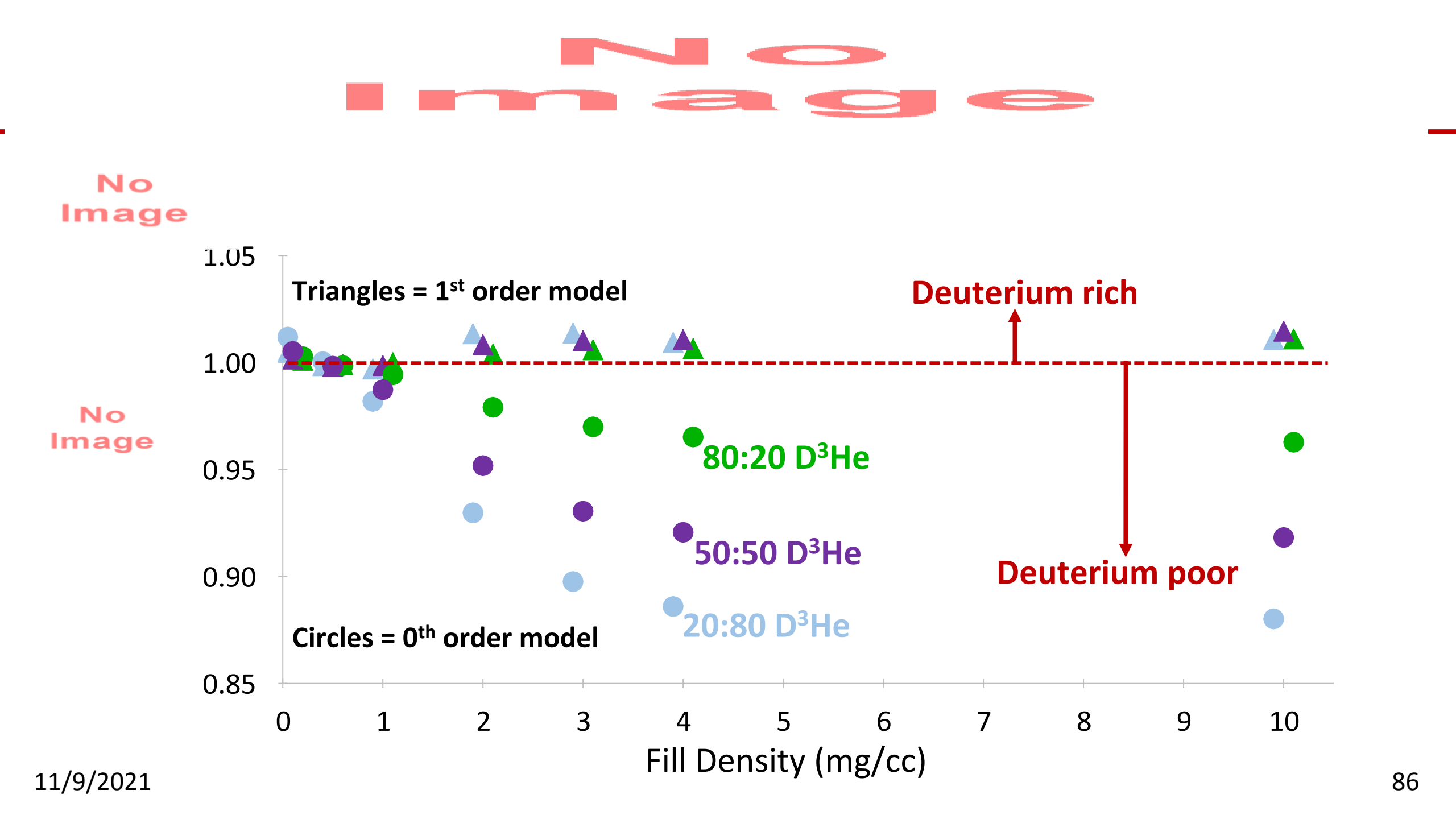
No Image
No Image
1.05
1.00
0.95
0.90
0.85
Triangles = 1st order model
Circles = 0th order model
Deuterium rich
Deuterium poor
80:20 D3He
50:50 D3He
20:80 D3He
0
1
2
3
4
5
6
7
8
9
10
Fill Density (mg/cc)

iFP consistently overpredicts the DTn and DDn ion temperatures indicating that some details of the ion distributions may not be properly captured

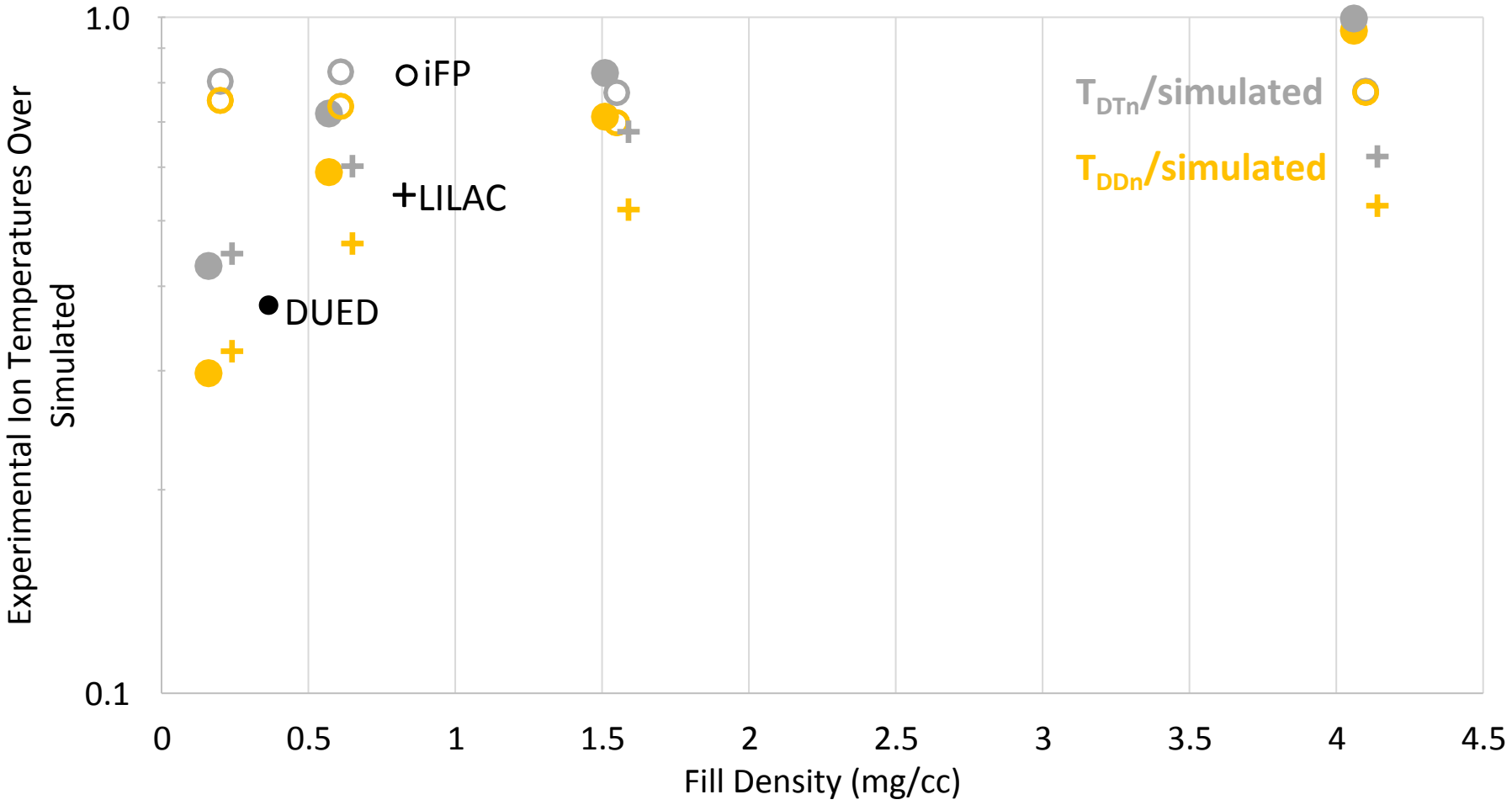

iFP temperatures are calculated by simulating the neutron spectra and using them to infer apparent temperatures.

The temperature ratio from iFP simulations is not consistent with the experimentally observed trend